Doctoral theses at NTNU, 2022:301

Nirmal Acharya

Erosion in Francis turbines due to geometrical positioning of runner and guide vanes

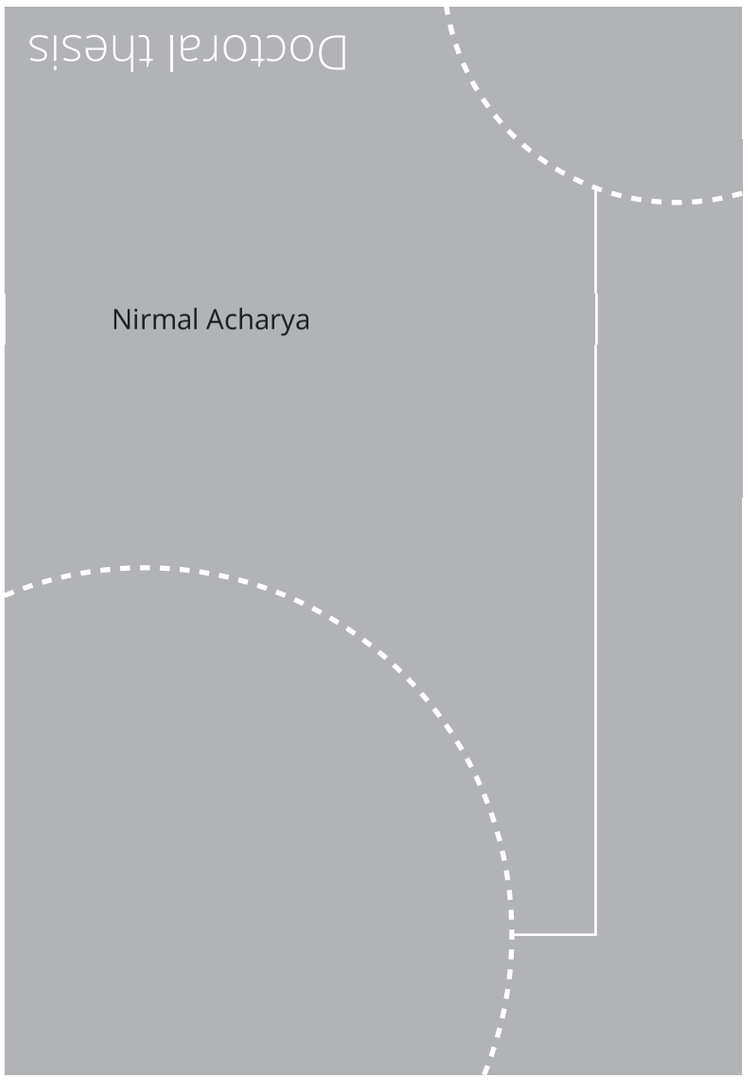

ISBN 978-82-326-6264-7 (printed ver.)
ISBN 978-82-326-6037-7 (electronic ver.)
ISSN 1503-8181 (printed ver.)
ISSN 2703-8084 (electronic ver.)

NTNU
Norwegian University of
Science and Technology

NTNU
Norwegian University of
Science and Technology
Thesis for the degree of
Philosophiae Doctor
Faculty of Engineering
Department of Energy and Process Engineering

Doctoral theses at NTNU, 2022:301

NTNU
Norwegian University of
Science and Technology

Doctoral theses at NTNU, 2022:301

NTNU

Nirmal Acharya

Erosion in Francis turbines due to geometrical positioning of runner and guide vanes

Thesis for the degree of Philosophiae Doctor

Trondheim, "OCTOBER" "2022"

Norwegian University of Science and Technology
Faculty of Engineering
Department of Energy and Process Engineering

NTNU
Norwegian University of
Science and Technology

NTNU
Norwegian University of Science and Technology

Thesis for the degree of Philosophiae Doctor

Faculty of Engineering
Department of Energy and Process Engineering

ISBN 978-82-326-6264-7 (printed ver.)
ISBN 978-82-326-6037-7 (electronic ver.)
ISSN 1503-8181 (printed ver.)
ISSN 2703-8084 (electronic ver.)

Doctoral theses at NTNU, 2022:301

PRINTED IN NORWAY
NO - 1598

NORDIC SWAN ECOLABEL
Printed matter
2041 0731

Printed by Skipnes Kommunikasjon AS

Dedicated to my parents, Mrs. Kamala Acharya and Mr. Nar Narayan Acharya

Preface

This PhD research work has been carried out at the Waterpower Laboratory, Department of Energy and Process Engineering (EPT) at Norwegian University of Science and Technology (NTNU) in Trondheim, Norway. Experimental works were executed at Turbine Testing Laboratory, Kathmandu University, Dhulikhel, Nepal. The work is presented as a collection of papers envisioned and written during the project period, October 2018- June 2021 and February 2022- July 2022. The research was conducted under research project FME- HydroCen which is a Centre for Environment- friendly Energy Research hosted by NTNU and funded by Research Council of Norway (RCN) and Norwegian Hydropower Industries. Professor Ole Gunnar Dahlhaug from NTNU was the main supervisor for this project (Project No. 90148312).

Abstract

Hydro-abrasive erosion in turbine components is one of the prominent operational challenges for hydropower plants located across basins of regions such as Himalayas in Asia, the Andes in South America, and Pacific coast. Large sediment concentration with higher percentage of hard minerals such as quartz and feldspar affect exposed hydromechanical components which can cause significant erosion resulting reduced efficiency over time, huge operation, and maintenance cost along with undesired shut-down causing loss of valuable energy generation. In case of Francis turbines, erosion is mostly observed around stay vanes, guide vanes, facing plates and runner blades. Quantity and pattern of erosion depends upon the operating conditions, amount, and size of sand particles in the flow along with type of flow phenomena in particular regions.

This study has conducted case study on the sediment erosion problems in one of the hydropower plants located in India that has collaboration with the project. Field reports from the power plant showed abundance of quartz particles contained in the water. A numerical analysis is conducted for turbine components in order to study the causes of various erosion patterns in the turbine components. The results from the CFD are compared with the actual erosion in the turbines. Leakage flow through the clearance gaps of guide vanes is found to be the primary cause of erosion at the inlet of the runner blades. This work comprehends a systematic investigation of spatial temporal progression of leakage vortex (LV) for varying operating conditions. The progression of LV at hub area is roughly classified into three forms i.e., elongation stage, disintegration stage and dissolving stage. Whereas few LV at the shroud area is found to pass through outlet of the runner, majority of it dissolves before reaching the mid-stream of the blade. Study was also conducted to find the optimal runner design with a trade-off between performance and erosion behavior by modifying blade angle distribution from inlet to outlet. Varying blade angle distribution changes the blade profile which also seemed to yield a better reduction in erosion.

This study has identified research gap as the investigation of flow pattern in sidewall gaps in Francis turbines which refers to the clearance region between the stationary and rotary components. For hydro-turbines operating in sediment laden water, sediment will pass through these gaps and erode the parent material. Due to continuous effects of abrasion and erosion, these side wall clearance region increases and consequently the leakages through these gaps. The work focusses on the study of flow behavior in those regions with an experimental setup. Experiments were

conducted in Rotating Disc Apparatus (RDA), which utilizes the method of rotating test specimen in a mixture of calculated amount of sand and water. It has a base plate which mounts test specimens that is attached to the shaft connected to the motor. First set of test specimens constitute three different slot width and another set has six different slot height. All experiments were carried out at Turbine Testing Laboratory, Kathmandu University, Nepal.

Results for different slot width show its positive correlation with the rotational speed and erosion loss. It shows that as rotational speed increases, the shift of erosion wear is more towards the higher width slot. Another set of results including specimens with different height shows the increase in erosion rate with the corresponding increase in slot height. It is observed that, fluid flowing from the outlet of the guide vanes hits the side wall of the rotor component normally at positive slot height. Some particles re-circulate in the slot width and again impinges the opposite side walls. Whereas in the case of negative slot, the direct impingement of sediment particle to the opposite face does not happen. However, during the flow re-circulation, the sediment again hits back to the guide vane face. For the specimen with height difference, weight loss in nearly constant at lowest rotational speeds. Erosion rate is observed increasing linearly up to zero height difference, but it increases significantly at the positive height difference.

Sidewall gaps and flow in such regions is inevitable in hydraulic machineries. Further investigation on the shape of slot and erosion around labyrinth rings should be done to get a complete picture of erosion phenomenon. Flow phenomenon associated with sidewall gaps should be well considered and alalyzed during the preliminary phase of machine design.

Keywords: Francis turbine, Hydro-abrasive erosion, Leakage vortex, Rotating disc apparatus, Runner, Sidewall gap.

Acknowledgements

I express my wholehearted gratitude to my supervisor Prof. Ole Gunnar Dahlhaug for providing me the opportunity to carry out the research works under his direct supervision and guiding me with his invaluable insights throughout this journey. His theoretical and practical knowledge in the field of hydropower with his relentless motivation and patience towards me has been a huge source of help and inspiration during the course of study. I am equally thankful to my co-supervisor Assoc. Prof. Chirag Trivedi who motivated me and shared his experiences and knowledge regarding numerical simulation and many more. It was a pleasure and privilege conducting research under their tutelage.

I would like to thank Prof. Torbjørn Kristian Nielsen, Assoc. Prof. Pål-Tore Storli and Bjørn Winther Solemslie for their valuable suggestions, endless support with valuable comments and recommendations. I am grateful to FME- HydroCen project for my PhD funding and its people in the office downstairs for all those festival gifts and parties. Such a nice gesture you people have!

A big thanks to my colleagues in Waterpower building who made this period smoother through spirited chats and regular newspaper quizzes during lunch time, frequent exchange of smiles and table tennis matches. I am also highly indebted to all my lab members, all batches of fellow students at the laboratory for the great working environment and for all the memorable moments we shared. Special thanks go to Dr. Igor Iliev who was always there as my unassigned supervisor for guiding me with CFD skills and hydro-machinery theories and for the fantastic co-operation we have had both in lab and outside. I would also like to remember my office roommates Kristian, Helene and Johannes for all the good time and bonhomie I had during my stay in the office. I am equally grateful to my colleagues Luiz, Ludwig, Truls, Gabriele and Jan Karl for all interesting discussions and parties. I am obliged to Ingrid Wiggen and Wenche Nygård from the administration department, for helping me in several ways.

I am most grateful to Mr. Saroj Gautam from Kathmandu University (KU) for assisting me during experimental works at Turbine Testing Lab (TTL), KU, Nepal. On the top of that, he was always readily available for project discussions and solutions. Dr. Sailesh Chitrakar deserves special credit for all the discussions, both funny and technical topics. I too like to remember my colleagues and faculty members at TTL and Department of Mechanical Engineering, KU.

I sincerely dedicate this work to my loving parents, Mommy and Daddy. I think I would not have come this far if you had not supported me in the way you have done. I am extremely thankful to my wife Prashna who was there with me in this time of rigorous dedication. Thank you for your love and support and listening my achievements and frustrations throughout this journey. I owe you a lot Prashna. Finding time with Aura, my cute little daughter to play and chatter amidst always boosted me with extra energy and motivation. Much love to my cutie pie!

Hjertelig takk!

Contents

List of Tables

List of Figures

List of Symbols

List of Symbols

c	Absolute velocity	ms^{-1}
C	Sediment concentration	kgm^{-3}
C_p	Normalized pressure	[-]
E_a	Area average sediment erosion rate density	[-]
E_r	Erosion rate	$kg\ m^{-2}s^{-1}$
f	Frequency	Hz
f_b	Blade Passing Frequency	Hz
g	Acceleration due to gravity	ms^{-2}
h	Size of Grid	M
H	Head	m
n_s	Specific speed	rpm
r	Grid refinement factor	[-]
p	Apparent order	[-]
S	Abrasion depth	mm

Greek Symbols

ρ	Density	kgm^{-3}
γ	Impingement angle	deg
ϕ	Variable for GCI calculation	[-]
*Ω	Speed number	[-]
τ	Torque	Nm

Abbreviations

CFD	Computational Fluid Dynamics
CG	Clearance Gap
GCI	Grid Convergence Index
GV	Guide Vane
HPP	Hydro Power Plant
IEC	International Electro-technical Commission
KU	Kathmandu University
LE	Leading Edge
LV	Leakage Vortex
NLS	No Load Speed
NTNU	Norwegian University of Science and Technology
PIV	Partice Image Velocimetry
PL	Part Load
RDA	Rotating Disc Apparatus
RPM	Revolutions Per Minute
RSI	Rotor-Stator Interaction
TTL	Turbine Testing Lab
TE	Trailing Edge
VFD	Variable Frequency Drive
3D	Three Dimensional

Structure of the thesis

The thesis is divided into three parts. Part I describes the background and the chronology of research works done to create the foundation for this thesis. Summary of the main research papers is included for quick overview of the work. Key outcomes of the research work are discussed in the conclusion.

Papers that highlight the main work of the author to fulfil the objectives are presented in part II. It comprises of the following six papers, as the main author.

Paper 1	Numerical study of sediment erosion in guide vanes of a high head Francis turbine
Paper 2	Investigation of sediment erosion phenomenon for different blade angle distribution in Francis runner
Paper 3	Leakage vortex progression through a Guide-vane's clearance gap and the resulting pressure fluctuation in Francis turbine
Paper 4	Development of simplified model for prediction of sediment induced erosion in Francis turbine's sidewall gaps
Paper 5	Application of hydro-abrasive erosion model from IEC 62364:2019 standard in Francis turbines
Paper 6	Experimental investigation on hydro-abrasive erosion due to geometrical positioning of Francis turbine's rotary-stationary components

Part III includes the additional papers produced in collaboration with Turbine Testing Lab, Kathmandu University, Nepal during this research work. Abstracts and relevance of the paper with this thesis are presented. It includes two papers as listed below.

Paper A	Sediment erosion in low specific speed Francis turbines: A case study on effects and causes
Paper B	Correlating sediment erosion in rotary-stationary gaps of Francis turbines with complex flow patterns

Part I

Summary

Chapter 1

Introduction

■ The chapter introduces the work conducted for this thesis and sheds some light on status and current research, objectives, and research contributions.

1.1 Background of study

Hydropower is a reliable and versatile source of clean energy production across the globe. The global development of hydropower is an important step towards a low-carbon society for the future. Hydropower sector generated a record 4,370 terawatt hours (TWh) of electricity in 2020 with a regional production of 2,141 TWh in Asia and Pacific and 690 TWh in South America alone [1]. Even though with such huge prospects and growth of hydropower sector globally, power plants located in these regions such as the Himalayas in Asia, the Andes in South America, and Pacific coast are mostly prone to hydro- abrasive erosion problems which has been a major challenge [2]. Sedimentation have proven to be technically, economically, and socio-ecologically challenging such as reduction of reservoir lifetime, wear and tear of hydromechanical components or impacts on downstream ecosystems etc. In order to address these challenges, it is essential to develop cost-effective methods for sediment handling.

Francis turbines which combine radial inflow and axial outflow concept are one of the most widely used reaction turbines. With higher efficiency and wide range of application, these turbines have history dated back to 1848 when James B. Francis proposed the design [3]. Water from the penstock enters the spiral casing, which transforms the hydraulic energy of water to mechanical energy. In between the runner and the spiral casing, two sets of vanes are distributed in circular rings. The first set of vanes are called stay vanes, which transfers water to guide vanes and provides structural support to spiral casing. Guide vanes are accompanied with shaft on both sides which change the opening angle for the flow regulation to runner. Runner blades are covered with upper crown plate (hub) and lower runner band (shroud), which rotate together with the blades. A gap is maintained between rotating runner and stationary covers for rotation. Labyrinth seals are fitted in hub and shroud to prevent

the leakage of the water from these gaps. With so many hydromechanical components associated, they are prone to erosion when operated in sediment laden river.

1.2 Status and current research

Scientific research on abrasive wear due to sand particles can be dated back to 1873 [4] and earlier. However intensive and most recognizable study on abrasive wear on hydraulic machinery in general was conducted by Truscott which got published in 1972 [5]. It tries to summarize several types of wear and factors associated with them. After that, many researchers have worked on sediment erosion problems and its effects on hydraulic turbines. Brekke [6] investigated the effects of sediment erosion in hydraulic turbines with the consideration of several hydropower plants as his case studies. Basic design criteria for hydro turbines operating in sediment-laden flows was proposed, and operation and maintenance strategies for the turbines operating in sediment-laden flows were also formulated during his research works.

An in-depth study of the erosion mechanism in hydraulic machineries has been done by Thapa [7]. In addition, he conducted experimental work with a high velocity jet on different materials and coating types, along with the study of particle separation in swirl flow. Neopane [8] implemented numerical models to estimate sediment erosion on Francis turbine components during his PhD study. Eltvik [9] performed parametric study on hydraulic design of Francis turbine and contributed on methods and numerical studies of optimized hydraulic design of Francis turbines for sediment handling. Gjosater [10] and Thapa [11] developed in-house design tool during their graduate studies which contributed to the optimized design of sediment laden Francis turbines. Poudel [12] conducted the computational and experimental study of effects of sediment shape on erosion of hydraulic turbines. Experimental studies have also been done to analyze the effects of different combinations of shape and size of hard particles on turbine material. It was observed that the particles with the irregular shape of smaller size induce higher erosion rates than that of the larger size with the same shape. Shrestha [13] made comparison for different shapes of runner blades and proposed the best suited one for sediment laden water. He also performed multi-disciplinary optimization on the selected design to conform structural integrity. Rajkarnikar [14] developed a rotating disc apparatus for testing erosion in Francis runner blade. He validated the optimized design of the runner blade with experimental investigations under different sediment loads. Thapa [15] developed an experimental setup for investigation of five different sized clearance gaps (CG) with symmetrical guide vane profile. Flow measurement done through particle image velocimetry (PIV) showed 2 mm CG having the highest effect on flow velocities and hence declared as critical size from his studies. Chitrakar [16] continued the research works on leakage flow through the CG of guide vanes of Francis turbines with both numerical and experimental techniques. His studies gave an indication of the flow behavior through the clearance gap of GV for different GV profiles. Hence past studies have shown that erosion in Francis turbines due to sediment particles is a function of many parameters such as particle velocity, impingement angle, type of mineral, size, shape, operating conditions etc.

1.3 Objectives

The major objective of this work is to understand the sediment erosion phenomenon in Francis turbines with the focus on the flow pattern around the gap between GV blade width and runner blade height.

Following are the specific objectives of this work:

1) Analysis of spatial temporal progression of leakage vortex through GV's clearance gap.
2) Investigate the flow pattern inside top and bottom sidewall gap in Francis turbine.
3) Investigate the effects of hydro-abrasive erosion due to geometrical positioning of Francis turbine's rotor- stator components.

1.4 Research Contributions

Papers presented in Part II of the thesis have general contribution which can be summarized as follow.

- A systematic investigation is provided on LV evolution and its progression from clearance gap to runner inlet. Moreover, analysis of vortex dynamics and pressure fluctuations helped to understand the complex phenomenon of LV. This is a contribution in accordance with first objective.

- An experimental set up with test specimens corresponding to rotary- stationary gap of Francis turbine is devised during this research work to understand the flow phenomenon in that region, which is in line with second objective.

- This study extends general erosion model predicted by previous studies with the consideration of width and height difference between rotary-stationary components. This is a contribution in accordance with third objective.

Chapter 2

Theoretical background

■ This chapter introduces the sediment erosion prone regions in Francis turbine, erosion models applicable for hydraulic turbines and methods used for the validation of numerical setup. More details are found in the papers from Part II.

2.1 Sediment erosion in Francis turbine components

Regions highly affected due to secondary flows and sediment erosion in the Francis turbine are discussed in this section. Brekke described the erosion damages in the stay vanes due to the secondary flow from the spiral casing and the presence of corner vortices [17]. In Francis turbines, other critical sediment erosion regions were suggested to guide vanes and runners. Figure 1 shows different locations of guide vane clearance gaps where secondary flow and sediment erosion occur. As suggested by literature [18 and 19], sediment contained flow affects the geometry of the guide vane and the clearance gap regions. This change in the geometry further increases the flow irregularities, also increasing the sediment erosion problem. Thus, the simultaneous effect of sediment erosion and leakage flow occurs in these regions.

Figure 1. Erosion due to secondary flows at the clearance gap of GVs (a) Towards bottom facing plate and (b) Towards upper facing plate & (c) Eroded GV towards the bottom end [Taken from *Paper B*].

In figure 2, erosion locations at different sections of the inlet of the reference runner are shown. Earlier research on the secondary flow from guide vanes suggested that

erosion in these regions was due to high-intensity leakage vortices travelling from guide vane clearance gaps [20]. However, towards the circumference of the band and crown side of the runner, the effect of erosion is present. At these locations, the leakage vortex does not hit at all. These oblique erosion locations at the runner inlet are due to the combined effect of leakage flow from guide vane clearance gaps (at the leading edge of the runner blade) and sidewall gaps (throughout the circumferential location). Sidewall gaps here refers to the minimum clearance region between the stationary and rotating component of the turbine. Based on the previous literature, erosion at sections 1-2 near the leading-edge geometry of the runner is due to high-intensity vortex flow from clearance gaps. Earlier studies [21,19 and 6] suggested that pressure oscillations are higher due to vortical flow at these locations. Thus, erosion due to the impact of high-intensity leakage vortex from guide vane clearance gaps is higher than the leakage from sidewall clearance gaps. This occurs towards the inlet of each runner blade, where the effect of Rotor-stator-interaction (RSI) dominates. However, based on the studies by [22-26], the leakage flow from sidewall clearance gaps cannot be neglected.

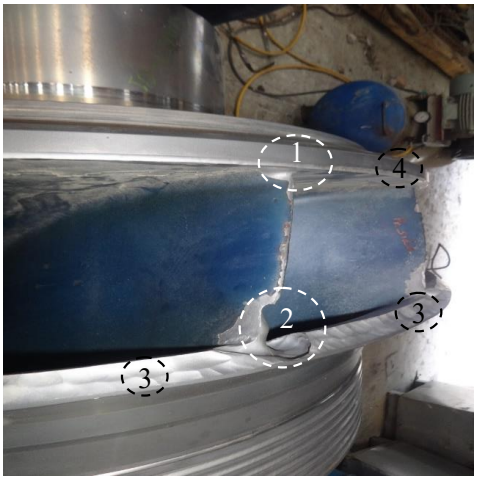

Figure 2. Erosion at different locations of runner inlet; Locations 1-2 refer to the region affected by the leakage flow from GV's clearance gap, and locations 3-4 are regions affected due to leakage flow from sidewall gaps.

When the flow leaving guide vanes enters the rotating domain, a small portion of the total flow escapes from top and bottom sidewall gaps. At design condition, Brekke [6] suggested that there would be a leakage of 0.5% of the total flow from these gaps. Trivedi et al. [27-29] used 1.65% of total inlet flow during the No-Load Speed (NLS) condition while investigating the leakage flow in the labyrinth seals. Schiffer et al. [23 and 30] reported that the hydraulic efficiency reduction due to leakage flow from this region is approximately 1% of the total efficiency. Since the study by Schiffer et al. was for clean water assumption, efficiency reduction can be predicted to be higher with sediment contained flow. Likewise, the flow leaving from sidewall gaps is

affected by the rotational speed of the runner. Hence, continuous abrasion and erosion due to sediment particles will severely affect those locations.

This flow escaping from the sidewall gaps enters the labyrinths of the turbine. Discharge from the bottom clearance gap enters the bottom labyrinth seals. The annular region of the fluid flow lies between two distinct areas: one domain rotating with the runner angular speed at a lower radius from the runner axis of rotation and the other stationary region at a higher radius. Moreover, since the runner is considered the most critical component of the Francis turbine, the rotating labyrinth's material is different from the stationary labyrinth. Therefore, erosion is higher towards the fixed end of the bottom labyrinth, which could be due to: (i) differences in the geometrical positions and (ii) variation in the materials used. Figure 3 depicts the erosion regions due to sediment flow towards the bottom labyrinth's rotary and stationary ends that validate the hypothesis as explained above.

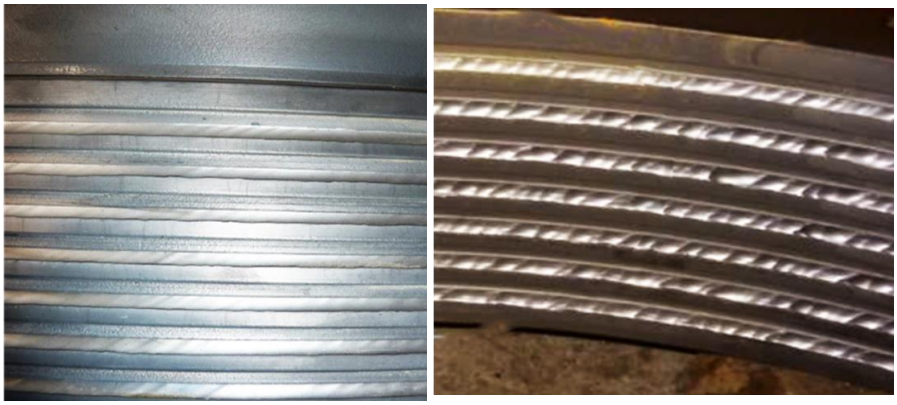

(a) (b)

Figure 3. Erosion at bottom labyrinths (a) Towards the rotating side and (b) Towards the stationary side [Taken from *Paper 3*].

Similarly, the flow escaping from the upper sidewall gaps reaches the upper labyrinth seals. In some cases, discharge from the upper labyrinth seal is lost in the total volumetric flow since it is released ultimately. Some manufacturers guide the water from the upper labyrinth through the runner's centre and into the draft tube. Towards the upper labyrinth regions, erosion effects towards the corner of the stationary domain are dominant, as shown in figure 4. Towards the rotating end, the eroded area is negligible. The erosion regions can also be seen at the circumferential positions of the holes for bolts. This is due to the presence of accelerated flow around the circular area of the bolts.

(a) (b)

Figure 4. Erosion at upper labyrinths (a) Towards the rotating side and (b) Towards the stationary side [Taken from *Paper 3*].

2.2 Flow related phenomenon in sidewall gaps

A review in flow inside sidewall gaps of hydraulic pumps and turbines done by Lucie et. al [22] points out three main phenomena in that region which are listed as.

1. *Disk friction losses*

Losses generated on a hub and shroud of an impeller; these types of losses are caused by shear stress arising on the surfaces. They are more pronounced in low specific speed turbines, which is also strongly influenced by operating conditions. The losses rise quite significantly in off- design conditions, especially at PL during which the flow rate is low and rotational speed is high [31]. It can increase rapidly with the inclusion of sediment particles in the flow.

2. *Hydraulic Axial thrust*

Axial thrust arises due to unbalanced forces acting on the rotor in the axial direction, which is strongly influenced by flow in sidewall gaps. With the increased capacity per turbine unit in these modern days, enormous axial loading can lead to bearing failure causing axial movement of rotor and subsequent damage of whole turbine.

3. *Rotordynamics*

Undesired flow in the sidewall gaps can be a source of eccentric displacement of the rotor. With a rising demand for efficiency and performance, higher speeds machines are increasing, which brings a need for proper prediction of their dynamic behaviors. Imbalance has a great impact on operating stability from a dynamics point of view. Moreover, it is also a cause of vibrations and noise, which obviously affect service life of the machine.

2.3 Erosion models applicable for hydro turbines

In turbines operating in sediment laden water, there are several factors that affects the turbine components. These factors can be categorized based on sediment properties or flow properties. The sediment properties refer to the geometrical shape, size,

distribution, concentration, hardness, etc. of the quartz contained in the sediment [6]. Similarly, the fluid properties refer to fluid velocity that is directly related to the particle velocity [6].

2.3.1 IEC 62634:2019 abrasion rate model

IEC 62364:2019 [32] aims to develop guidelines for methods of minimizing hydro-abrasive erosion in hydro turbines based on experience data. With the consideration of different critical parameters, a model for hydro-abrasive erosion depth in a Francis turbine is proposed by IEC 62364: 2019, as shown in equation 1.

$$S = W^{3.4} \text{ x } PL \text{ x } K_m \text{ x } K_f / RS^p \quad (1)$$

where, S is the numerical value of hydro-abrasive erosion depth in mm.

Characteristic velocity W is unique for each machine component and is used to quantify hydro-abrasive erosion damage. Similarly, PL variable is introduced in the equation to find a simple and reasonably accurate estimate of the time integral. It is used to quantify the particles that pass through the turbine which is related to the hydro-abrasive erosion potential in a certain period. PL integrates particle concentration I, hardness factor ($K_{hardness}$), size factor (K_{size}) and shape factor (K_{shape}) over time.

$$PL = \int_0^T C(t) \text{ x } K_{size}(t) \text{x } K_{shape}(t) \;\; K_{hardness}\,(t) dt \quad (2)$$

$$\approx \sum_{n=1}^{N} C_n \text{ x } K_{size,n} \text{ x } K_{shape,n} \text{ x } K_{hardness,n} \text{ x } T_{s,n} \quad (3)$$

The details of the terms used in above equations are presented in Table 1.

Table 1. Terms, definitions and symbols used in IEC 62364 standard [32].

Symbol	Term	Nomenclature/Definition	Unit
C	Particle concentration	Mass of all solid particles per volume of water-particle mixture	kg/m^3
K_f	Flow coefficient	Coefficient characterizing abrasion with flow around each component	[-]
$K_{hardness}$	Hardness factor	Factor relating abrasion with the hardness of abrasive particles	[-]
K_m	Material factor	Factor relating abrasion with material properties of the base material	[-]
K_{shape}	Shape factor	Factor characterizing abrasion with shape of the base material	[-]
K_{size}	Size factor	Factor characterizing abrasion with size of the base material	[-]
PL	Particle load	Integral of modified particle concentration over time	kg h/m^3
RS	Turbine reference size	For Francis turbine, it is the reference diameter	m
P	Size exponent	Exponent that describes size dependant effects of hydro- abrasive erosion while evaluating RS	[-]
S	Hydro-abrasive erosion depth	Depth of material removed (measured perpendicular to the original surface) component due to hydro-abrasive erosion	mm

T_s	Sampling interval	Time interval between two samples for determination of abrasive particles in the water	h
W	Characteristic velocity	Relative velocity between the abrasive particles and turbine parts	m/s

2.3.2 Finnie Erosion Model

In Finnie model, particles tend to slide on the base metal when it hits at a lower impact angle and leaves away the erosion damage, which are commonly observed in hydraulic machine exposed to sediments [33]. At the higher angle of attack of sediment particles, horizontal velocity of particles nearly tends to zero, creating pits on the surface. Erosion in case of Finnie model is found vary with impact angle and velocity as;

$$E = kV_p^2 f(\gamma) \tag{4}$$

where, E= dimensionless mass

V_p = particle impact velocity

$f(\gamma)$ = dimensionless function of the impingement angle

$$f(\gamma) = 1/3\, cos^2\, \gamma \; if \; tan\, \gamma > 1/3$$

$$f(\gamma) = sin(\, 2\gamma) - 3\, sin^2\, \gamma \; if \; tan\, \gamma \leq 1/3$$

2.3.3 Tabakoff Erosion Model

Tabakoff erosion model introduces the combination of higher and lower angle of attack of sediment particles on the surface. It can capture a realistic scenario of sediment erosion in hydraulic machines because it considers more parameters and combines all angles of attack of sediment particles [34]. Tabakoff erosion model determines erosion rate *E* from the following relations:

$$E = f(\gamma)(V_p/V_1)^2\, cos^2\, \gamma\, [1 - R_T^2] + f(V_{PN}) \tag{5}$$

where, $f(\gamma) = [1 + k_2 k_{12}\, sin(\gamma \frac{\pi/2}{\gamma_0})]^2$

$$R_T = 1 - V_p/V_3\, sin\, \gamma$$

$$f(V_{PN}) = (V_p/V_2\, sin\, \gamma)^4$$

$$k_2 = \begin{Bmatrix} 1.0\; if \gamma \leq 2\gamma_0 \\ 0.0\; if\; \gamma > 2\gamma_0 \end{Bmatrix}$$

Erosion of a wall due to a particle is computed from the following relation:

$$Erosion\ Rate = E \times N \times m_p \tag{6}$$

where, m_p is the mass of the particle and N is its number rate. The overall erosion of the wall is then the sum over all particles. This gives an erosion rate in [kg s^{-1}], and

erosion rate density in [kg s^{-1} m^{-2}] to indicate the erosion area visually on the wall surface.

2.4 Validation and verification of numerical model

2.4.1 Grid independence study

A grid independence test was conducted using the Grid Convergence Index (GCI) technique to estimate discretization error [35]. In this technique, three generated meshes with varying number of discretized elements is tested. For this study, the number of elements at each edge in a 3-D surrounding geometry block is increased by two times while generating successive finer grids. Therefore, three different meshes were created as G1, G2, and G3 suffix 1, 2 and 3 represents fine mesh respectively. The overall increment was such that the mesh refinement factor 'r >1.3'. This technique uses the approximate and extrapolated error values to calculate the final grid sensitivity in terms of GCI. Discretization error for the numerical was determined as follows:

(i) The average length of each element for a 3-D mesh was determined as,

$$h = \left[\frac{1}{N}\sum_{i=1}^{N}(\Delta V_i)\right]^{\frac{1}{3}} \tag{7}$$

(ii) Let $h_1 < h_2 < h_3$ and $r_{21} = h_2/h_1, r_{32} = h_3/h_2$, the apparent order was solved as in equations 7, 8 and 9 using the fixed-point iteration method,

$$p = \frac{1}{ln(r_{21})}|ln|\varepsilon_{32}/\varepsilon_{21}| + q(p)| \tag{8}$$

$$q(p) = ln\left(\frac{r_{21}^{p} - s}{r_{32}^{p} - s}\right) \tag{9}$$

$$s = 1.sign(\varepsilon_{32}/\varepsilon_{21}) \tag{10}$$

(iii) The extrapolated values were calculated as,

$$G_{ext}^{21} = \frac{r_{21}^{p}G_1 - G_2}{r_{21}^{p} - 1} \tag{11}$$

(iv) Approximate and extrapolated relative error was calculated as,

$$e_a^{21} = \left|\frac{G_1 - G_2}{G_1}\right| \tag{12}$$

$$e_{ext}^{21} = \left|\frac{G_{ext}^{21} - G_2}{G_{ext}^{21}}\right| \tag{13}$$

$$GCI_{fine}^{21} = \frac{1.25e_a^{21}}{r_{21}^{p} - 1}$$

(14)

2.4.2 Experimental validation

Steady-state simulations were conducted at design and off-design conditions in the initial stage. Another set of simulations was carried out with the total pressure as the inlet boundary condition. The mass flow rate was calculated in a postprocessing step. Flow rate data available for the prototype turbine at different operating points [36] were compared with the results from the simulation as shown in figure 5.

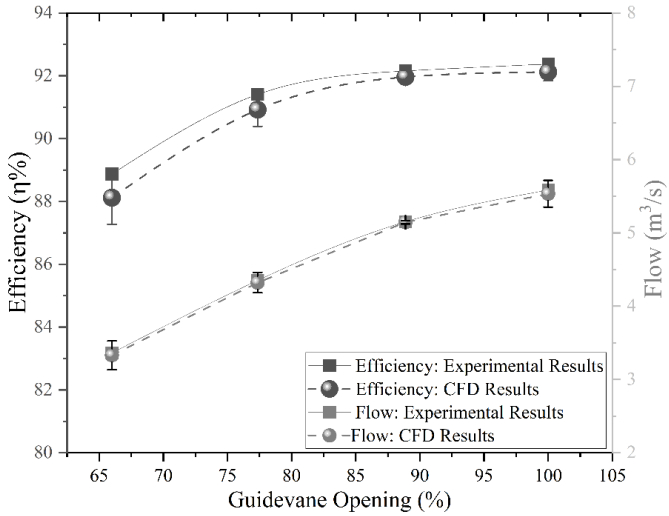

Figure 5. Prototype discharge and efficiency comparison with the simulated results for various operating condition. [Taken from *Paper 3*]

It can be inferred from this figure that at the same guide vane opening angles, the resultant flow obtained from the CFD analysis closely matches the field data. Moreover, the efficiency comparison from the CFD calculation shows lower efficiency than the prototype measurement, which could be due to the overprediction of losses by the turbine with the use of the turbulence model. It can be noticed at a deep part load condition that the efficiency variation is higher than the design point. In off-design conditions, the losses predicted by the numerical model are higher. Figure 5 also shows the error bar which was constructed with the difference of numerical and experimental value for each GV opening angle.

Furthermore, validation of numerical model was also carried out by measuring the pressure around the middle GVs in three-GV cascade rigs developed by Chitrakar et al. [37]. The arrangement has a trapezoidal slot with holes with a diameter of 2 mm around the middle GV with a 2-mm offset from the GV surface. Piezoresistive pressure transducers were connected to these holes, which were used to determine GV loading. Figure 6 shows the experimental test section of the 3-GV cascade rig that consists of a pressure measurement location at the middle GV (GV2). A pressure transducer was calibrated with a dead weight calibrator with an uncertainty of ±0.2%.

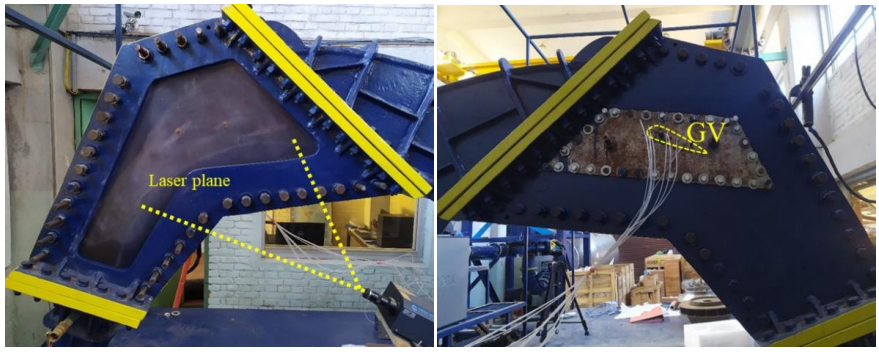

(a) (b)

Figure 6. The three-GV test setup for experimental validation: (**a**) Experimental set up which shows the test section in the lab ; (**b**) Locations of holes for tapping the value of pressure at GV [Taken from *Paper 3*].

Normalized pressure (C_p) calculated with CFD analysis, was validated with the data obtained from the pressure transducer measurement around the circumferential positions from the leading edge (LE) to the trailing edge (TE). Local pressure measurement at each measurement location was normalized by the pressure value at the LE of GV. Thus, the blade loading characterizing the flow around the GV was observed experimentally with a maximum normalized pressure where $C_p = 1$ at the leading edge [16]. It was observed that using the current numerical model, the maximum error in pressure measurement was 8.8% towards the LE in the pressure side of the GV. This might be due to the influence of GV1 and inappropriate stagnation as compared to the numerical solution. At all other locations of pressure measurement, the errors in the pressure measurement were less than 5%. Figure 7b shows the blade loading distribution of the reference GV profile.

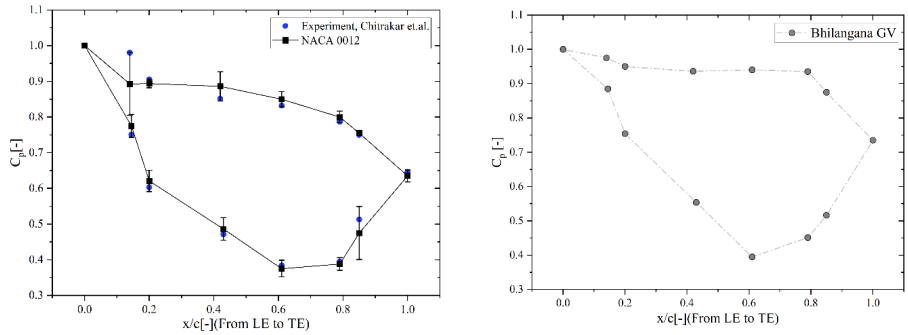

(a) (b)

Figure 7. Validation of the CFD results with the experiment: (**a**) Velocity normal to camber line from LE to TE and pressure distribution in GV for NACA 0012 hydrofoil; (**b**) reference case GV profile [Taken from *Paper 3*].

Chapter 3

Summary of main publications

■ In this chapter, main papers presented in Part II are summarized. It attempts to develop the scenario and background of the PhD project and methodology in the research work.

Paper 1- Numerical study of sediment erosion in guide vanes of a high head Francis turbine

N. Acharya, C. Trivedi, N. M. Wahl, S. Gautam, S. Chitrakar, and O. G. Dahlhaug Published in Journal of Physics: Conference Series 2019

Building the framework for this PhD project, the paper presents the research on flow and erosion pattern around guide vanes of the high head Francis turbine. As a part of HydroCen project, Bhilangana- III hydroelectric plant in India was identified and collaborated for the reference study. The paper investigates the erosion pattern, erosion rate density and nature of vortices originating from the leakage flow on existing guide vanes. It aims to understand the nature of significant leakage flow passing from pressure side to suction side of guide vanes along with sediment particles which disturbs the main flow. The paper focuses on sediment erosion analysis giving indication of relative erosion intensity and critical zones of erosion damage of turbine components. Erosion was observed mostly in regions downstream of the mid-chord position inside clearance gap due to local separation and vortex. Secondary flow erosion might have been caused by horse-shoe vortices which can be seen on facing plates along the guide vane contours. Clearance gaps sizes varies from 0.5 mm, 1 mm to 1.5 mm for the numerical study. It shows that strong vortices are generated from the guide vanes with clearance gap of 1.5 mm which might be accountable for the high erosion on runner blade inlet. At this point, earlier studies on sediment erosion in Francis turbines components were understood and research direction for this PhD thesis was identified.

Paper 2- Investigation of sediment erosion phenomenon for different blade angle distribution in Francis runner

N. Acharya, C. Trivedi, S. Gautam, and O. G. Dahlhaug Published in IOP Conference Series: Earth and Environmental Science 2021

This paper tries to investigate optimal runner design with a trade-off between performance and erosion behaviour. It presents comparative results of sediment erosion behaviour of five different types of shapes which were proposed for parametric study. It utilizes the design program which has been made to generate blade profiles corresponding to blade angle distribution as input parameter. It controls how much hydraulic energy is converted to the mechanical energy in each section of blade. Adjusting the blade angle distribution influences blade loading which will affect the blade shape as well. Energy distribution is the distribution of product of peripheral velocity, U and peripheral component of absolute velocity, C_u. As U is only dependent on the radius and angular velocity, which

is known for all points, C_u is strongly corelated to the blade angle distribution. Different blade angle distribution causes different transition from inlet to outlet velocity, which might explain the difference in erosion factors. Investigations are made on sediment erosion rate density for all blades normalized with erosion for reference case. Results show the highest erosion rate for reference blade followed by blade with linear blade angle distribution. In addition, results prove the co-relation between relative velocity and erosion i.e., the higher possibility of erosion with higher values of relative velocity at runner outlet.

Paper 3- Leakage vortex progression through a Guide-vane's clearance gap and the resulting pressure fluctuation in Francis turbine

N. Acharya, S. Gautam, S Chitrakar, C. Trivedi, and O. G. Dahlhaug Published in Energies, 2021

The paper comprehends a systematic investigation across both space and time i.e., spatial temporal progression of leakage vortex (LV) through clearance gaps of guide vanes in a high head Francis turbine for three operating conditions. Important dynamic characteristics on leakage vortex evolution and progression are revealed. LV evolution and trajectory, LV progression from clearance gap to runner blades, vortex dynamics and pressure fluctuations are analyzed based on numerical simulations. LV pattern and trajectory are obtained from transient simulations. Results shows that vortex core intensity in leakage flow decreases along the progression. Progression of leakage flow at hub area is classified into 3 stages viz: elongation stage, disintegration stage and dissolving stage. Leakage flow at shroud area is transported all the way until mid-section of the blade before majority of vortex is dissolved and few seems to pass from outlet of runner as well. During pressure pulsations monitoring, frequency spectrum of pressure signals at vaneless space shows the highest amplitude at guide vane passing frequency (f_{gv}) and its successive harmonics; $2f_{gv,}$ $3f_{gv,}$ $4f_{gv}$ and so on due to rotor stator interaction. The paper shows that low frequencies of 0.32, 0.64 and 0.96 times the runner rotational frequency corresponds to rotating vortex rope frequency and its harmonics whereas higher frequencies of 200 Hz, 400 Hz and 600 Hz correspond to guide vane passing frequency and its harmonics. In addition, it is observed that the highest fluctuation of the torque is observed at part load condition followed by full load condition and lowest of all for BEP condition.

Paper 4- Development of simplified model for prediction of sediment induced erosion in Francis turbine's sidewall gaps

N. Acharya, S. Gautam, S. Chitrakar, and O. G. Dahlhaug Published in IOP Conference Series: Earth and Environmental Science 2022

The paper focusses on the investigation of flow pattern in sidewall gaps which refers to the clearance region between the stationary and rotary components. A simplified numerical model based on the concept of rotating disc apparatus (RDA) is conceptualized to make analogy with the gap available between runner blades and guide vanes (GVs). Fillet gaps were introduced in the model to emulate the gaps available between runner blade and GV for real case scenario. Four samples with 90° separation of each are mounted on the disc rotating at 750 rpm. Two different types of models i.e., equal, and unequal heights of the gap were investigated in this study. It was found that inside the gap of a model rotating at certain angular speed, the vortex develops from lower radius, accumulates to the higher radius and leaves with high intensity. This phenomenon can be observed for both cases having equal heights between the slot gaps and unequal height. However, in the case of the model having unequal heights another region of vortex development was also observed. It can be directly related to the

difference in guide vane outlet height and runner inlet height in case of Francis turbine. Results from experiment showed two different regions of erosion in the specimen. Region 1 is at the farthest end from the centre where all the vortices accumulate and has the distinct region of erosion due to flow re-circulation whereas in region 2, the scaled effect of erosion at an angle less than 90 degrees to the slot length is observed. The presence of gap induces the vortices that has severe effect due to sediment contained flow. The continuous interaction between the sediment particle and the surface of material gives rise to erosive and abrasive wear.

Paper 5- Application of hydro-abrasive erosion model from IEC 62364:2019 standard in Francis turbines

N. Acharya, S. Gautam, S Chitrakar, C. Trivedi, and O. G. Dahlhaug IOP Conference Series: Published in Earth and Environmental Science 2022

This paper outlines the terms used in the theoretical model of abrasion rate for Francis turbine proposed by IEC 62364:2019 guideline. Abrasion depth for the different turbine components of reference hydropower plant was calculated. Theoretical expected erosion depth for runner inlet, runner outlet, guide vanes facing plates and labyrinth seals was calculated with the estimation of characteristic velocities of runner and guide vanes. Particle load was calculated based upon the sampling data available from the site. Measurements of abrasion depth in various components were conducted in the site during shut down. Discrepancies in depth value for the same components were calculated and presented in the results. Abrasion depth for guide vanes and runner outlet was slightly under-predicted by calculation. The discrepancy for this might be pressure difference between two sides of guide vane which varies with flow. For the runner outlet region, it can be explained with part load (PL) condition. At PL there are two phenomenon which influence hydro abrasive erosion. First one is that the average velocity will decrease with low discharge. Another one is that flow distribution will lose uniformity increasing degree of turbulence. These two phenomena will influence hydro abrasion in opposite way but considering turbulence factor will be dominant, erosion will increase. For other components like facing plates, runner inlet and labyrinth seal, there is slight difference in two values. Although abrasion depth formula gives a reasonable accuracy in case of Francis turbine but still it is challenging to obtain complete and exact observations. An optimized solution can thus be devised based on the evaluation of hydro-abrasive erosion along with energy production and maintenance expenses.

Paper 6- Experimental investigation on hydro-abrasive erosion due to geometrical positioning of Francis turbine's rotary-stationary components

N. Acharya, S. Gautam, S Chitrakar, and O. G. Dahlhaug – SUBMITTED FOR PUBLICATION

This paper focusses on the erosion pattern at clearance region between the stationary (guide vanes) and rotary components (runner blades) mentioned as sidewall gap. For hydro turbines operating in sediment laden water, sediment will pass through these gaps and erode the parent material. Due to continuous effects of abrasion and erosion, these side wall clearance region increases and consequently the leakages through these gaps. A simplified model is conceptualized to make analogy with the sidewall gap and experimental works were carried out in rotating disc apparatus (RDA) with four specimens mounted at 90° separation on the disc in one run. Sediment size of 150-250 μm diameter with particle mass flow rate based on the maximum amount of sediment passing through the

reference turbine was used. Slotted specimens with different sizes width and height were used for the experiments. Results show that the slot width is positively correlated with the rotational speed and erosion loss. Similarly trend of erosion with different height difference is compared at different rotational speeds and time. It was observed that for both rotational speed factor and time factor, erosion rate increases with the increase in slot height. This study aims to extend the existing erosion model with consideration of width and height difference between rotor-stator component.

Chapter 4

General discussions

■ This chapter presents a general discussion on the results and topic.

4.1 Research Gap

This research work is intended on the investigation of flow pattern in sidewall gaps in Francis turbines. It refers to the clearance region between the stationary and rotary components as highlighted with brown squares in figure 8. For hydro turbines operating in sediment laden water, sediment will pass through these gaps and erode the parent material. Due to continuous effects of abrasion and erosion, these side wall clearance region increases and consequently the leakages through these gaps. Although research has been done on clearance region between guide vanes and cover plates, this sidewall gaps has still been unexplored. Experimental test set up is designed to study the flow behavior in those regions.

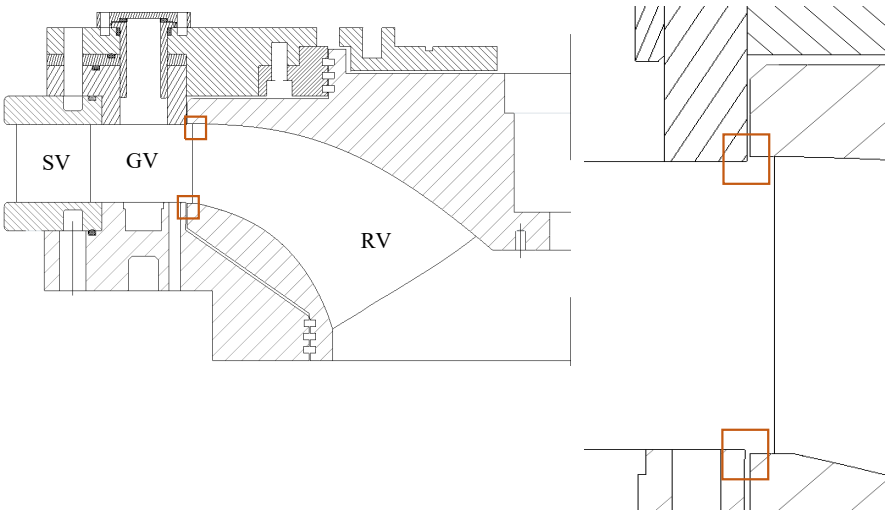

Figure 8. Cross section of Francis turbine with the enlarged view of sidewall gap [Taken from *Paper 6*].

Building the framework for this research work, initial studies on flow and erosion pattern around guide vanes of the high head Francis turbine for the reference power plant was conducted which is discussed in *Paper 1* in detail. It was followed by the numerical simulation of runner and the results from CFD compared with the actual erosion in turbines. It is found that the leakage flow through clearance gaps of guide vanes is the primary cause of erosion at the inlet of the runner blades. A systematic investigation was then conducted across both space and time i.e., spatial temporal progression of leakage vortex (LV) for varying condition operating conditions, i.e., BEP, part load and full load. As presented in *Paper 3*, the progression of LV at hub area is classified into three stages namely elongation stage, disintegration stage and dissolving stage. Results shows few LV at the shroud area passing through outlet of the runner whereas majority of it dissolving before reaching the mid-stream of the blade. Frequency spectrum of pressure oscillations in the vaneless space, in the runner blade and inside the draft tube are also analyzed to observe the peak pressure pulsation and its harmonics. Unsteady fluctuations of runner output torque are also studied to identify the pattern and magnitude of torque oscillations.

4.2 Special purpose rig: Rotating Disc Apparatus

In a special purpose rig such as Rotating Disc Apparatus (RDA), an arm or disc that is turned by a high-speed motor is part of the rotating disc/arm type of sediment testing equipment. The test specimens are fixed to a revolving disc or arm that is immersed in a fluid-erodent mixture (generally water). One of these test rigs is the rotating disc apparatus (RDA) utilized by Thapa et al [38] to investigate the synergistic effect of erosion and cavitation in turbine materials. This also applies to Clark's [39] usage of the slurry pot tester. The test specimens are mounted on the edge of a rotor in the centrifugal accelerator type of testing facility, and sand slurry is delivered into the rotor's center. In RDA, sand particles accelerate radially because of centrifugal force when the rotor rotates at a high speed and collide with the test specimen's surface. One of these testers is the Coriolis slurry erosion tester designed for improved slurry dynamics [40].

4.3 Experimental measurements

Experiments for this research work were conducted in RDA. It utilizes the method of rotating test specimen in a mixture of calculated amount of sand and water. Figure 9 shows CAD model of setup with base plate and specimen used during experiments. Test specimens are mounted on the disc with the help of counter sunk screw. Rotor assembly comprises of rotating disc with test specimens mounted that are attached to the shaft connected to the motor. Rotational speed of motor is adjusted by Variable Frequency Drive (VFD) connected to the setup. Housing of RDA consists of two chambers viz; inner chamber which is the cooling chamber and outer chamber which encloses the base plate with specimens and sand-water mixture.

Sediment particles were collected from the Jhimruk hydropower plant, Nepal for the analysis of mineral content in the sample. Sieve analysis was done to characterize sediment size progressively from coarse to fine. Six layered sieve analyzer was deployed which is vibrated to separate each sample by size in its respective sieve plate. From the sieve analysis, about 90% of the sediment sample size ranges from 90 μm – 300 μm. It consists of very fine sand particles in abundance which passes through the turbine. Sediment sample observed under the microscope showed the presence of quartz mineral in plentiful amount along with other elements such as feldspar and muscovite. Sediment sizes ranging from 150-250 μm were utilized to investigate the effect of sediment on the test specimen during this experiment. The concentration of sediment used for the experiment was 60 g/L of water. A higher concentration of sediment was used for the experiment to get the accelerated erosion wear in the runner blade specimen.

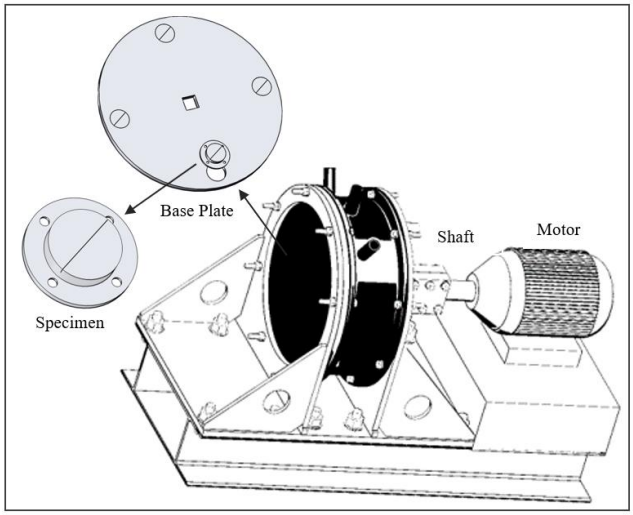

Figure 9. 3D representation of RDA along with base plate and test specimens [Taken from *Paper 5*].

Experimental set up consists of 4 test specimens fitted in 90-degree periodic positions inside the disc. Figure 10 shows two reference geometries without slot represented by RG1 and RG2 and two test geometries TG1 and TG2. Two similar reference geometries were mounted each time for checking the uniformity of erosion pattern for each observation. Similarly right-side sketches show types of geometries used as the test specimens. '*s*' and 'δ' in the sketch represent the slot width and height of the opposite ends of slot respectively. Details of the specimens sizes are explained in Paper 6. Aluminum was used as the specimens material to accelerate the erosion process.

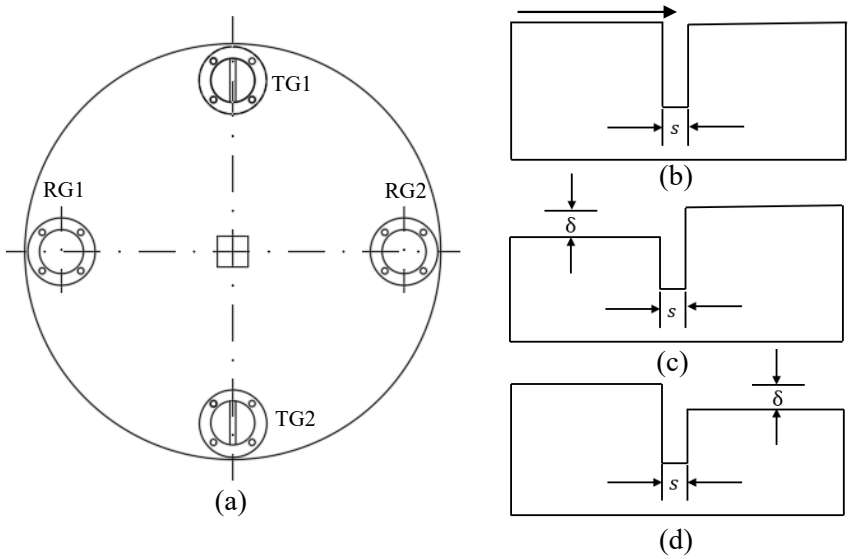

Figure 10. (Left)View of reference geometry (Right) Cases adopted [Taken from *Paper 6*].

A thermistor temperature sensor with a resolution of 0.1°C was installed in the set-up for monitoring temperature below 35°C. The test set-up consists of a control system with the provision for automatic shut-down of the system at high temperatures. When the temperature of the system reaches above 35°C, the system goes off automatically and the experiment needs to be repeated after cooling down. For the observation of the effects of erosion in varying rotational speed, motor was coupled with the Delta C200 VFD. Speed of the specimen with rotor-disc was varied from 800 to 1100 RPM. The measurement of the weight loss in the test specimen after each run was done in a precise weight measurement device with an accuracy of 0.001 gm. Brief procedures and description of parameters are listed in Table 2.

Table 2: Various parameters in test set-up

Parameters	**Value**	**Unit**
Disc diameter	300	mm
Rotation variations	800-1100	rpm
No. of specimens/ run	4	[-]
Specimens	2 reference and 2 test geometries	[-]
Concentration of sediment	60	g/L
Time of each run	60*	min
Temperature	<35	°C
Sediment size	150- 250	µm
Material of specimen	Aluminium	[-]

**Total 5 hours for single run: 60 min, 120 min, 180 min, 240 min and 300 min*

The major objective of this research work was to observe abrasion pattern and estimate the amount of hydro-abrasive erosion. After each test run, test specimens were dismantled from the disc, and washed thoroughly with clean water. Test specimens were then dried, and weights were recorded with device with accuracy 0.001 gm. Weight loss was then calculated after each run using relation as shown in equation 15.

$$m^*[-] = \frac{m_{t=0} - m_{t=t_n}}{m_{t=0}} * 100\ \% \tag{15}$$

where $m_{t=0}$ is the initial weight before run and $m_{t=\ tn}$ is the weight after one run.

Experiments were carried out RDA on simplified test specimens to make analogy with the sidewall gap. Slotted test specimens with different sizes width and height were used during the experiments. Results show that the slot width is positively correlated with the rotational speed and erosion loss. Bar chart as shown in figure 11 gives the clear indication of slight increase of weight loss from 800 rpm to 1100 rpm for 2.5 mm slot width whereas it incresaes significantly for 3.5 mm slot width.

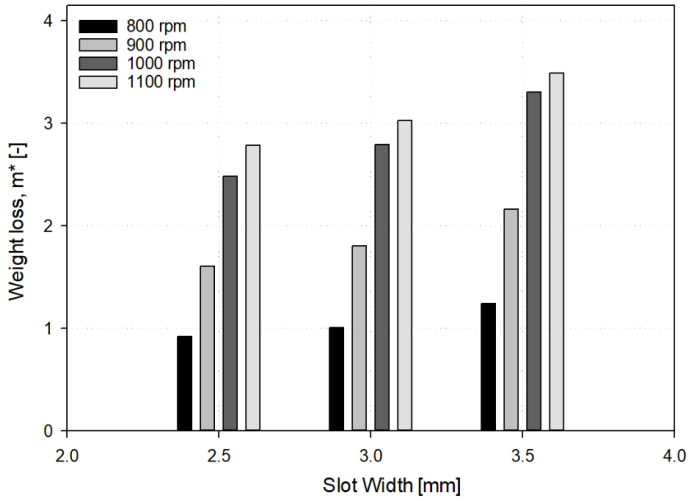

Figure 11. Effect of slot width at varying rpm

Similarly trend of erosion with different height difference is compared at different rotational speeds and time. Negative height difference as seen to the left of the dotted line in figure 12 shows lesser impact of erosion. At lowest rotational speeds, the material loss in nearly constant. However, at higher rotational speed the erosion rate increases linearly up to zero height difference. At the positive height difference, the erosion rate increases significantly, highest for highest rotational speed.

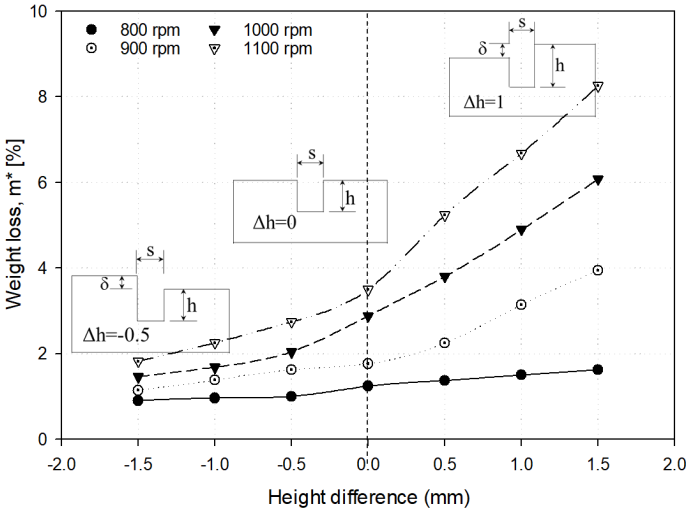

Figure 12. Effect of slot height at varying rpm [Taken from *Paper 6*].

4.4 Theoretical Implications

A small portion of its flow escapes from the sidewall gaps when high-velocity fluid leaves the GV. The fluid flow in the sidewall gaps can be investigated as a flow in the annular gap between two concentric cylinders. One cylinder rotates at a certain angular speed, and the other is fixed.

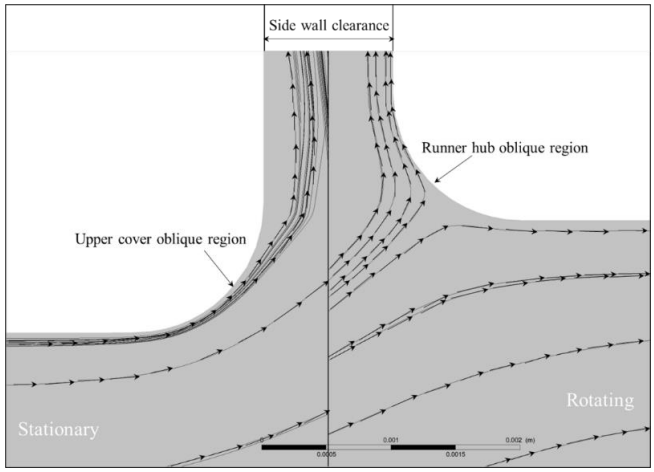

Figure 12. Fluid flow between sidewall clearance gaps between rotary and stationary body [Taken from *Paper B*].

A clearance region is made between these two components through which a portion of the fluid escapes. The escaping fluid moves towards labyrinths interacting with the near-wall surfaces. The fluid velocity in these regions will be sufficiently higher than those in oblique fillet regions. Likewise, the angular speed of the runner also has a significant effect on the velocity of the escaping fluid. Therefore, towards the rotating end, the impact of high-velocity fluid can be observed while the fluid velocity is comparatively small towards the stationary end. This leakage flow reduces the overall efficiency of the turbine.

Even though magnitude of sidewall gaps and volume of fluid involved in this region is very small as compared to the size of turbine itself, nature of flow there can have huge impact on the machine in general. From the past studies on erosion prediction in the hydro-turbines, the geometrical parameters of the turbine are not considered for erosion prediction. In this study the general erosion model predicted by previous studies is extended apart from properties of particles and base materials. It includes the width and height difference between rotary-stationary components as well and can be expressed in simple form as:

$$E_r \approx f(V^n \times K_{time} \times K_{material} \times K_{size} \times K_{shape} \times K_{concentration} \times K_{width} \times K_{height})$$

Chapter 5

Conclusion and further work

■ This chapter discusses about the research results and final conclusions of the work. It also lists few suggestions for further work on the topic.

As a large part of untapped global hydropower potential falls in areas with high sediment yields, erosion issue will be prominent one in the days to come. Since each hydropower plant is a tailored project, a trade-off is essential among several factors for the contribution to energy and cost-efficient usage. In the presented work, experimental investigations of erosion pattern have been carried out in a simplified test set up which aims to replicate the gap between GV blade width and runner inlet height which was unexplored yet.

Erosion trend in the reference test specimen shows that at lesser time the erosion wear is low regardless of the rotational speeds, but it increases gradually when the time of operation increases. At individual rotational speeds, the erosion wear increases significantly, highest for highest rotational speed. It can be justified with the assumptions that with higher time period, the gradual erosion of the turbine material changes the impact angle and hence accelerated erosion can be predicted for such case. This sharp increment in the erosion rate with respect to time indicates the scenario of hydro-turbines that are prominently affected when operated for longer time.

Test specimens with three varying slot widths 2.5 mm, 3.0 mm and 3.5 mm show the positive co-relation with the rotational speed and erosion loss. It is observed that vortex develops from lower radius, accumulates to the higher radius and leaves with high intensity inside the slot rotating at certain angular speed. Erosion loss between 2.5 mm slot and 3 mm slot is very low for the lowest rotational speeds compared to highest rotational speeds. However, as the rotational speed increases the shift of erosion wear is more towards the higher width slot. Similarly during initial time, erosion wear is nearly constant regardless of the slot width. As the time period increases, the particle interactions during the continous vortices formation inside the

slot gap erodes the parent material abruptly. This continous interaction causes the particle to impact the substrate material at maximum angle of attack after certain hours of operation.

Another test specimens set up include height difference between the two sides of slots keeping the width constant. The height was varied as 0.5 mm, 1.0 mm and 1.5 mm which corresponds to the positive height difference between GV blade width and runner inlet height. In this case, fluid flow from GVs hit the sidewall of rotor directly. Some fluid carrying particles re-circulate in the slot width and again imparts the opposite side walls. For next set of experiments, test specimen's height was varied as -0.5 mm, -1.0 mm and -1.5 mm which corresponds to the negative height difference between GV blade width and runner inlet height. In this case, the direct impingement of sediment particles to the opposite face does not happen but they strike back to the guide vane face during the flow re-circulation. Due to continuous impact the impingement angle increases and reaches maximum that causes maximum erosion in the rotor-stator sidewall gaps. Results show that erosion rate increases with the increase in slot height for both the rotational speed factor and time factor. Negative height difference shows lesser impact of erosion compared to positive one. The significant increment in the erosion rate is observed for positive height difference, at higher time period. This signifies the fact that installing the stator component with higher height compared to rotor inlet height is catastrophic for operation in sediment laden flow condition.

It is quite obvious that presence of sidewall gaps and flow in such regions is inevitable in hydraulic machineries. Hence the design process should ensure sidewall gaps flow as well for efficient machine design. Flow phenomenon associated with sidewall gaps should be well considered and analyze them during the preliminary phase of machine design.

Based on general discussions in Chapter 3, and the results presented in papers of Part II, following recommendations could be considered for any further work.

- Expand the experimental investigations on the slot shape which might include radius of edge factor .
- Study the erosion effects in labyrinth region and method to minimize it.

Bibliography

[1] IHA 2021, Hydropower Status Report: Sector trends and insights

[2] Winkler, K., 2014 Hydro-abrasive erosion: Problems and solutions, *IOP Conf. Series: Earth and Environmental Science,* 22 052022.

[3] J.B. Francis, "Lowell Hydraulic Experiments" *Little Brown, Boston* 1855.

[4] O. Reynolds, "On the action of a blast of sand in cutting hard materials," *Philos. Mag. (Fourth Ser.),* vol. 46, pp. 337-343, 1873.

[5] G. F. Truscott, "A literature survey on abrasive wear in hydraulic machinery," *Wear,*vol. 20, pp. 29-50, 1972.

[6] H. Brekke, "Design of hydraulic machinery working in sand laden water," in *Abrasive erosion and corrosion of hydraulic machinery*, C. G. Duan and V. Y. Karelin, Eds., ed London: Imperial college press, pp. 155-181, 2002.

[7] B. Thapa, "Sand erosion in hydraulic machinery", *PhD thesis*, Norwegian University of Science and Technology, Faculty of Engineering Science and Technology, 2004.

[8] H. P. Neopane, "Sediment erosion in hydro turbines", *PhD thesis*, Norwegian University of Science and Technology, Faculty of Engineering Science and Technology, 2010.

[9] M. Eltvik, "Sediment erosion in Francis turbines," *PhD thesis*, Norwegian University of Science and Technology, Faculty of Engineering Science and Technology, 2013.

[10] K. Gjosater, "Hydraulic Design of Francis Turbine Exposed to Sediment Erosion", *Masters Thesis*, Norwegian University of Science and Technology, 2011.

[11] B. S. Thapa, "Hydraulic design of Francis turbine to minimize sediment erosion", *Masters Thesis*, Kathmandu University, 2012.

[12] L. Poudel, B. Thapa, B. P. Shrestha, B. S. Thapa, K. P. Shrestha and N. K. Shrestha, "Computational and Experimental study of effects of sediment shape on erosion of hydraulic turbines," in 26th *IAHR Symopsium on Hydraulic Machinery and Systems,* Beijing, 2012.

[13] K. P. Shrestha, O. G. Dahlhaung, B. Thapa, H. P. Neopane and B. S. Thapa, "Innovative Design of Francis Turbine for Sediment Laden Water," in *TIM International Conference*, 2012.

[14] B. Rajkarnikar, H. N. Neopane and B. S. Thapa, "Development of rotating disc apparatus for test of sediment-induced erosion in Francis runner blades," *Wear*, vol. 3, no. 6, pp. 119-125, 2013.

[15] B. S. Thapa, "Effects of sediment erosion in guide vanes of Francis turbines", *PhD thesis*, Norwegian University of Science and Technology, Faculty of Engineering Science and Technolog, 2016.

[16] S. Chitrakar, B. S. Thapa, O. G. Dahlhaung and H. N. Neopane, "Numerical and Experimental Study of the Leakage Flow in Guide Vanes with Different Hydrofoils", *Journal of Computational Design and Engineering*, 2017

[17] H. Brekke, A review on oscillatory problems in Francis turbines, in: *New*

Trends in Technologies: Devices, Computer, Communication and Industrial Systems, Sciyo, 2010, pp. 217-232.

[18] S. Chitrakar, H. P. Neopane, and O. G. Dahlhaug, "Study of the simultaneous effects of secondary flow and sediment erosion in Francis turbines," Renew. Energy, vol. 97, pp. 881–891, 2016, doi: 10.1016/j.renene.2016.06.007.

[19] S. Gautam, H. P. Neopane, B. S. Thapa, S. Chitrakar, and B. Zhu, "Numerical investigation of the effects of leakage flow from guide vanes of francis turbines using alternative clearance gap method," *J. Appl. Fluid Mech.*, vol. 13, no. 5, pp. 1407–1419, 2020, doi: 10.36884/JAFM.13.05.30792.

[20] S. Gautam, H. P. Neopane, N. Acharya, S. Chitrakar, B. S. Thapa, and B. Zhu, "Sediment erosion in low specific speed francis turbines: A case study on effects and causes," *Wear*, vol. 442–443, p. 203152, 2020, doi: 10.1016/j.wear.2019.203152.

[21] N. Acharya, S. Gautam, S. Chitrakar, C. Trivedi, and O. G. Dahlhaug, "Leakage Vortex Progression through a Guide Vane's Clearance Gap and the Resulting Pressure Fluctuation in a Francis Turbine," *Energies*, vol. 14, no. 14, p. 4244, 2021, doi: 10.3390/en14144244.

[22] L. Zemanová and P. Rudolf, "Flow inside the sidewall gaps of hydraulic machines: A review," Energies, vol. 13, no. 24, 2020, doi: 10.3390/en13246617.

[23] J. Schiffer, H. Benigni, H. Jaberg, and T. Schneidhofer, "Numerical simulation of the flow in a Francis turbine including the runner seals on crown and band side," *Hydro – Int. Conf. Exhib. – Bordeaux, Fr.*, no. October, pp. 3–10, 2015.

[24] W. Zhao, "Investigation of seal technology for Francis turbine," Norwegian University of Science and Technology, 2012.

[25] K. Yonezawa and T. Watamura, "Experimental and Numerical Investigations of Erosion on Runner Seal of a Francis Turbine," *IOP Conf. Ser. Earth Environ. Sci.*, vol. 774, no. 1, 2021, doi: 10.1088/1755-1315/774/1/012034.

[26] X. Hou, Y. Cheng, Z. Yang, K. Liu, X. Zhang, and D. Liu, "Influence of clearance flow on dynamic hydraulic forces of pump-turbine during runaway transient process," Energies, vol. 14, no. 10, 2021, doi: 10.3390/en14102830.

[27] C. Trivedi and O. G. Dahlhaug, "Interaction between trailing edge wake and vortex rings in a Francis turbine at runaway condition: Compressible large eddy simulation," *Phys. Fluids*, vol. 30, no. 7, 2018, doi: 10.1063/1.5030867.

[28] C. Trivedi, "Time-dependent inception of vortex rings in a Francis turbine during load variation: large eddy simulation and experimental validation," *J. Hydraul. Res.*, vol. 58, no. 5, pp. 790–806, 2020, doi: 10.1080/00221686.2019.1671514.

[29] C. Trivedi, "Compressible large eddy simulation of a Francis turbine during speed-no-load: Rotor stator interaction and inception of a vortical flow," *J. Eng. Gas Turbines Power*, vol. 140, no. 11, 2018, doi: 10.1115/1.4039423.

[30] J. Schiffer, H. Benigni, and H. Jaberg, "Analysis of the leakage behavior of Francis turbines and its impact on the hydraulic efficiency – A validation of an analytical model based on computational fluid dynamics results," *J. Fluids Eng. Trans. ASME*, vol. 139, no. 2, 2017, doi: 10.1115/1.4034865.

[31] C. Trivedi, M. Cervantes and O. G, Dahlhaug, "Experimental and Numerical

Studies of a High-Head Francis Turbine: A Review of the Francis-99 Test Case", *Energies* 2016, 9 (2), 74

[32] IEC 2364:2019Hydraulic machines- Guide for dealing with hydro-abrasive erosion in Kaplan, Francis and Pelton turbines, *International Electro technical Commission*, Geneva, Switzerland, Edition 2.0 2019-01.

[33] Finnie I. Erosion of surfaces by solid particle. *Wear* 1960; 103:3–87.

[34] M. Eltvik, "Sediment erosion in Francis turbines", *Master Thesis*, Norwegian University of Science and Technology, 2009

[35] I. B. Celik, U. Ghia, P. J. Roache, C. J. Freitas, H. Coleman, and P. E. Raad, "Procedure for estimation and reporting of uncertainty due to discretization in CFD applications," *J. Fluids Eng. Trans. ASME*, vol. 130, no. 7, pp. 0780011–0780014, 2008.

[36] R. Thapa, S. Sharma, K. M. Singh, and B. K. Gandhi, "Numerical investigation of flow field and performance of the Francis turbine of Bhilangana-III hydropower plant," *J. Phys. Conf. Ser*., Vol. 1608, p. 012010.

[37] Chitrakar S., Neopane H. P., and Dahlhaug O. G. (2019) Development of a test rig for investigating the flow field around guide vanes of Francis turbines, *Flow Meas. Instrum*., Vol. 70, p. 101648.

[38] B. Thapa, P. Chaudhary, O. G. Dahlhaug and P. Upadhyay, "Study of combined effect of sand erosion and cavitation in hydraulic turbines", International conference on small hydropower- Hydro Sri Lanka 22-24 October 2007.

[39] H. M. Clark and R. B. Hartwich, "A re-examination of the particle size effect in slurry erosion", *Wear*, vol. 248, p. 147-161, 2001.

[40] H. M. Hawthorne, Y. Xie and S. K. Yick, "A new Coriolis slurry erosion tester design for improved slurry dynamics", *Wear*, vol. 255, p. 170-180, 2003.

Part II

Main Papers

Paper 1

Numerical study of sediment erosion in guide vanes of a high head Francis turbine

N. Acharya, C. Trivedi, N. M. Wahl, S. Gautam, S. Chitrakar, O. G. Dahlhaug
Journal of Physics: Conf. Ser. **1266** 012004, 2019
doi:10.1088/1742-6596/1266/1/012004

A numerical study of sediment erosion in a high head Francis turbine

N. Acharya[1*], C. Trivedi[1], N. M. Wahl[1], S. Gautam[2], S. Chitrakar[2], O. G. Dahlhaug[1]

[1]Waterpower Laboratory, Department of Energy & Process Engineering, Norwegian University of Science and Technology, NO-7491, Trondheim, Norway
[2]Turbine Testing Lab, Department of Mechanical Engineering, Kathmandu University, Dhulikhel, Nepal

*Corresponding author (nirmal.acharya@ntnu.no)

Abstract. Erosion of guide vanes (GVs) has been reported from several power plants in Himalayan and Andes basins which affects the efficiency of turbine. Wear in clearance gaps (CGs) increases with the sediments passing through them resulting in increased gap size, which disturbs the flow into the runner inducing more losses. This paper investigates the flow and erosion pattern around GVs along with the leakage flow. Simulations are carried out in full GV and runner model with varying CGs with the inclusion of sediment. 3 types of clearance gaps viz., 0.5 mm, 1 mm and 1.5 mm are analyzed and numerical results obtained are compared with the photograph of the erosion affected guide vanes. Result shows that erosion was prevalent in regions downstream of the mid-chord position inside the CG due to high pressure difference between two sides of GVs and the leakage flow induced from the pressure difference mixes with the main flow forming a vortex filament, which is driven towards the runner inlet.

Keywords: Francis turbine; sediment erosion; guide vanes; vortex; clearance gap; leakage flow

1. Introduction

Sediment transport in Himalayan rivers reaches their peak during the monsoon period which comprise quartz as a main constituent (more than 50%), along with feldspar and other hard minerals. Hard sediment constituents cause erosive and abrasive types of wear in turbine components. Francis turbines cover the high head range of reaction turbines, which will get the most serious damage from sand erosion due to high velocities and accelerations [1].

Guide Vanes (GVs) are symmetrical or asymmetrical hydrofoils attached with shafts which act as the flow control apparatus responsible for flow governance in turbine setup. They are subjected to entering flow from stay vane and exiting flow to runner, and major physical factors such as hydrofoil profile, clearance gaps, angle of attack, presence of shafts in high velocity etc. are associated with this flow. Gaps on the passage induce leakage and other secondary flows which disturb the main flow downstream. Some research had been done earlier for sediment erosion induced leakage flow from GV's clearance gap in Francis turbine. Brekke [2] studied the influence of varying size of GV's clearance gap on turbine's efficiency in which it was observed that the clearance gap has a high influence on overall efficiency of Francis turbine. Another work showed that all sizes of clearance gap larger than 1 mm induces turbulent cross-flow which mixes with main flow and disturbs the runner inlet flow conditions [3]. Numerical analysis done to investigate the effect of leakage flow on performance of the turbine showed that the symmetrical GV profile was not suitable for best efficiency and part load conditions [4]. Similarly changing GV profile shape can get much lower velocity difference between the two sides with a clear improvement of leakage flow and observation of weaker and smaller filament vortex in the new design [5].

This paper focuses on a high head Francis turbine operating under 207 m nominal head and 4.33 m^3/s rated discharge. Petrographic study of silt samples from the site shows composition of loose grains of coarse sand to fine silt and clay which comprise of quartz & lithic fragments, feldspar, mica (muscovite and biotite), hornblende, and magnetite. Figure 1(a) and 1(b) shows the representation of GV with dry clearance and inclusion of clearance gaps representing eroded profile respectively. As depicted in figure, original width of clearance gap is t, which increases to t+Δt after erosion [6]. Actual eroded surfaces are non-uniform and erratic but assumption of uniform clearance gap is done to get the general sense of leakage flow through GVs.

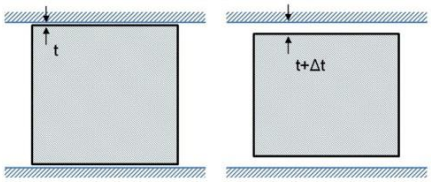

Figure 1 (a) GV with dry clearance and (b) Eroded GV profile representation

2. Methodology

2.1. Numerical Model

2D geometry of GVs obtained from the power plant was used for the numerical work. An in-house developed code was used to produce a reference turbine, as there was limitation for the availability of design and drawings of installed prototypes. CFD simulations were carried out for 1 GV profile and 3 clearance gaps at best efficiency point (BEP). The full model of the turbine consists of 13 runner blades and 24 GVs, as shown in Figure 2. The domain was divided into 3 sub domains, GV (stationary), runner (rotating) and a portion of draft tube (stationary). Full passage modelling was carried out in this study to avoid shifting of vortex filament in the interface due to mismatch in pitch angles between the domains of GVs and runner. Mass flow rate of 4330 kg/s at inlet and atmospheric pressure at outlet were chosen as boundary conditions. Designed mass flow rate of the turbine representing 100% flow was taken as BEP. SST turbulence model was used due to its robustness in predicting both near and away wall boundary flows. This numerical analysis is focused on the flow pattern around guide vane profiles with varying clearance gap corresponding to sediment erosion which would influence erosion pattern in the runner blades as well. Steady state analyses were conducted to study the leakage flow through the clearance gap and transient analyses were done to predict the true transient interaction of the flow between GV and runner blades.

2.2. Erosion Model

Sediment particles are defined as solid particles and size distribution is uniform in diameter. For this case, quartz is considered as it affects the most and hence particles are modelled based on quartz properties. Particle size and density is given and mass flow rate of sediments is obtained from the sediment data of Bhilangana-III (B-III) HEP.

Tabakoff erosion model was chosen over Finnie for the simulations as it considers more parameters and is relatively more reliable and gives more realistic erosion rate indication [7]. Tabakoff erosion model in ANSYS CFX, determines erosion rate *E* from the following relation:

$$E = f(\gamma)(V_p/V_1)^2 cos^2\gamma\left[1 - {R_T}^2\right] + f(V_{PN}) \quad (1)$$

where,

$$f(\gamma) = [1 + k_2.k_{12}.sin(\gamma^{\pi/2/\gamma_0})]^2 \quad (2)$$

$$R_T = 1 - {V_p/V_3} sin\gamma \quad (3)$$

$$f(V_{PN}) = ({Vp/V_2} sin\gamma)^4 \quad (4)$$

$$k_2 = \begin{cases} 1.0 \ \ if\ \gamma \leq\ 2\gamma_0 \\ 0.0 \ \ if\ \gamma >\ 2\gamma_0 \end{cases} \quad (5)$$

Here E is the dimensionless mass (mass of eroded wall material divided by the mass of particle). V_p is the particle impact velocity, γ is the impact angle in radians between the approaching particle track and the wall, γ_0 being the angle of maximum erosion. k_2 and k_{12} are model constants and depend on the particle/wall material combination.

Erosion of a wall due to a particle is computed from the following relation:

$$ErosionRate = E.N.m_p \quad (6)$$

Where, m_p is the mass of the particle and N is its number rate. The overall erosion of the wall is then the sum over all particles. This gives an erosion rate in [kg s^{-1}], and erosion rate density in [kg s^{-1} m^{-2}] to indicate the erosion area visually on the wall surface.

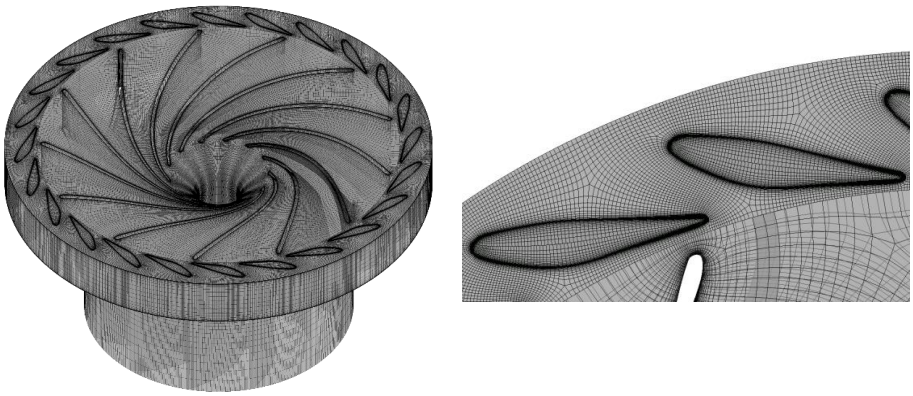

Figure 2 Computational domain showing entire mesh and the enlarged one near guide vanes

3. Mesh Sensitivity Analysis

Estimation of discretization error and extrapolation values was done by using the GCI method [8]. This technique is found to be effective in predicting numerical uncertainties for the case of Francis turbines [9]. For uncertainty analysis, three mesh were created with number of elements in each mesh equal to 1.6, 4.9 and 16.7 million. Mesh refinement was done by increasing the distribution in each direction. Efficiency was chosen as monitored variable. These values obtained by the three mesh densities are noted as η_1, η_2 and η_3, where η_1 represents the results of the fine mesh and η_3 represents that of the coarse mesh.

The fine- grid convergence index was estimated as:

$$GCI_{fine}^{21} = \frac{1.25e_a^{21}}{r_{21}^p - 1} \quad (7)$$

Table 1 shows the uncertainties and extrapolated values. The numerical uncertainties in the efficiency was calculated to be 1.46% and 3.69% for the medium and fine grid densities respectively.

Table 1. Discretization errors in the numerical solution

Efficiency as a variable measured for various sizes mesh										
r_{21}	r_{32}	η_1	η_2	η_3	p	η_{ext}^{21}	e_a^{21}	e_{ext}^{21}	GCI^{21}_{fine}	GCI^{32}_{med}
1.78	1.43	90.11%	90.79%	89.81%	0.86	89.06%	0.0075	0.0118	0.0146	0.0369

4. Results and discussions

Numerical erosion model calculates the forces that acts when the particles (sediment in this case) collide with the wall where erosion rate indicates loss of material per square meter per second, and are seen as colored spots in Figure 3. Complete blue area denotes zero erosion and red areas are highly affected areas with maximum erosion intensity. Along the pressure side of the blade, erosion in observed near the trailing edge and some erosion is detected on the suction side as well in the middle portion and near trailing edge area. One of the studies [2] shows that kinetic energy increases from about 10% to about 50% from guide vanes inlet to the runner inlet for a high head Francis turbine which clearly indicates availability of very high accelerated flow inside the guide vane which can resulting secondary flow, aggravating the erosion problems. Figure 3 shows the turbulence erosion pattern in guide vane in which fine particles erode the GV outlet both pressure and specially towards suction side.

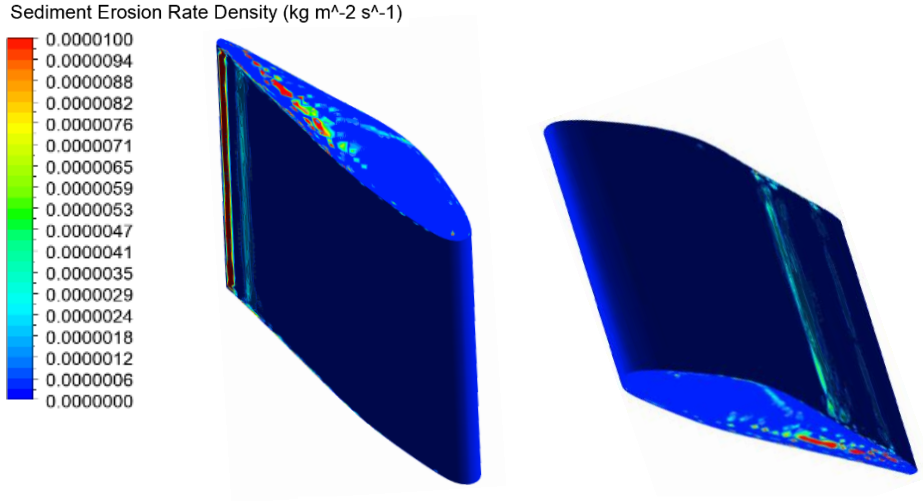

(a) (b)

Figure 3 Erosion pattern on GV (a) Pressure Side and (b) Suction side

Erosion can also be seen in GV's facing ends, both in the upper and lower facing ends as shown in Figure 4(a). Figure 4(b) shows the GV profile in Unit-I after 6170 hours of operation which shows similar pattern with the numerical one and Figure 4 (c) shows erosion pattern in facing plate along

with GV contour which is secondary flow type of erosion which occurs in the corners between facing plates and guide vanes. More erosion was observed downstream of the mid-chord due to larger intensity of the leakage flow in this region. The high leakage flow is governed by the pressure difference between two sides of the GVs [6]. It is to be noted that in the current CFD model, the shafts have not been modeled. Erosion downstream of the shaft is more severe due to high turbulences in these regions.

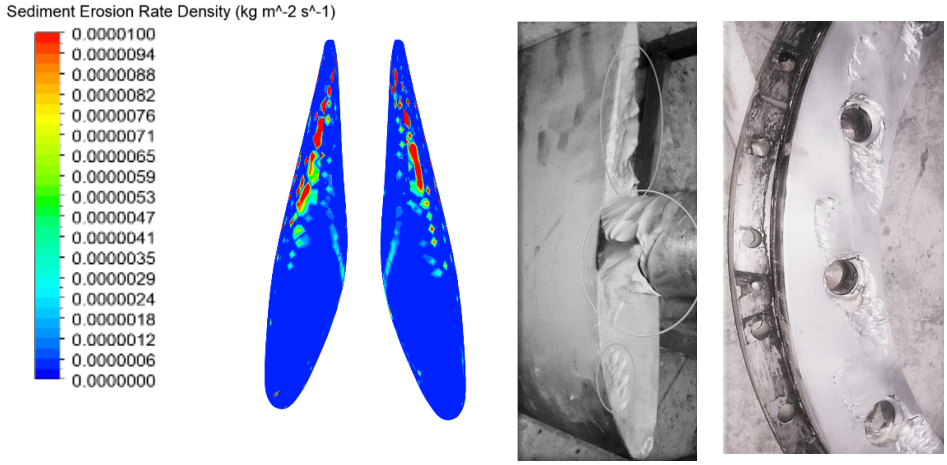

(a) (b) (c)

Figure 4 (a) Erosion pattern in GV's face ends and (b) Photograph of eroded GV profile and (c) Facing plates

Guide vanes consist of a small clearance gap at both ends to adjust the opening angle based on various operating conditions. In case of sediment affected power plants, hard fine particles mixed in water erode the connecting ends due to horse-shoe vortices. This erosion together with the head cover deflection due to water pressure increases the size of the gap. Leakage flow refers to the flow passing from high pressure side to low pressure side of GV inside clearance gaps as depicted in Figure 5. At high acceleration, when the sediment particles enter in to the gap, it further causes abrasion on the guide vane ends and facing plates as seen on Figure 4(b) and 4(c). This leakage flow mixes with the main flow which might cause more disturbances in runner inlet.

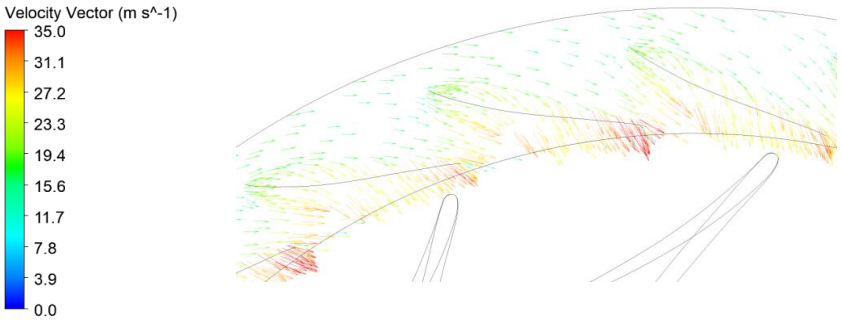

Figure 5 Leakage flow pattern as seen by velocity vectors

Figure 6 shows iso-surface of swirling strength obtained from transient analysis for different CGs. It is one of the methods to visualize the vortex, which represents the strength of swirling motion around local centers. GV profiles with three CGs are compared at same swirling strength of 500 Hz and velocity on the vortex core to justify the comparison. It is observed that the strength of the vortices and velocity of the flow is higher for higher thickness of clearance gap i.e. with 1.5 mm CG among the three gaps studied in this paper (only 2 shown). This vortex flow tends to hit the runner inlet and move towards trailing edge at a high velocity thus aggravating the erosion problem.

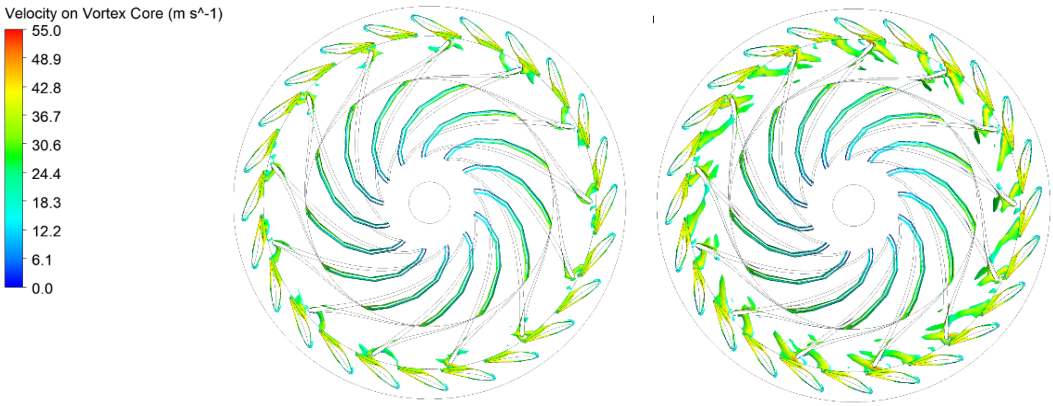

(a) 1 mm (b) 1.5 mm

Figure 6 Iso-surface contours of swirling strength with velocity for (a) 1 mm (b) 1.5 mm clearance gaps

5. Conclusion

Sediment erosion analysis of a turbine gives an indication of relative erosion intensity and critical zones of erosion damage of turbine components. Numerical analysis on guide vanes of B-III HEP was carried out with existing design. Erosion pattern, erosion rate density and nature of vortices originating from leakage flow were observed during the process.

It was seen that erosion pattern in GVs predicted by CFD matches with erosion in actual turbine as seen in Figure 4(b) and 4(c). Velocity vectors on the upper plane of GV shows the significant leakage flow passing from high pressure side to low pressure side as observed in Figure 5. This leakage flow disturbs the main flow causing swirl which never enters the runner channel and leaves energy unutilized. Erosion was seen mostly in regions downstream of the mid-chord position inside the clearance gap due to local separation and vortex. Secondary flow erosion might have been caused by horse-shoe vortices which can be seen on facing plates along the guide vane contours as observed in Figure 4(c). Comparatively, strong vortices are generated from the guide vanes with clearance gap of 1.5 mm which might be accountable for the high erosion on runner blade inlet. In addition to gap erosion, erosion on foil surfaces causes friction drag resulting high friction losses.

Other hydrofoil profiles, angle of attack, inclusion of GV shaft, sediment size & concentration, GV opening angle should be investigated to draw the conclusion on the erosion pattern, localization, and quantity. For the ease of calculation, uniform clearance gaps were considered for this case. Accurate results might be obtained from the exact or at least similar type of non-uniform gaps.

6. Future works

Numerical simulation in existing guide vanes with non- uniform clearance gaps and more accurate runner from the power-plant considering erosion phenomenon will be continued as further works. For

this paper, simulations were carried out for one GV opening conditions i.e. for BEP obtained from the in-house code but other openings conditions will be considered. Most optimum shape of guide vanes with suitable hydrofoil and runner blades design will be investigated to address erosion challenges in sediment- laden projects.

References

[1] Brekke H, Wu Y.L. and Cai B.Y 2001 Design of hydraulic machinery working in sand laden water Abrasive erosion and corrosion of hydraulic machinery, volume 2, chapter 4, page 155-181 Imperial College Press

[2] Brekke H, The influence from the guide vane clearance gap on efficiency and scale effect for Francis turbines. Proc 14th IAHR Symposium, section on hydraulic machinery equipment and cavitation, 1988

[3] Thapa B.S, Dahlhaug O.G and Thapa B 2017 Sediment erosion induced leakage from guide vane clearance gap in a low specific speed Francis turbine, *Renewable Energy* Vol 107, July 2017, p. 253-261

[4] Chitrakar S 2018 *Secondary flow and sediment erosion in Francis turbines*, PhD Thesis, Norwegian University of Science and Technology

[5] Nora L P 2016 Study of sediment erosion in guide vanes of Francis turbine, Master Thesis, Norwegian University of Science and Technology

[6] Chitrakar S, Dahlhaug O G and Neopane H P 2018 Numerical investigation of the effect of leakage flow through erosion- induced clearance gaps of guide vanes on the performance of Francis turbines, *Engineering Applications of Computational Fluid Mechanics*, 12:1 662-678

[7] Eltvik M 2009 *Sediment erosion in Francis turbines*, Master Thesis, Norwegian University of Science and Technology

[8] Celik I, Ghia U, Roache P, Freitas C, Coleman H and Raad P 2008 Procedure for estimation and reporting of uncertainty due to discretization in CFD applications, *Journal of Fluids Engineering, ASME,* 130(7), 078001

[9] Trivedi C, Cervantes M, Gandhi B and Dahlhaug O 2013 Experimental and numerical studies for a high head Francis turbine at several operating points, *Journal of Fluids Engineering, ASME,* 135(11), 111102

Acknowledgment

The numerical study was conducted under research project FME-Hydrocen. This project (No. 90148312) was funded by Norwegian Research Council and Norwegian Hydropower Industries. Authors would like to acknowledge the support from B-III HEP for provided necessary detail to carry out this work.

Paper 2

Investigation of sediment erosion phenomenon for different blade angle distribution in Francis runner

N. Acharya, C. Trivedi, S. Gautam, and O. G. Dahlhaug
IOP Conference Series: Earth and Environmental Science **774** 012017
doi:10.1088/1755-1315/774/1/012017

Investigation of sediment erosion phenomenon for different blade angle distribution in Francis runner

N Acharya[1*], C Trivedi[1], S Gautam[2] and O G Dahlhaug[1]

[1]Waterpower Laboratory, Department of Energy & Process Engineering, Norwegian University of Science and Technology, NO-7491, Trondheim, Norway
[2]Turbine Testing Lab, Department of Mechanical Engineering, Kathmandu University, Dhulikhel, Nepal
*Corresponding author (nirmal.acharya@ntnu.no)

Abstract. Wear and tear of hydraulic turbine due to sediment erosion is one of the major problems in hydropower plants located in the Himalayan and Andes regions. High sediment concentration in water of such areas wears down the mechanical components rapidly which causes significant operational challenges. In the present work, a prototype high head Francis runner with speed number 0.32 has been considered as reference case and other designs have been obtained modifying the blade angle distribution with same hydraulic parameters. Full turbine steady state numerical calculations were carried out at the best efficiency point and corresponding performance and erosion pattern are observed. Hydraulic efficiency and sediment erosion rate density are compared for the different cases taken into consideration. Sediment erosion analysis gives an indication of relative erosion intensity and critical zones of erosion damage in runner. Erosion was observed at the inlet near hub and shroud region and was mostly concentrated at the outlet of runner blades for all cases, where relative velocity is higher. Numerical results from CFD are also compared with the actual eroded turbine from the powerplant.

Keywords: CFD, Erosion rate density, Francis turbine, Runner blade, Sediment erosion

1. Introduction

Sediment particles along with water erodes the material surface of hydraulic turbine components in contact. Erosion effect in hydraulic turbine differs with the nature of flow inside the turbine. Francis runners cover the high head range of reaction turbines, which will get most serious damage from sand erosion due to availability of high velocities and high accelerations within [1]. Damage on the component depends on hardness of sediment, its shape and grain size along with the amount as well as the velocity. High relative velocity at the outlet and due to leakage flow carried out from clearance gaps of guide vanes (GVs), runner is exposed to the erosion phenomenon [2].

This paper examines the sediment erosion effect on runner at best efficiency point (BEP). Previous work focussed on the numerical analysis of guide vane of the same power plant [3]. Erosion pattern, erosion rate density and nature of vortices originating from leakage flow were observed during that study [3]. GV profiles with three different clearance gaps were compared and velocity on the vortex core was analyzed. To investigate the performance of Francis turbines and their erosion phenomenon, a MATLAB based code is applied to generate various blade profiles followed by CFD analysis on them.

2. Methodology

2.1 A brief description of the reference case and variation of blade angle distribution

Guide vanes and runner blades from prototype with speed number of 0.32 is considered as the reference case for this study, and the specifications are presented in Table 1.

Table 1. Design data for reference case

S.N.	Parameters	Value	Unit
1	Design head (H)	207	m
2	Discharge per unit (Q)	4.33	m^3/s
3	Rotational speed (N)	750	rpm
4	Power Output (P)	8	MW

Hydraulic design of the runner has a significant impact on the overall performance of the turbine [4]. The following study focusses to find the optimal runner design with a trade-off between performance and erosion behavior. This study focuses on comparison of sediment erosion investigation of 5 shapes of runner blades which were proposed for parametric study in previous works [5] [6] presented in Figure 1. Graph in fig. 1 shows relative length along the streamline in x- axis and distribution relative to inlet along y- axis which is enlarged for fig. 1(a) only whereas all other figures have similar parameters in x and y axis.

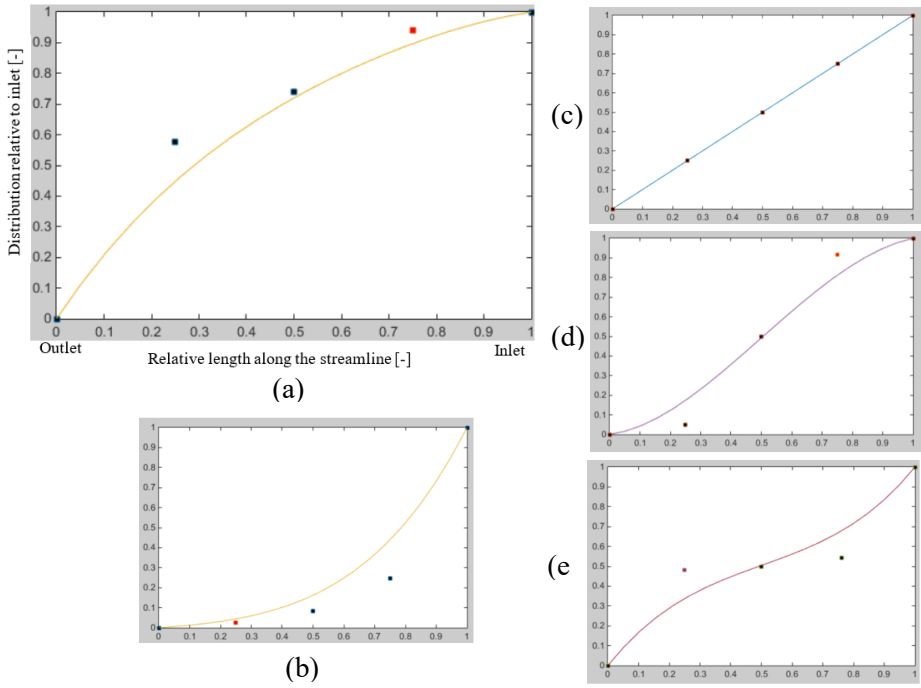

Figure 1 Blade angle distribution for various blades (a) Shape 1 (b) Shape 2 (c) Shape 3 (d) Shape 4 & (e) Shape 5

Velocities comprises of peripheral (U), absolute (C) and relative (W) at inlet and outlet of the runner as shown in fig. 2. Different shapes were obtained modifying the blade angle distribution from inlet to outlet. Blade angle is calculated from the equation 1 as follows:

$$tan\,\beta = \frac{C_m}{U - C_u} \quad [-] \tag{1}$$

where, C_m and C_u are meridional and tangential components of C respectively (Refer Fig.2)

Design program has been made to generate blade profiles corresponding to blade angle distribution as input parameter. It controls how much hydraulic energy is converted to the mechanical energy in each section of blade. Adjusting the blade angle distribution influences blade loading which will affect the

blade shape as well. In terms of energy conversion, shape 1 shows the blade angle distribution with low energy extraction at runner inlet and high energy extraction at the runner outlet as shown in fig. 1 (a), while shape 2 is opposite of it as shown in fig. 1 (b). A linear blade angle distribution is represented by shape 3 as in fig. 1 (c). Similarly, shape 4 & 5 shows the energy distributions with combinations of high and low energy distribution at the inlet and the outlet respectively which are depicted in fig. 1 (d) & 1 (e) [5].

Full model of the turbine consists of 13 runner blades and 16 GVs similar as in the power plant. Figure 3 shows isometric view of the reference runner.

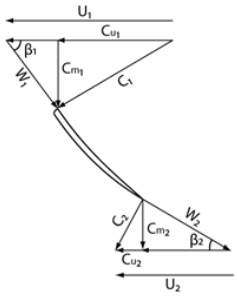

Figure 2 Velocity components on Francis runner blade

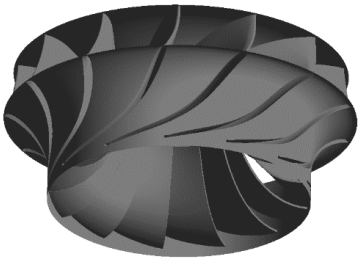

Figure 3 Isometric view of reference

2.2 Description of numerical and erosion model

Numerical calculation was done using ANSYS CFX by solving steady state RANS equations coupled with SST model for the turbulence quantities. Calculation was done using reduced geometry of the turbine that includes the guide vane cascade and runner blades. CFD simulations were carried out for reference runner blades with generated one together with same set of guide vanes ring. Numerical model of turbine was divided into 2 domains, GV (stationary) and a runner (rotating) at 750 rpm depicted in Figure 4. Mass flow rate of 4330 kg/s with prescribed velocity components in cylindrical co-ordinates at the inlet and static pressure outlet condition were chosen as boundary conditions. Non-slip wall condition is used for all wetted surfaces while frozen rotor interface is used for connecting non-conformal meshes with both stationary and rotating domains. High resolution advection scheme is used for all equations being solved. Designed mass flow rate of the turbine representing 100% flow was taken as BEP.

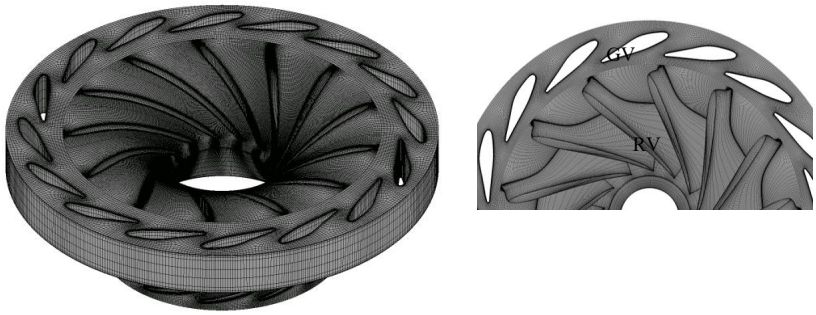

Figure 4 Domain with entire mesh size of 4.98 million elements

Sediment particle was defined as a spherical quartz material with a density of 2.65 gm/cm^3. Particle size distribution analysis of the collected sediment samples from the site showed the presence of particles with 150 μm diameter abundantly which can't be settled in desilting chamber and hence

passes through the runner blades [7]. Particle mass flow rate was based on the maximum amount of sediment passing through the turbine unit that corresponds to 26028.7 tonnes /year recorded in the site in year 2013-2014 [8].

Tabakoff erosion model was chosen over Finnie for the simulations as it considers more parameters and is relatively more reliable and gives more realistic erosion rate indication [9]. It introduces the combination of higher and lower angle of attack of sediment particles in the surface. It considers the influence of quartz particles colliding with the ductile material which is somehow similar to the real scenario.

Tabakoff erosion model in ANSYS CFX, determines erosion rate E from the following relation:

$$E = f(\gamma)(V_p/V_1)^2 \cos^2\gamma\,[1 - R_T^2] + f(V_{PN}) \tag{2}$$

where,
$$f(\gamma) = [1 + k_2 k_{12}\, sin(\gamma \frac{\pi/2}{\gamma_0})]^2$$

$$R_T = 1 - V_p/V_3 \sin\gamma$$

$$f(V_{PN}) = (V_p/V_2 \sin\gamma)^4$$

$$k_2 = \begin{Bmatrix} 1.0 & if\ \gamma \le 2\gamma_0 \\ 0.0 & if\ \gamma > 2\gamma_0 \end{Bmatrix}$$

Here E is the dimensionless mass (mass of eroded wall material divided by the mass of particle). V_p is the particle impact velocity, γ is the impact angle in radians between the approaching particle track and the wall, γ_0 being the angle of maximum erosion. k_2 and k_{12} are model constants and depend on the particle/wall material combination.

Erosion of a wall due to a particle is computed from the following relation:

$$ErosionRate = E \times N \times m_p \tag{3}$$

Where, m_p is the mass of the particle and N is its number rate. The overall erosion of the wall is then the sum over all particles. This gives an erosion rate in [kg s^{-1}], and erosion rate density in [kg s^{-1} m^{-2}] to indicate the erosion area visually on the wall surface.

2.3 Mesh Sensitivity Analysis

Estimation of discretization error and extrapolation values was done by using the Grid Convergence Index (GCI) method [10]. It is considered as the effective method in predicting numerical uncertainties in the case of Francis turbines. Three types of structured hexahedral meshes with varying resolution were generated (coarse, medium and fine), initially starting from the coarsest grid that can achieve acceptable mesh quality and then increasing the element count throughout a structured refinement in all directions. Number of elements in each mesh equal to 1.67, 4.98 and 17.7 million. Turbine efficiency was chosen as monitored variable. These values obtained by the three mesh densities are noted as η_1, η_2 and η_3, where η_1 represents the results of the fine mesh and η_3 represents that of the coarse mesh. Overall grid refinement factor was then calculated with the ratio of the length of consecutive mesh scheme i.e. for $h_1 < h_2 < h_3$ and $r_{21} = h_2/h_1$, $r_{32} = h_3/h_2$. GCI value of the mesh was calculated as:

$$GCI_{fine}^{21} = \frac{1.25 e_a^{21}}{r_{21}^p - 1} \quad [-] \tag{4}$$

Where, e_a represents error in absolute value and r_{21} represents the grid refinement factor from medium mesh to fine mesh respectively. Results are summarized in Table 2. Considering the low discretization error that fine mesh has, it can be assumed that a fully grid independent solution has been achieved.

However, as the medium mesh too gives balance results in terms of accuracy and computational time, the same has been used for all simulation cases.

Table 2. Discretization errors for B-III reference case

Efficiency as a variable measured for various sizes mesh		
No. of cells	N1, N2, N3 [10^6]	17.7, 4.98, 1.67
Grid refinement factor	r_{21}, r_{32}	1.52, 1.43
Efficiency	$\eta_1, \eta_2 \eta_3$	95.92, 96.83, 95.62
Apparent order	p	0.75
Extrapolated values	η_{ext}^{21}	94.18
Error estimates	e_a^{21}	0.95%
Extrapolated relative error	e_{ext}^{21}	1.84%
Fine grid convergence index	GCI $^{\eta}{}_{fine}$	2.26%
Medium grid convergence index	GCI $^{\eta}{}_{medium}$	3.6%

3. Results and discussions

3.1 Blade to blade plot for various shapes

Contour in the mid span of all blades is presented in Figure 5, which shows the velocity distribution from inlet to outlet for all blades. Blade to blade transformation in turbo mode was acquired to observe the difference in blade profile for all shapes. Compared to reference blade profile, other blades are bit longer. Various velocity distributions were observed for different blade profile as depicted from Figure 5 (a) to 5 (f). It shows that the highest relative velocity is concentrated at the trailing edge in the reference blade clearly exhibited in fig. 5 (a) among all.

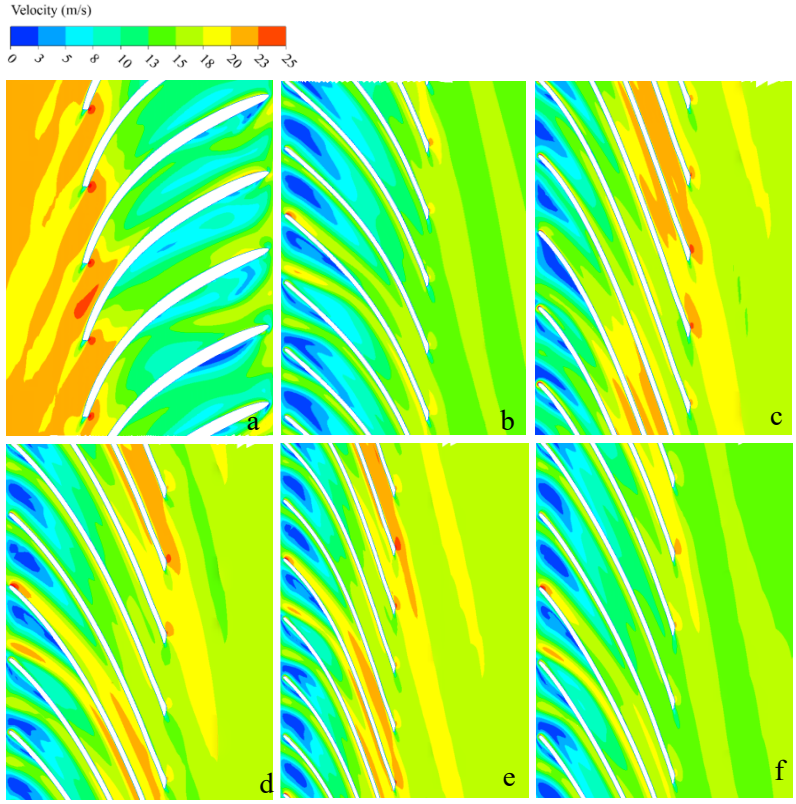

Figure 5 Velocity contours in runner at mid span (a) Reference (b) Shape 1 (c) Shape 2 (d) Shape 3 (e) Shape 4 & (f) Shape 5

3.2 Comparison of sediment erosion for various shapes

Variation in pattern and amount of erosion in runner blade was observed with the effect of change of runner blade shapes. This study only focusses on the erosion of runner blades, so guide vanes erosion is excluded. As discussed in methodology section above, various shapes of the blades were obtained with the variation in blade angle distribution. Energy distribution is the distribution of product of peripheral velocity, U and peripheral component of absolute velocity, C_u. As U is only dependent on the radius and angular velocity, which is known for all points, C_u is strongly corelated to the blade angle distribution. Different blade angle distribution causes different transition from inlet to outlet velocity, which might explain the difference in erosion factors.

Figure 6 shows the normalized sediment erosion rate for different blades. Sediment erosion rate density for all blades is normalized with the erosion for reference case. From the bar graph, it is seen that reference blade shows the highest erosion factor of all followed by shape 3 which corresponds to the linear blade angle distribution. Shape 5 shows the lowest erosion rate of all which was followed by shape 1 and shape 2.

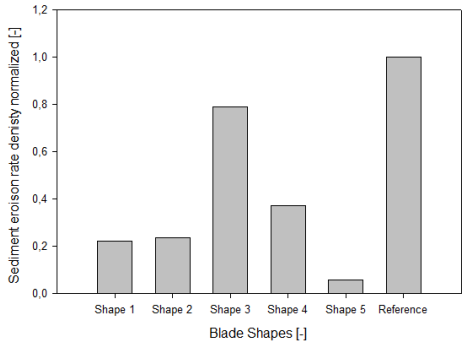

Figure 6 Erosion rate normalization for all blades

Figure 7 shows the plot of relative velocity versus streamwise location from inlet to outlet for all shapes. Values shows that the highest relative velocity is for the reference case followed by shape 3. Similarly, the smooth transition with the lowest relative velocity is acquired in case of shape 5. Shape 1 follows shape 5 closely with slight increase in velocity from middle section. Relative velocities for shape 2 and 4 fall in between maximum and minimum values. Figures 6 and 7 strongly exhibits the co-relation between relative velocity and erosion i.e. the higher possibility of erosion with the higher values of relative velocity at runner outlet.

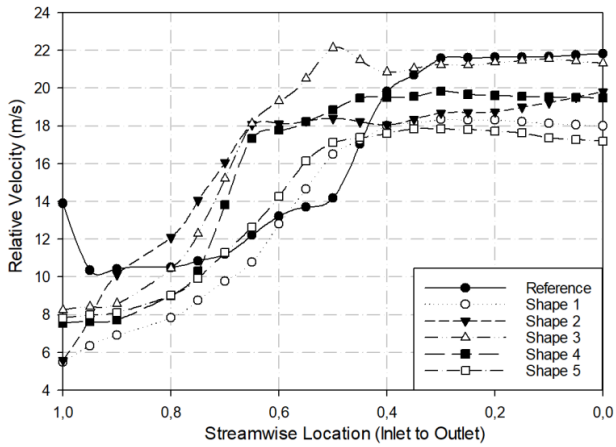

Figure 7 Comparison of relative velocity along blade span for all shapes

Numerical erosion model calculates the forces that acts when the particles (sediment in this case) collide with the wall where erosion rate indicates loss of material per square meter per second. Figure 8 shows the comparison of erosion at the inlet and outlet of the reference runner with CFD and field inspection. Erosion from CFD seen at the inlet and pattern of erosion near hub and shroud region was found to be similar as the inspected runner in the power plant as seen in figure 8 (a) & (b). Erosion was observed more adverse towards the outlet, where the relative velocity is higher. Erosion pattern obtained at the outlet is shown in figure 8 (c) which is quite similar with the eroded profile obtained from the site i.e., figure 8 (d). Erosion in the runner blades was mainly due to vortices travelling from clearance gaps that hits the inlet of runner and leaves the outlet with higher velocity. As the study was only done for best efficiency point (BEP) conditions, different erosion phenomena might occur for full load and part load conditions. At BEP, particle carried by flow regime is less turbulent and hence they glide with water rather than striking the blade surface and hence, minimum erosion is observed [11].

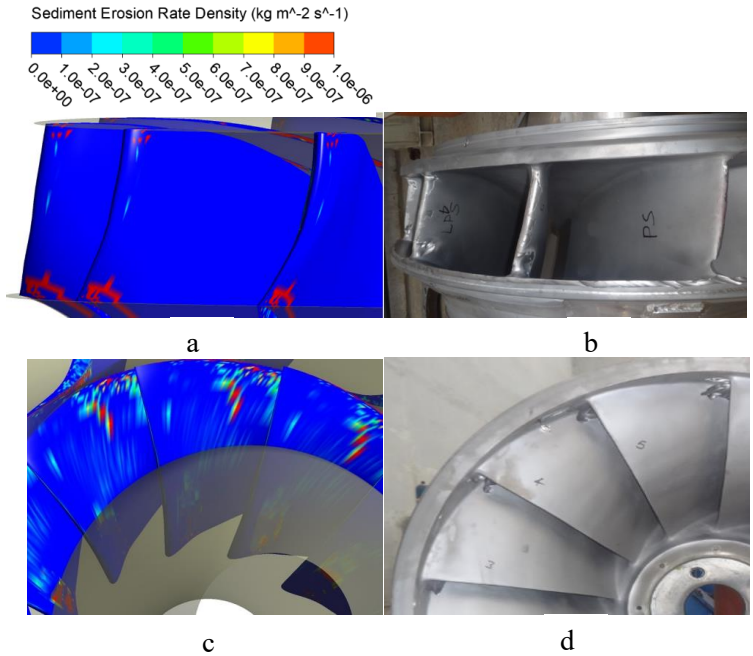

Figure 8 (a) Erosion at inlet of runner (b) Photograph of eroded profile at inlet (c) Erosion at outlet of runner and (d) Photograph of eroded profile at outlet

3.3 Comparison of efficiency for various shapes

Figure 9 shows the efficiency for five different types of runner blades generated. which is normalized upon reference blade. η* plotted on y-axis in figure 9 is the normalized efficiency based upon the reference blade.

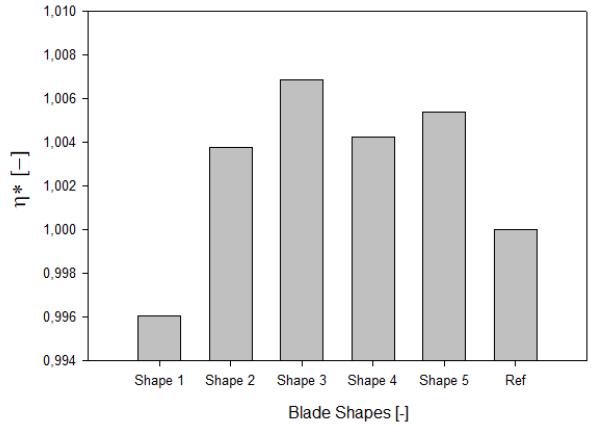

Figure 9 Normalized efficiency for various blades

In all cases, flow conditions are represented by GV opening angles corresponding to best efficiency point (BEP). Shape 3 shows the best efficiency followed by shape 5. Shape 2 and 4 shows somehow similar efficiency. Shape 1 shows the lowest efficiency among all blade designs.

4. Conclusion

Sediment erosion analysis gives an indication of relative erosion intensity and critical zones of erosion damage in turbine components. Numerical analysis on reference runner and 5 other different designs as per varying blade angle distribution was carried out. Erosion pattern, erosion rate density and efficiency were compared during the process.

It was seen that erosion pattern in runner blades predicted by CFD matches with erosion in actual turbine as seen in figure 8. Erosion was observed at the runner inlet near hub and shroud region and was mostly concentrated at the outlet of runner blades for all cases. Comparing the erosion rate for different blade profiles, shape 5 showed the optimum result whereas shape 3 showed the highest efficiency. Reference blade has highest relative velocity at outlet among all with rapid transition from section to section, which might be one of the major causes for highest erosion density rate. Shape 3 representing linear blade angle distribution, which has been commonly accepted for Francis runner design [5] stands out with highest efficiency but due the high relative velocity, it is also subjected to high sediment erosion. Varying blade angle distribution changes the blade profile which also seemed to yield a better reduction in erosion.

Optimization approach used for this study uses the same energy distribution from shroud to hub together with all streamlines for one shape. Better results can be obtained from different sort of energy distribution from hub to shroud in a single shape as well, which is yet to be investigated. Other operating conditions and sediment size & concentration should also be investigated. Several other distributions and combinations should be attempted to obtain the best trade-off between performance and erosion phenomenon during optimization process.

5. Further Works

Parametric design tool is being developed in MATLAB to carry out its hydraulic design and consequently optimization of the same. The main design philosophy is to minimize the velocity of water along the components such that sediment velocity will also be reduced. Erosion tendency function will be incorporated in the program and it can be used to develop several designs to look at measures for reducing erosion.

References

[1]. Brekke H, Wu Y.L. and Cai B.Y 2001 Design of hydraulic machinery working in sand laden water Abrasive erosion and corrosion of hydraulic machinery, volume 2, chapter 4, page 155-181 Imperial College Press

[2]. Thapa B.S, Thapa B and Dahlhaug O.G, Empirical modeling of sediment erosion in Francis turbines, *Energy* 4 (1) (2012) 386–391

[3]. Acharya N, Trivedi C, Wahl N. M, Gautam S, Chitrakar S and Dahlhaug O. G, Numerical study of sediment erosion in guide vanes of a high head Francis turbine 2019 Journal of Physics: Conference Series1266 012004

[4]. Iliev I, Trivedi C and Dahlhaug O.G 2018 Simplified hydrodynamic analysis on the general shape of the hill charts of Francis turbine using shroud- streamline modeling Journal of Physics: Conference Series1042 012003

[5]. Eltvik M 2013 *Sediment erosion in Francis turbines*, PhD Thesis, NTNU

[6]. Gjøsæter K, 2011, *Hydraulic Design of Francis Turbine Exposed to Sediment Erosion*, Master's Thesis, NTNU

[7]. Gautam S, Neopane H.P, Acharya N, Chitrakar S, Thapa B.S and Zhu B 2019 Sediment erosion in low specific speed francis turbines: A case study on effects and causes, *Wear*

[8]. Koirala R, Thapa B, Neopane H.P, Zhu B 2017 A review on flow and sediment erosion in guide vanes of Francis turbines, *Renewable and Sustainable Energy Reviews*

[9]. Eltvik M 2009 *Sediment erosion in Francis turbines*, Master Thesis, Norwegian University of Science and Technology

[10]. Celik I, Ghia U, Roache P, Freitas C, Coleman H and Raad P 2008 Procedure for estimation and reporting of uncertainty due to discretization in CFD applications, *Journal of Fluids Engineering, ASME,* 130(7), 078001

[11]. Shrestha K.P, Chitrakar S, Thapa B and Dahlhaug O.G 2018 Performance comparison of optimized designs of Francis turbines exposed to sediment erosion in various operating conditions, Journal of Physics: Conference Series1042 012001

Acknowledgment

This work was conducted under research project FME-Hydrocen. This project (No. 90148312) was funded by Norwegian Research Council and Norwegian Hydropower Industries.

Paper 3

Leakage vortex progression through a Guide-vane's clearance gap and the resulting pressure fluctuation in Francis turbine

N. Acharya, S. Gautam, S Chitrakar, C. Trivedi, and O. G. Dahlhaug
Energies, **2021**, *14*(14), 4244
doi.org/10.3390/en14144244

Leakage vortex progression through a guide-vane's clearance gap and the resulting pressure fluctuation in Francis turbine

N. Acharya[1*], S. Gautam[2] , S. Chitrakar[2] , C.Trivedi[1] and O. G. Dahlhaug[1]

[1]Waterpower Laboratory, Department of Energy & Process Engineering, Norwegian University of Science and Technology, NO-7491, Trondheim, Norway
[2]Turbine Testing Lab, Department of Mechanical Engineering, Kathmandu University, Dhulikhel, Nepal

*Corresponding author (nirmal.acharya@ntnu.no)

Abstract. A clearance gap (CG) between guide vanes (GVs) and facing plates exists at both ends of a Francis turbine and allows the opening angle to be adjusted for varying operating conditions. Leakage flow is induced through this gap due to the pressure difference between the two sides of the guide vanes. While some research works have used qualitative approaches to visualize and predict the strength of a leakage vortex (LV), this paper presents a method for quantifying vortices along a trajectory. In this paper, a prototype high-head Francis runner with specific speed of 85.4 is considered as a reference case. A systematic investigation across both space and time is carried out, i.e., analysis of the spatial temporal progression of LV for three operating conditions. While travelling from the CG to runner leading edge, LV evolution and trajectory data are observed, and the values of vorticity and turbulent kinetic energy are calculated for the LV trajectory. Frequency spectrum analyses of pressure oscillations in the vaneless space, runner blade, and draft tube are also performed to observe the peak pressure pulsation and its harmonics. Unsteady fluctuations of the runner output torque are finally studied to identify the patterns and magnitudes of torque oscillations.

Keywords: clearance gap; leakage vortex; rotor stator interaction; pressure pulsation

1. Introduction

Francis turbines are the most prevalent reaction turbines, which are normally adopted for medium-head and medium-flow conditions. In these turbines, the flow rate is regulated with guide vanes (GVs) that exist upstream of a runner. Water leaving from the guide vanes enters the runner blades with the desired angle at a high velocity which is consequently converted into rotary motion. In addition, GVs are incorporated with a small clearance gap (CG) at both ends so that they can pitch around their axis, which enables the adjustment of the opening angle based on various operating conditions. Several studies [1–5] have suggested that the sizes of CGs increase with head cover deflection due to water pressure, which results in the disturbance of the runner inlet flow conditions and a loss in overall efficiency. Brekke [1] studied the influence of varying CG and GV sizes on flow behavior and turbine efficiency, observing that the size of the CG has a high influence on the overall turbine efficiency. Thapa [2] developed an experimental setup with a GV cascade representing the flow inside the distributor of a Francis turbine. Pressure and velocity data obtained from his experiments showed that all CG sizes greater than 1 mm induced a turbulent cross-flow jet which mixes with the main flow and disrupts the runner inlet flow conditions. A critical size for maximum leakage flow effects was identified to be 2 mm from his experiments. Chitrakar [3] investigated flow phenomena around GV parameters computationally and compared and validated their results with the experimental results from Thapa [2]. The results showed that flow on the suction side is significantly affected by pressure-to-suction side flow through the gap and that the reduction of the pressure gradient reduces leakage through GVs. Koirala [4] performed a study on GVs at the Kaligandaki Hydroelectric Power Station, Nepal, with a capacity of 144 W. One of his major observations was that the CG at the trailing edge was larger than leading edge, which was due to the increasing cross flow velocity with a decreasing pressure for a decreasing diameter of the runner. Koirala [5] also studied the effects of the CG on turbine performance. Higher flow-affected regions were observed with a larger gap, which might be due to the substantial pressure variation across vanes. Moreover, the leakage flow rate has been found to increase with an increase in the CG, which ultimately causes pressure drops and efficiency loss in a turbine. Liu [6] investigated a leakage vortex in a mixed flow pump as a turbine (PAT) in the pump mode numerically, which was validated with experimental measurements. He concluded that,

although the gap in the study was narrow, it could induce severe leakage vortex and flow separation effects which could remarkably deteriorate the subsequent flow state in the pump and turbine. As GVs have adjacent pressure and suction sides, flow passes through the gaps from the high-pressure side to the low-pressure side or suction side. The fluid flow behavior from a GV is difficult to predict because of the wakes passing through the trailing edge combined with the cross-leakage flow through the CG [1]. This leakage flow is intermixed with the primary flow in the suction side of the GV, thus disturbing the overall flow characteristics.

Over the last few years, both numerical and experimental works have been carried out for the investigation of leakage flow through CGs in Francis turbines. A numerical investigation of the leakage flow in a three-GV cascade rig conducted by Chitrakar et al. showed that leakage flow depends on GV loading and that an asymmetrically profiled GV can improve turbine performance in terms of erosion, efficiency, and pressure pulsations of the runner [7,8]. Chitrakar [7] investigated the performance of a Francis turbine, including erosion induced CGs on GVs. With a case study of sediment-prone hydropower in Nepal, he concluded that vortices containing sediment erode the inlet of the runner blade towards the hub and shroud. Moreover, asymmetrical GV profiles have been found to have a minimal influence on pressure pulsations at the runner inlet. Chitrakar [8] investigated flow through a CG with cambered hydrofoil shapes by using a particle image velocimetry (PIV) technique. He has inferred that the pressure distribution around the hydrofoil affects the velocity field, leakage flow, and characteristics of the vortex filament developed inside the cascade. Gautam et al. [9] studied leakage flow using an alternative CG method for both asymmetrical and symmetrical GV profiles. The results show that vortices leaving the GV with a NACA 4412 profile travel towards GV surface, whereas in the case of NACA 0012, it strikes the runner inlet. Moreover, FFT analysis depicts that the frequency spectrum at the same operating condition shows lower amplitude regarding pressure pulsation in the case of an asymmetrical GV profile when compared to a symmetrical one for all CG sizes.

During operation, a Francis turbine is subjected to pressure fluctuations that originate from the interactions between rotating and stationary parts of the machine, which is defined as rotor–stator interaction (RSI). RSI describes the unsteady interaction between the rotating flow caused by runner blades (the rotating part) and the flow disturbances caused by the guide vane blades (the stationary parts). This interaction induces pressure waves that propagate through the overall hydraulic machine and hence should be considered; however, the phenomenon and characteristics of pressure fluctuation become more complex and unpredictable when a CG exists [10]. Figure 1a shows an illustration of a pressure pulse occurring as a runner blade passes through a guide vane cascade. The wake originating from the guide vanes enters the runner blade as depicted in Figure 1b [11]. It is well documented in various studies that flow instabilities, such as pressure fluctuation, vortex formation, cavitation, etc., deteriorate the hydraulic turbine efficiency and operating lifetime. Vortex evolution and propagation is a complicated phenomenon and there are several examples of vortex-induced instabilities in hydropower turbines [12]. The unsteady phenomenon in turbomachines can be classified into periodic and non-periodic types [13]. RSIs are associated with the periodic class, whereas vortex rope formation and cavitation, observed at the exit of the runner and in the cone of draft tube, which rely on the operating points, are associated with the non-periodic class.

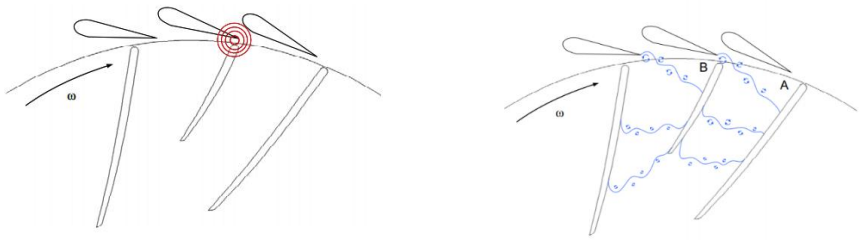

(**a**) (**b**)

Figure 1. (**a**) Occurrence of a pressure pulse as a runner blade passes through a guide vane cascade; (**b**) GV wake progressing towards the runner. Adapted with permission from Einar Kobro (2010) [11]. [11].

Vortex identification can lead to an increased understanding of complex flow phenomena. In complex flow scenarios, as in Francis turbines, there are several interacting vortices which may be bent or twisted, thus resulting in rotation in several different planes for each single vortex. Several systematic procedures for the identification of vortices have been developed and proposed [12–16]. Zhang [12] has performed a review of methods for vortex identification in hydraulic turbines. He has also discussed and summarized experimental techniques for vortex observation. Similarly, Qian [13] has experimentally investigated unsteady flows at the stator level in a Francis turbine model in his doctoral thesis. Chakraborty [14] proposed a local vortex identification criterion and requirements with the introduction of spiraling compactness for material orbits in vortices. Elsas [15] introduced an alternative vortex identification method which he termed as the "vorticity curvature criterion", which is fundamentally based on the local properties of the vortex field. He has carried out a realistic comparative study for vortex identification for the direct numerical simulation of a turbulent channel flow. Likewise, ANSYS® has devised several methods to detect vortices as spatial regions with a specified set of equations [16]. The most popularly used criteria include the Q criterion [17], $\lambda 2$ criterion, [18], Δ criterion [19], and swirling strength criterion (λci) [20]. The Q criterion is relevant for identification of a vortex in incompressible fluid, especially in large scale vortices in turbulent flow. The details of the Q criterion, which is the method of vortex identification in this paper, are discussed in the results section. The $\lambda 2$ criterion corresponds to the pressure minimum in a plane when the contributions of unsteady irrotational straining and viscous terms in Navier–Stokes equations are discarded. The Δ criterion defines vortices in regions with a complex velocity gradient. A higher value of Δ denotes stronger spiraling within a vortex region. The λci criterion identifies a vortex structure based on the imaginary eigenvalues of the velocity gradient with the quantification of the swirling strength in the vortex. The spatiotemporal evolution of a leakage vortex (LV) in a Francis turbine is still unpredictable and the relationship between flow instability and LV progression has not been revealed completely. Hence, this work is intended to understand the spatiotemporal evolution of LVs and related steady and unsteady flow phenomena in a reference case of a Francis turbine. Moreover, the frequency spectra of pressure signals at various locations inside a turbine are analyzed to understand the RSI and vortex rope phenomena.

1. Methodology

This study uses a prototype turbine with nominal head size of 207 m, rated discharge of 4.33 m^3/s, and rated speed of 750 rpm from the Bhilangana-III Hydroelectric Power Plant, Uttarakhand, India, which is mentioned as the reference turbine onwards. Figure 2 shows the methodology adopted for this research work.

Numerical studies were performed using ANSYS® CFD™ by solving steady-state Reynolds-averaged Navier–Stokes equations. The calculations were conducted at 77%, 100%, and 130% loads and the respective flow rate values were 3.36, 4.34, and 5.64 m^3/s [21]. A 100% load corresponds to the best efficiency point (BEP), whereas the 77% and 130% loads correspond to a partial load (PL) and full load (FL), respectively. Figure 3 shows a numerical model of the reference turbine, which has a runner rotating at 750 rpm and four stationary domains. The GVs of this powerplant were numerically studied by Acharya et al. earlier with a different runner [22]. Shaft allowance was also included in the GVs for this study to make the numerical case as close as the prototype [22,23]. The full model of the turbine consists of 13 runner blades and 16 GVs, as shown in Figure 2. The draft tube mesh is not shown in the figure. Spiral casing and stay vanes were excluded in the domain during simulation.

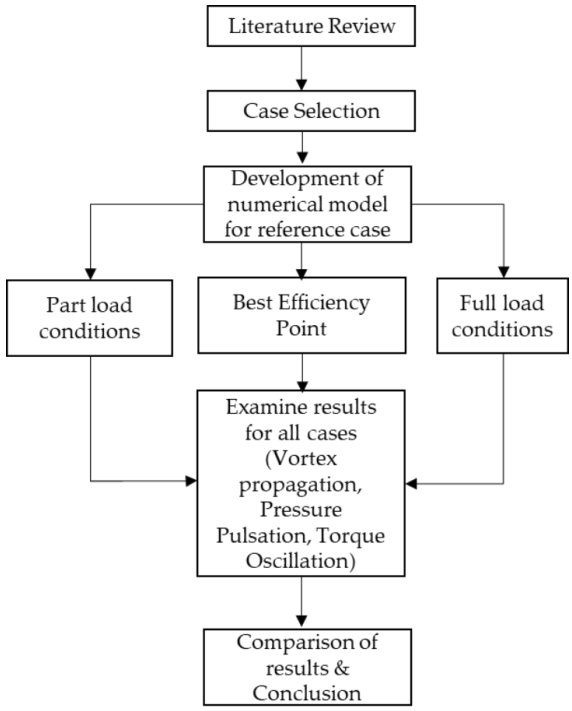

Figure 2. Flow chart showing the methodology adopted in this work

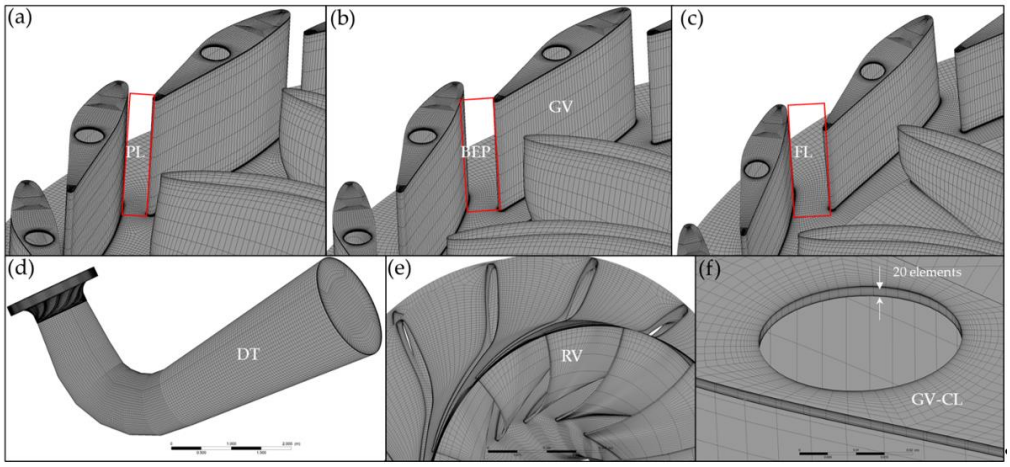

Figure 3. Structural grid for the runner, guide vanes with clearance gaps, and draft tube consisting of 7 million (approx.) elements. (**a**) GV at a partial load; (**b**) GV at the best efficiency point; (**c**) GV at a full load; (**d**) Draft tube; (**e**) Runner; (**f**) Clearance gap.

2.1 Mesh Generation and Boundary Conditions

Full passage modelling was carried out and the computational domain was discretized with a hexahedral structured mesh. ANSYS® Turbogrid™ was applied to generate the meshes in the runner and guide vanes, while the meshes in clearance gaps and draft tube were generated in ANSYS® ICEM CFD™. Meshes on the overall domain were well defined and the values of positive y-values were maintained below 30. A mass flow rate of 4330 kg/s at the circumferential inlet of guide vanes and average static pressure of 0 Pa at the outlet were chosen as boundary conditions for BEP case [24,25]. The designed mass flow rate of the turbine, representing 100% flow, was taken as the BEP. Interfaces between the stationary and rotational domain were considered with a frozen rotor method for steady-state analysis. This forms a local coupling which uses the rotating reference frame to save on computation by converting transient turbomachinery flow into a steady state. For transient analysis, a transient rotor–stator model was used as it accounts for all interaction effects between components that are in relative motion to each other and hence predicts the true transient interaction of the flow between a stator and rotor passage [26]. Transient simulations were carried out for total time corresponding to three runner revolutions, and at a time step of 1° of angular rotation for runners. The turbulence model selected for this study was the shear stress turbulence model developed by Meter [27], which was determined based upon the literature [28–30]. The details of the simulation settings are listed in Table 1.

Table 1. Numerical settings for the simulation

Item	Setting
Inlet boundary condition	Mass flow rate at 4330 kg/s at BEP with a cylindrical flow component
Outlet boundary condition	Average static pressure of 0 Pa
Wall	No slip wall
Turbulence model	Shear stress transport
Turbulence intensity	Medium (5%)
Advection scheme	High resolution
Turbulence numeric	High resolution
Solver precision	Double
Convergence criteria	RMS residual below 1×10^{-5}

2.2. Mesh Sensitivity Analysis

The grid convergence index (GCI) method was used for the estimation of the discretization error and value extrapolation [31]. This particular technique has been found to be effective in predicting numerical uncertainties in the case of a Francis turbine [32,33]. For uncertainty analysis, three structured hexahedral meshes with different resolutions were created. Mesh refinement was performed by increasing the distribution in each direction. Uncertainties in the simulation were monitored by monitoring the torque and pressure inside the domain for three different points, i.e., VL1 (vaneless space), RV1 (runner blade) and DT1 (draft tube).The discretization error for the numerical model was determined as follows:

Average length of each element for a 3D mesh was determined as follows:

$$h = \left[\frac{1}{N}\sum_{i=1}^{N}(\Delta V_i)\right]^{1/3} \quad (1)$$

Let $h_1 < h_2 < h_3$ and$r_{21} = h_2/h_1, r_{32} = h_3/h_2$. The apparent order was solved as in Equations (2)–(4) using a fixed point iteration method:

$$p = \frac{1}{ln(r_{21})}|ln|\varepsilon_{32}/\varepsilon_{21}| + q(p)| \quad (2)$$

$$q(p) = ln\left(\frac{r_{21}^{p} - s}{r_{32}^{p} - s}\right) \quad (3)$$

$$s = 1.sign(\varepsilon_{32}/\varepsilon_{21}) \quad (4)$$

The extrapolated values were calculated as follows:

$$\varphi_{ext}^{21} = (r_{21}^{p}\varphi_1 - \varphi_2)/(r_{21}^{p} - 1) \quad (5)$$

The approximate and extrapolated relative errors were calculated as follows:

$$e_a^{21} = \left|\frac{\varphi_1 - \varphi_2}{\varphi_1}\right| \quad (6)$$

$$e_{ext}^{21} = \left|\frac{\varphi_{ext}^{12} - \varphi_1}{\varphi_{ext}^{12}}\right| \quad (7)$$

$$GCI_{fine}^{21} = \frac{1.25e_a^{21}}{r_{21}^{p} - 1} \quad (8)$$

Table 2 shows the uncertainties and extrapolated values. The numerical uncertainties in pressure at points 1 and 2, with a fine mesh and medium mesh, were 0.0151% and 0.2568%, respectively. Efficiency was calculated as the ratio of power output to input. Power output was calculated from the torque of the runner and its rotational speed, whereas power input was obtained from the net head. From the efficiency measurement, uncertainty for the fine mesh was 0.0307%.

Table 2. Discretization error for the reference case.

Parameter	Pressure 1 (Pa, Φ_1)	Pressure 2 (Pa, (Φ_2)	Efficiency (η, (Φ_3)
Coarse (G3)	366,912	344,516	90.15
Medium (G2)	367,151	344,112	91.84
Fine (G1)	367,236	345,083	92.03
ϕ_{ext}^{21}	367,280	345,791	92.05
e_a^{21}	0.02314%	0.0028%	0.0021%
GCI_{fine}^{21}	0.0151%	0.2568%	0.0307%

Figure 4a shows the normalized velocity at the outlet of the GV along the circumferential position at the trailing edge of GVs. Velocity in this case is normalized in terms of net head of the turbine as expressed in Equation (9).

$$v^*[-] = \frac{v}{\sqrt{2gH}} \quad (9)$$

where v = local velocity at the outlet of the GV, which is given as $v = \sqrt{v_x^2 + v_y^2}$.

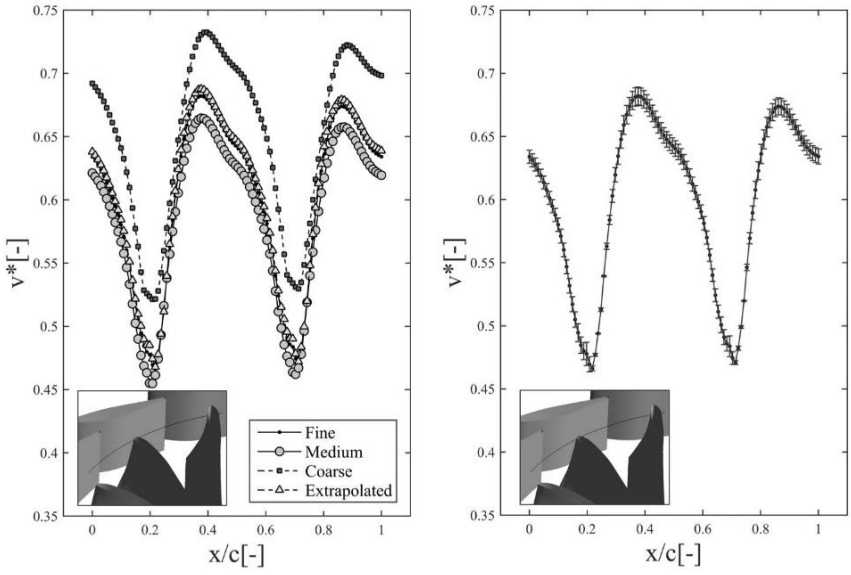

Figure 4. Uncertainty in velocity measurement at the outlet of the GV. (**a**) Different mesh schemes; (**b**) Discretization error bar.

For the numerical measurement of velocity, circumferential locations of the outlets of two GVs were considered such that the flow beneath the trailing edge of GV could be distinguished. A dimensionless term *x/c* was used in the *x*-axis, which denotes the position (*x*) from LE with respect to the chord length (c). In Figure 4, two different low velocity regions were observed due to the influence of the wake travelling from the trailing edge of the GV. Because of the influence of wakes and vortices travelling from the trailing edge, the uncertainties at these locations are higher, as shown in Figure 4b. As clearly observed in Figure 4a, the graph representing the coarse mesh has higher discrepancies as compared to the medium and fine meshes. Hence, the coarse mesh was discarded and the medium one was used for further numerical calculations.

2.3. Validation with Prototype Data

Steady-state simulations were conducted at designed and off-design conditions in the initial stage. Another set of simulations was carried out with the total pressure as the inlet boundary condition. The mass flow rate was calculated in a postprocessing step. Flow rate data available for the prototype turbine at different operating points [21] were compared with the results from the simulation as shown in Figure 5. It can be inferred from this figure that at the same guide vane opening angles, the resultant flow obtained from the CFD analysis closely matches the field data. Moreover, the efficiency comparison from the CFD calculation shows lower efficiency than the prototype measurement, which could be due to the overprediction of losses by the turbine with the use of the turbulence model [21]. It can be noticed at a deep partial load condition that the efficiency variation is higher than the designed point. In off-design conditions, the losses predicted by the numerical model are higher [7]. Figure 5 also shows the error bar which was constructed with the difference of numerical and experimental value for each GV opening angle.

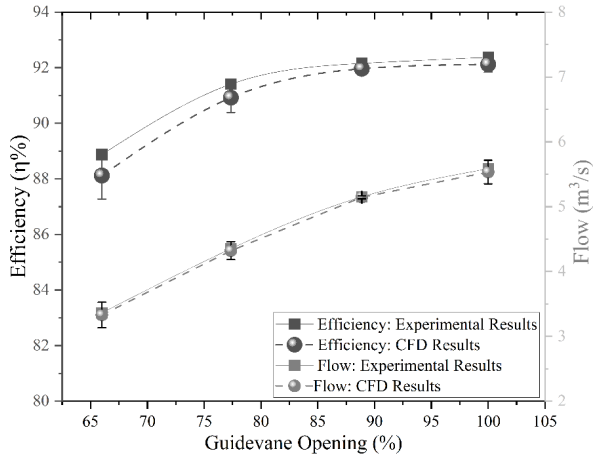

Figure 5. Prototype discharge and efficiency comparison with the simulated results for various operating condition.

Furthermore, validation of numerical model was also carried out by measuring the pressure around the middle GVs in three-GV cascade rigs developed by Chitrakar et al. [34]. The closed loop test setup was equipped with a pump delivering water from a lower reservoir. A flow meter was mounted at the outlet of the rig and two pressure taps were mounted at the inlet and outlet to acquire the correct operating points for measurement. The arrangement has a trapezoidal slot with holes with a diameter of 2 mm around the middle GV with a 2-mm offset from the GV surface. Piezoresistive pressure transducers were connected to these holes, which were used to determine GV loading. Figure 6 shows the experimental test section of the three-GV cascade rig that consists of a pressure measurement location at the middle GV (GV2). A pressure transducer was calibrated with a dead weight calibrator with an uncertainty of ±0.2%.

(**a**) (**b**)

Figure 6. The three-GV test setup for experimental validation: (**a**) Experimental set up which shows the test section in the lab ; (**b**) Locations of holes for tapping the value of pressure at GV.

Normalized pressure (Cp), which is the ratio of the pressure at a point to the pressure at an inlet as found by CFD analysis, was validated with the data obtained from the pressure transducer measurement around the circumferential positions from the leading edge to the trailing edge. Local pressure measurement at each measurement location was normalized by the pressure value at the

leading edge of GV. Thus, the blade loading characterizing the flow around the GV was observed experimentally with a maximum normalized pressure where Cp = 1 at the leading edge [35]. In the CFD pressure measurement, at same experimental pressure measurement locations, pressure values were measured. It was seen that using the current numerical model, the maximum error in pressure measurement was 8.8% towards the leading edge in the pressure side of the GV. This might be due to the influence of GV1 and inappropriate stagnation as compared to the numerical solution. At all other locations of pressure measurement, the errors in the pressure measurement were less than 5%. The blade loading distribution of the current GV profile in the reference case is shown in Figure 7b.

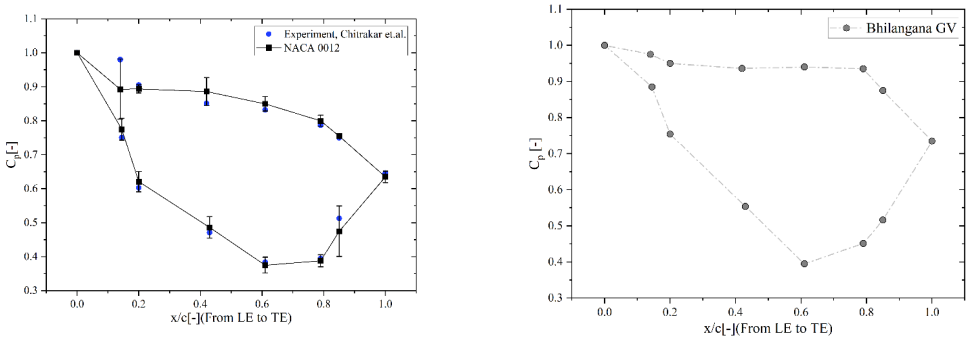

(**a**) (**b**)

Figure 7. Validation of the CFD results with the experiment: (**a**) Velocity normal to camber line from LE to TE and pressure distribution in GV for NACA 0012 hydrofoil; (**b**) reference case GV profile.

3. Results and Discussions

3.1. Leakage Vortex from GV

Figure 8a shows the overall pattern of the GV leakage vortex obtained from the transient simulation for the BEP condition whereasFigure 8bshows three distinct leakage flow (LF) areas. Part 1 shows a LF initiating from the leading edge of GV, whereas part 2originates from the GV shaft region. From Figure 8b, it is clearly observed that LF from part 1 mixes with part 2 which ultimately strikes the leading edge of runner. Similarly, another LF is set up from the trailing edge of GV, which is further divided in part 3a and part 3b in Figure 8b. The intensity of these vortices can be related with the guide vane loading curve shown in Figure 7b. The pressure difference between the two sides of GV is maximum in the stream-wise location (x/c) of 0.5–0.7. As a result, the leakage flow is driven with higher acceleration, increasing the intensity of the vortex filament. Due to the difference in number of GVs and runner blades in the turbine, the region of vortices hitting the runner is different for each blade and in every revolution.

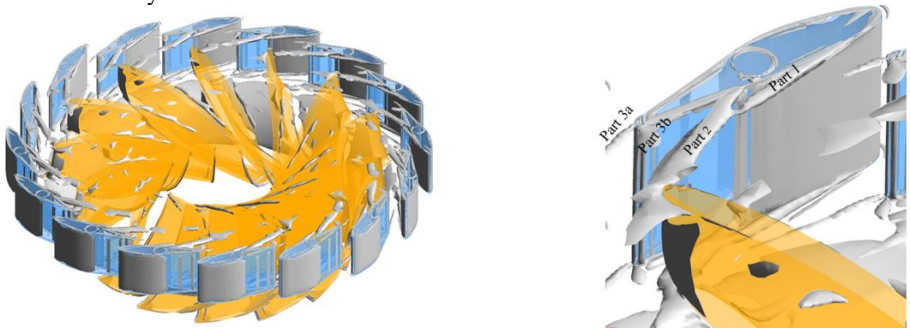

(**a**) (**b**)

Figure 8. Leakage vortex from the GV: (**a**)Pattern as observed for complete set of GVs and runner blades; (**b**) Single GV and runner blade showing three distinct leakage flow areas.

3.2. Leakage Vortex Progression

Figure 9 shows the LV trajectory obtained by transient simulation. Among several vortex identification methods as discussed in the introduction part above, the Q criterion is considered for this work. It is usually suitable for vortex identification in incompressible fluid, especially in large scale vortex in turbulent flow [12]. The Q criterion identifies vortices using second invariant of velocity gradient tensor which is defined as follows:

$$Q = {}^{1}/_{2}\, tr(\nabla v) r^2 - tr\,(\nabla v^2) \tag{10}$$

where $\nabla \boldsymbol{v}$ is the velocity gradient tensor and tr is the trace of the matrix.

A total of 13 points (P1 to P13) were located based on the vortex trajectory, as shown in Figure 9a, and vorticity was calculated on those points. Figure 9b shows the values of vorticity along LV trajectory for three operating conditions. Vorticity value was normalized in correspondence with BEP case, as shown in y axis of Figure 9b. Considering the propagation of LV from point P1, vorticity increases until point P2 for all cases and after point P3, it sharply drops until point P6. From point P6 to P9, it decreases slowly, and from P10 to P12, it is vorticity is almost lowest for the BEP and full load conditions as compared to the partial load condition from point P6 to P13 before striking the runner.

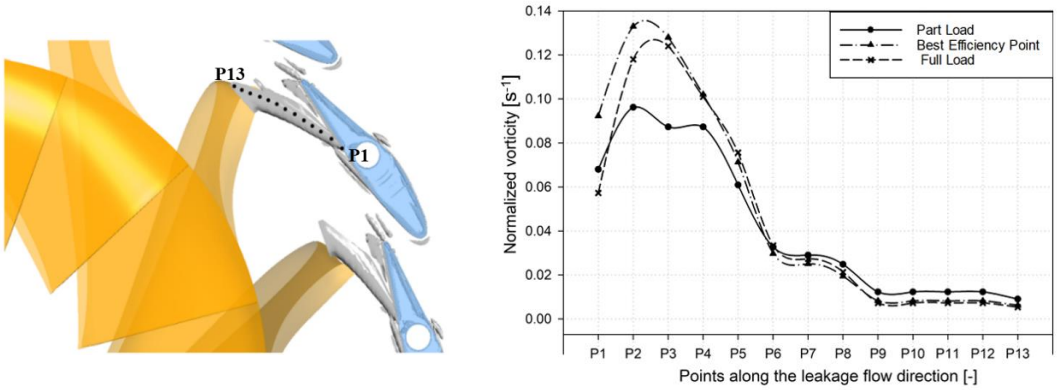

(**a**) (**b**)

Figure 9. (**a**) LV pattern with 13 points along the trajectory for the calculation of vorticity value ; (**b**) Vorticity graph normalized with corresponding BEP case along the LV trajectory.

Similarly, Figure 10 depicts values of turbulence kinetic energy (TKE) along the LV trajectory. The fluid undergoes irregular fluctuations or mixing during turbulent flow which can be visualized with irregular swirls of motions called eddies. Values of the TKE are directly related to the strength of turbulence in the flow. TKE, as seen in y-axis of Figure 10, was normalized with values corresponding to the BEP. TKE increased from points P1 to P3 steadily and then produced a sharp increase until point P5, i.e., almost approaching the middle of the trajectory. The value of TKE from point P5 fell rapidly until P9, where it then stabilized until the end of propagation. The TKE strength was lowest for the BEP and full load conditions in comparison with partial load condition after point 6 as the LV reached the leading edge of runner, which is a similar pattern to that observed for the vorticity graph shown in Figure 9b.

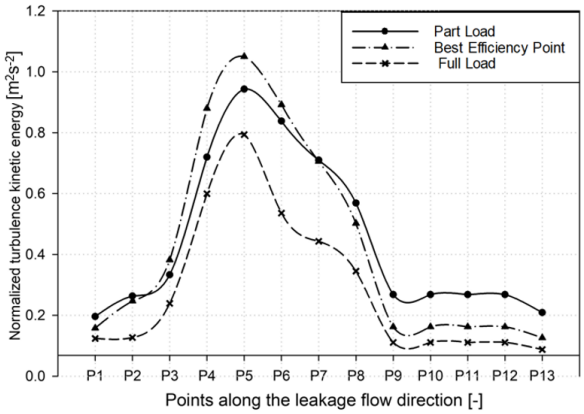

Figure 10. Turbulence kinetic energy variation along the LV trajectory.

Transient simulations were performed for three operating conditions to inspect spatial-temporal progression of LV before it hits the leading edge of runner blades. Figure 11a–f show the evolution of the LV as one runner blade passes from one GV to the consecutive GV. It shows the vortex for a 10° revolution, capturing 2° at a time. For the investigation of the progression of the part II LV of the hub region, which strikes the leading edge of runner, it can be categorized into three stages, namely (a) the elongation stage, (b) disintegration stage, and (c) dissolving stage. The elongation stage represents some shedding and the LV being slender and weaker as seen in Figure 11b,c. Figure 11d,e shows the disintegration stage, in which LV becomes more stretched with a decrease in volume and length. Only a few traces of the LV can be observed in Figure 11f, which can be described as the dissolving stage. The same process is expected to continue as the runner rotates. The LV at the shroud region is shown by the green ellipse in Figure 11a and is transported all the way until the mid-section of the blade before the majority of the vortex is dissolved.

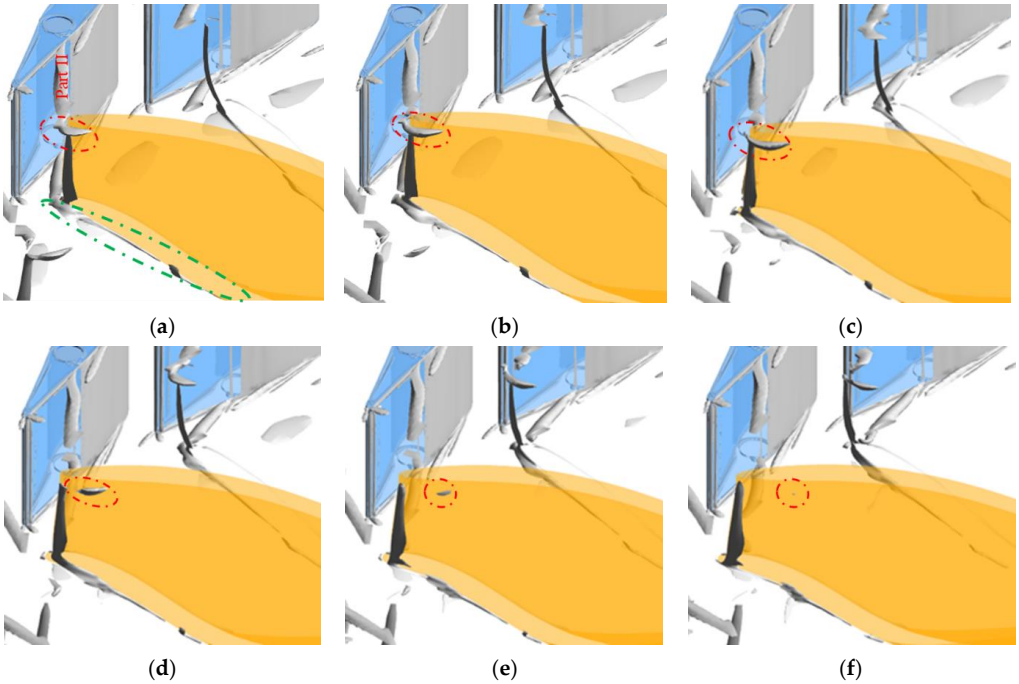

Figure 11. Progression of leakage vortex during runner rotation at BEP: (**a**) T_0; (**b**) T_0 + 1/5 of X°; (**c**) T_0 + 2/5 of X°; (**d**) T_0 + 3/5 of X°; (**e**) T_0 + 4/5 of X°; (**f**) T_0 + X°.

Figure 12a–f show the propagation of LV during 10° of rotation of the runner during the partial load condition. It also follows the same trend as in case of BEP, but the vortex disintegrates and dissolves earlier than BEP. For this condition, vortex almost disappear in Figure 12e but while compared to the same position for BEP, there is still some traces of vortex during that time. In partial load conditions, the pressure difference between the two sides of the GVs rises (because of the closing), so logically the intensity of the vortex should also rise. In this case, we saw that the intensity dropped instead, and this may be due to the reduced flow rates in the part load condition.

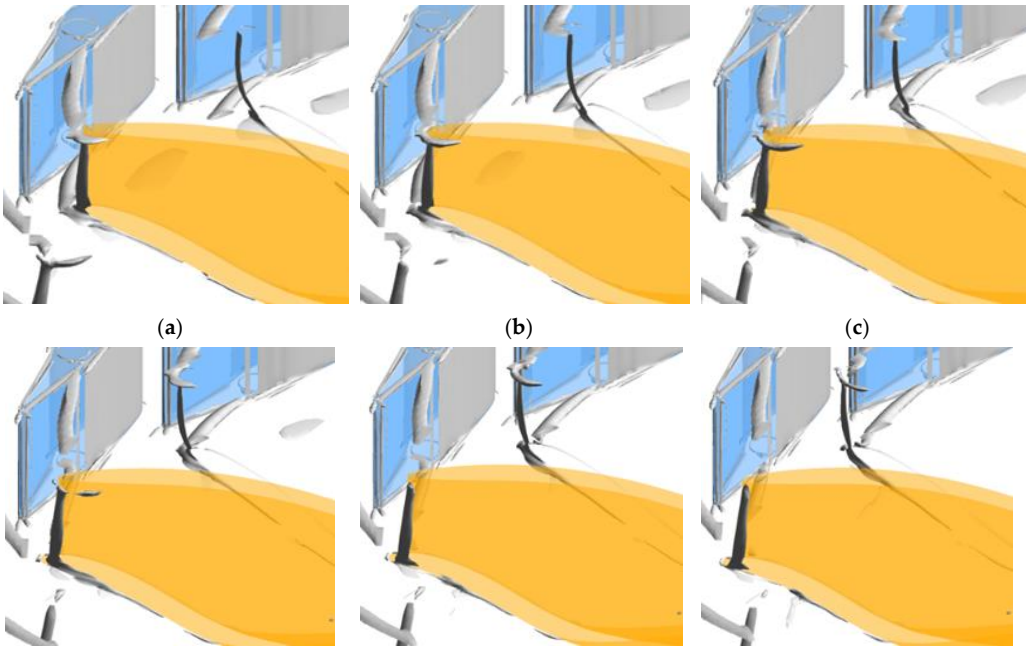

Figure 12. Progression of leakage vortex during runner rotation at part load: (**a**) T_0; (**b**) T_0 + 1/5 of X°; (**c**) T_0 + 2/5 of X°; (**d**) T_0 + 3/5 of X°; (**e**) T_0 + 4/5 of X°; (**f**) T_0 + X°.

Similarly, the progression of the leakage vortex for full load conditions is depicted in Figure 13a–f. In this case, the strength and volume of LF at the hub and shroud is higher than in previous cases. Some amount of a vortex still exists before another set of LF from consecutive GV hits the runner blade. At full load conditions, due to opening, the pressure difference should be minimum; however, in this case, the flow rate is high, and this could be the reason why we see high intensity vortices compared to other cases.

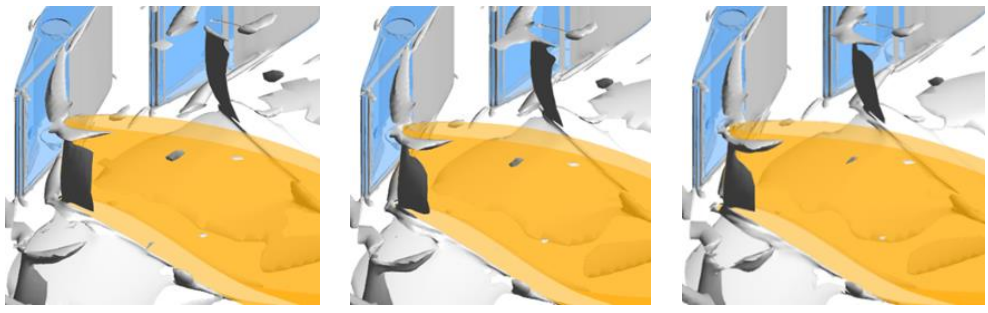

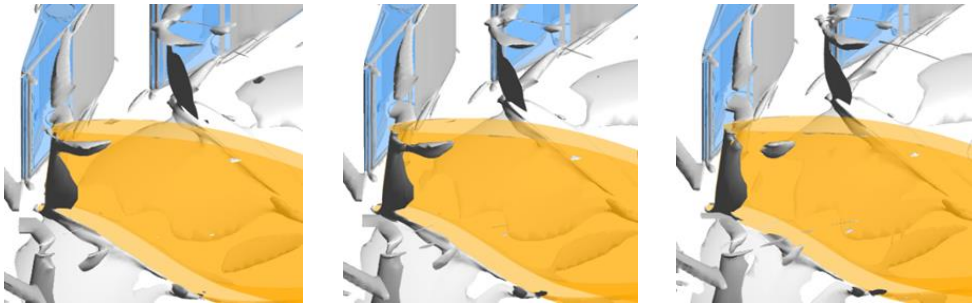

(**d**) (**e**) (**f**)

Figure 13. Progression of leakage vortex during runner rotation at full load: (**a**) T_0; (**b**) T_0 + 1/5 of X°; (**c**) T_0 + 2/5 of X°; (**d**) T_0 + 3/5 of X°; (**e**) T_0 + 4/5 of X°; (**f**) T_0 + X°.

The formation of complex vortices can represent significant influences on the performance and flow stability of hydraulic machinery. Insertion of points in the trajectory which corresponds to LV progression helped to compute the value of vorticity and TKE which are the vital parameters with major influence on the flow pattern. Intensity of these vortices can be related to GV loading curve. Similarly, the strength of turbulence in the flow can be related to the value of the TKE.

3.3. Pressure Pulsations Inside Runner

The stationary domain experiences pressure fluctuations at a frequency corresponding to the number of rotating blades (z_b) and the rotational speed of the runner (n), as shown in Equation (11). Likewise, rotating domain experience a frequency (f_{gv}) corresponding to number of guide vanes (z_{gv}) and rotational speed of runner (n), as shown in Equation (12) [33,36,37].

$$f_b = n \,.\, z_b \quad [Hz] \tag{11}$$

$$f_{gv} = n \,.\, z_{gv} \quad [Hz] \tag{12}$$

A total of sixteen points were located in the vaneless space, runner blade and draft tube, as shown in Figure 14a,b, to analyze frequency spectra. Among the sixteen points, six points from DT1 to DT6 were located in the draft tube passage from the runner outlet to the draft tube outlet. Similarly, four points, from VL1 to VL4, starting from hub area to shroud area, were defined in the vaneless space before the leading edge of runner. The remaining six points, namely, RV1 to RV6, starting from leading edge to trailing edge of the blade, were inserted along the runner blade. Pressure pulsation was calculated by subtracting the mean pressure (p) from the instantaneous pressure ($\bar{p}$) and was normalized by the reference pressure $(\rho E)_{BEP}$ [38].

$$p* = \frac{p - \bar{p}}{(\rho E)_{BEP}} \quad [-] \tag{13}$$

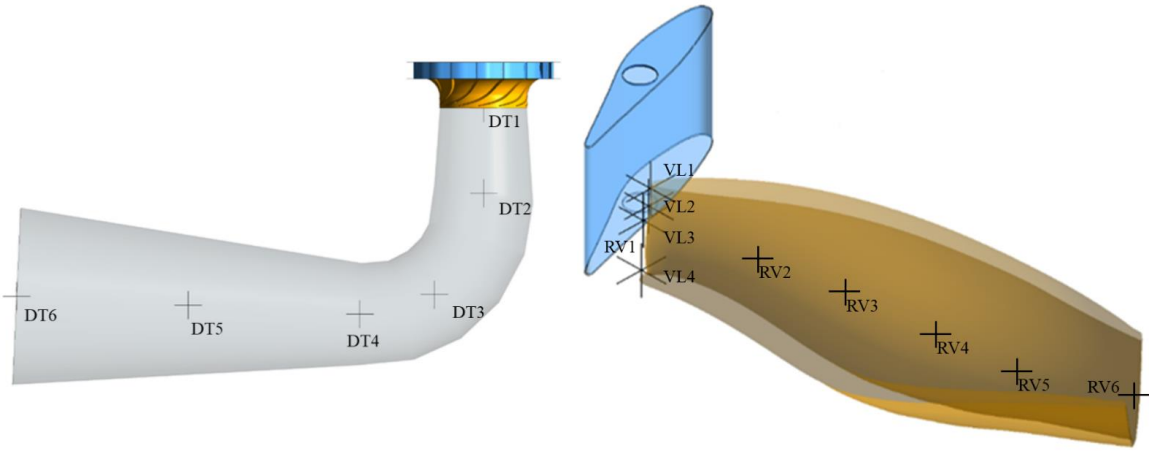

(**a**) (**b**)

Figure 14. Points for measurement of pressure pulsations at: (**a**) Six points from DT1 to DT6 inside the draft tube domain ; (**b**) Four points from VL1 to VL4 inside the vaneless space and six points from RV1 to RV6 in the runner blade surface for pressure monitoring.

In a high-head Francis turbine, as in the reference case of this study, the vaneless space between the guide vane and runner blade is small. Pressure fluctuations associated to RSI are a major concern in such an area, as several failures related to hydraulic turbines are related to this phenomenon [39]. Figure 15 shows the Fourier-transformed pressure pulsation for three operating conditions at vaneless space with a sampling frequency of 4500 Hz. The research case presented here is comprised of 16 guide vane blades. For the runner rotation of 750 rpm, the value of f_{gv} for the runner is 200 Hz. The first peak observed in Figure 15 represents the guide vane passing frequency. Consequently, other successive harmonics occurs at $2f_b$ = 400 Hz, $3f_b$ = 600 Hz, and so on. The pulsating signal is seen in every point for each operating conditions. It shows that pressure pulsating amplitude is most significant while operating the runner in part load conditions.

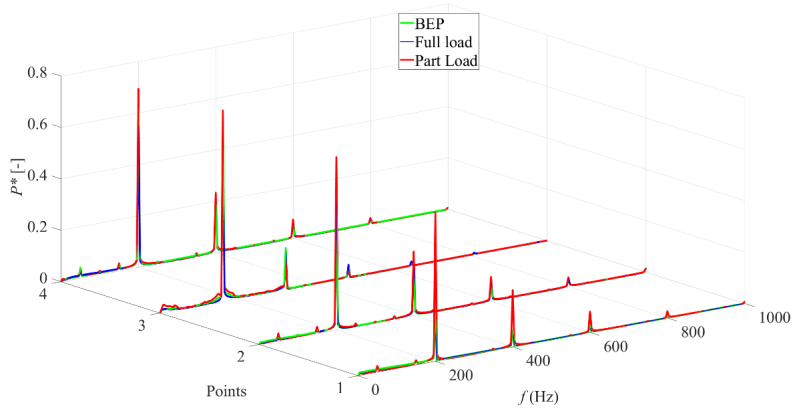

Figure 15. Frequency spectrum of pressure time signals at vaneless space.

Figure 16 shows FFT analysis of pressure pulsation inside the draft tube. As demonstrated in the figure, peak pressure pulsation is at 4 Hz for all measured points which is 0.32 times that of runner rotational frequency. After that, other pulsations occur at 8 Hz, 12 Hz, 16 Hz which corresponds to 0.64, 0.96, and 1.28 times the runner rotational frequency, respectively. This phenomenon can be related with the hydroacoustic pressure waves investigation by Arpe et al. [40], where about two types

of pressure fluctuations related to vortex precession (a) in the range of 0.3–0.4 f_n, and (b) in the range of 2–4 f_n, as pointed out during the experiment.

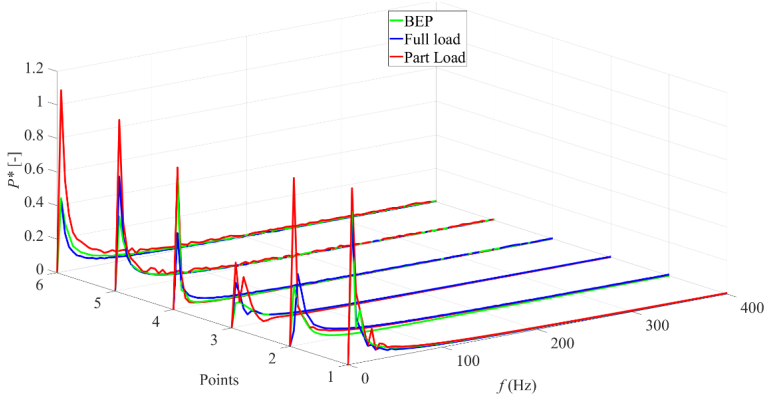

Figure 16. Frequency spectrum of pressure time signals inside draft tube.

FFT plot of pressure fluctuation from points RV1 to RV6 along the runner blade is presented in Figure 17. It is assumed that the points located in the runner surface rotate with the runner, hence the value obtained is during runner operation. It is evident from the figure that the periodic behavior of pressure fluctuation is governed by both frequencies. The low frequencies of 0.32, 0.64, and 0.96 times the runner rotational frequency correspond to the rotating vortex rope (RVR) frequency and its harmonics [41]. The bigger frequencies of 200 Hz, 400 Hz, and 600 Hz correspond to the guide vane passing frequency and its harmonics.

Frequency spectrum of pressure time signals showed that operation outside the BEP can result in high amplitudes and vortex roping, which can cause serious damage to the runner and other components. A swirling component will occur in the draft tube outside BEP operation. The high velocities in vortex core can decrease the pressure, resulting in a vapor-filled cavity core. This can cause operational challenges when coinciding with dynamics oscillations in a system.

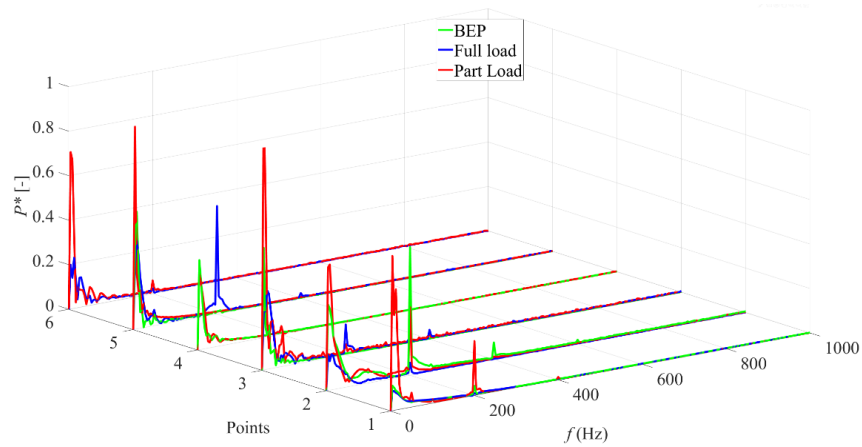

Figure 17. Frequency spectrum of pressure time signals along runner blade.

3.4. Torque Oscillations

RSI between guide vanes and runner induces pressure fluctuations inside the runner, which causes torque fluctuation. Fluctuation in torque inside the runner is caused by the expanding wakes from the guide vanes, which progresses until runner blades [42]. Hydraulic torque (T_h) from the water acts on the runner, thus accelerating it. T_h is a function of hydraulic power (P_h) and angular velocity (ω), as

expressed in Equation (14). Figure 18 shows the dynamic forces in runner blade showing an average torque for three operating conditions plotted against runner angular position.

$$T_h = {}^{P_h}/_{\omega} \text{ [Nm]} \tag{14}$$

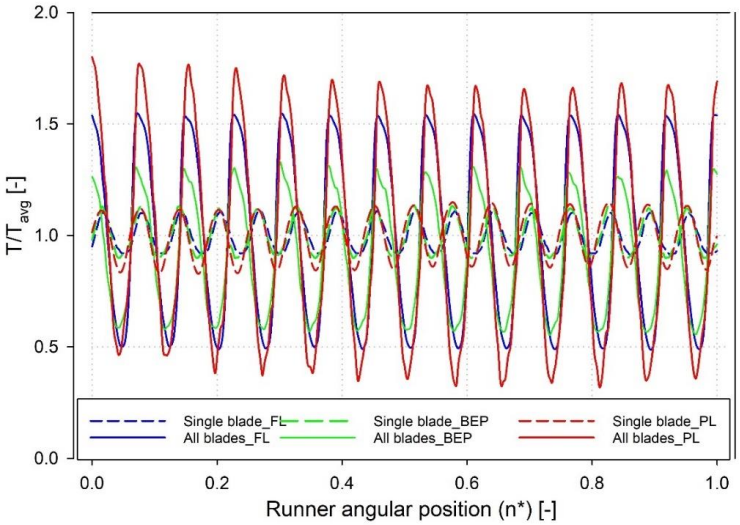

Figure 18. Torque oscillations for various operating conditions.

Torque is normalized with the value corresponding for the BEP conditions. The patterns of torque fluctuations across different operating conditions are quite similar but the amplitude varies for all. The highest fluctuation of torque is observed at part load condition of operating stage shown by red graph in Figure 18, which is followed by the full load condition shown by the blue graph. The lowest torque fluctuation of all can be seen in BEP condition as shown by the green graph. The larger fluctuations were obtained for the full runner as compared to single blade for all cases, which agrees with the work done by Nicolle et al. [43]. For the single blade, a total of 16 peaks can be seen which is due to RSI arising from pressure fields around the guide vane and it corresponds to guide vanes number; however, for the full runner, 13 peaks are seen for all cases. The reason behind this is that the number of runner blades is a prime number and has no common integer with the number of guide vanes. As such, the torque variation for the runner must be completed in one pitch, i.e., 360/13. This phenomenon can also be explained with the assumption that when we consider full runner, more than one blade is experiencing RSI at the same time.

4. Conclusions

This work features an exploration of the spatial temporal progression of a leakage vortex in a high-head Francis turbine. The LV evolution and trajectory, LV progression from the clearance gap to runner blades, vortex dynamics, and pressure fluctuations have been analyzed in this study based on numerical simulations.

LV pattern and trajectory data were acquired from transient simulations. Vortex core intensity in the leakage flow decreased along the progression. The progression of leakage flow at the hub area was classified into three forms, i.e., the elongation stage, disintegration stage, and dissolving stage. Leakage flow at the shroud area is transported until the mid-section of the blade, i.e., before the majority of vortex is dissolved, and seems to pass from the outlet of the runner as well. The values of vorticity and TKE along the LV trajectory somehow gave a clear picture of the complex vortices and turbulence phenomena for varying operating cases.

Unsteady pressure fluctuations were investigated with the reference turbine at three operating conditions, i.e., BEP, partial loading, and full loading. A total of sixteen points were located in the vaneless space, runner blade, and draft tube to study the pressure pulsations in the stationary and rotating domains. The frequency spectra data of pressure signals in the vaneless space showed the highest amplitude at the guide vane passing frequency (*fgv*) and its successive harmonics, i.e., 2*fgv*, 3*fgv*, 4*fgv* and so on, due to RSI. Monitoring the points at the draft tube showed peak pressure pulsation that was 0.32 times that of the runner rotational frequency and subsequent peaks for its harmonics. The points located along the runner blade from the leading edge to the trailing edge showed that the frequency spectrum was affected by both available frequencies. Low frequencies of 0.32, 0.64, and 0.96 times the runner rotational frequency corresponded to the rotating vortex rope frequency and its harmonics, whereas higher frequencies of 200 Hz, 400 Hz, and 600 Hz corresponded to the guide vane passing frequency and its harmonics. Moreover, while taking torque fluctuations for different operating conditions into account, it was observed that the patterns were quite similar in terms of the variation of amplitude. The highest fluctuation of the torque was observed at partial load condition, followed by the full load condition, and least for the BEP condition.

In summary, important dynamic characteristics for leakage vortex evolution and progression have been revealed in this work. The frequency spectra of pressure signals at various locations in the turbine provide some information regarding pressure fields in the blade channel; however, the spatial temporal evolution of a vortex is complex phenomenon which is governed by several factors. Further investigation is needed for overall energy improvement and the elucidation of a novel technique for vortex suppression before hitting a runner. Grooves or shapes can be added and studied which could reduce the flow separation and pressure gradient between two sides of the CG and hence suppress the LV along the way. This method should be extensively developed for implementation in real scenarios.

Author Contributions: "Conceptualization, N.A..; methodology,N.A. and S.G.; software, N.A. and S.G..; validation, S.C., and S.G..; formal analysis, N.A..; investigation, N.A..; resources, O.G.D.; data curation, N.A. and S.G. ; writing—original draft preparation, N.A.; writing—review and editing, N.A.; visualization, N.A.; supervision, O.G.D, C.T. and S.C.; project administration, O.G.D.; funding acquisition, O.G.D. All authors have read and agreed to the published version of the manuscript."

Funding: This work was conducted under the research project FME HydroCen. This project (No. 90148312) was funded by Norwegian Research Council and Norwegian Hydropower Industries.

Data Availability Statement: Not Applicable

Acknowledgments: Authors would like to thank Igor Iliev, a post-doctoral fellow at Waterpower laboratory, NTNU, for addressing some queries during the manuscript writing process.

Conflicts of Interest: Authors declare no conflict of interest.

Nomenclature

GCI_{fine}	Grid convergence index of the fine mesh [-]
e_a	Approximate relative error [-]
e_{ext}	Extrapolated relative error [-]
f_b	Blade passing Frequency [Hz]
f	Frequency [Hz]
H	Head [m]
n	Rotation of the runner [rpm]
P_h	Power [kW]
P*	Normalized Pressure [-]
T_h	Hydraulic torque [Nm]
T_{avg}	Average torque [Nm]
ω	Angular velocity [$rads^{-1}$]
Φ	Variable for GCI calculation [-]
v*	Normalized velocity [-]

v	Local velocity [ms^{-1}]
Cp	Normalized pressure [-]
ρ	Density [kgm^{-3}]
E	Specific hydraulic energy of turbine [$J\ kg^{-1}$]
Z_b	Number of rotating blades [-]
Z_{gv}	Number of guide vanes [-]

References

1. Brekke, H. The influence from the Guide Vane Clearance Gap on Efficiency and Scale Effect for Francis Turbine. In Proceedings of the IAHR Symposium on Progress within Large and High Specific Energy Units, Trondheim, Norway, 20–23 June **1988**, Volume 14; pp. 825–837.
2. Thapa, B.S.; Dahlhaug, O.G.; Thapa, B. Sediment Erosion Induced Leakage Flow from Guide Vane Clearance Gap in a Low Specific Speed Francis Turbine. *Renew. Energy* **2017**, *107*, 253–261, doi:10.1016/j.renene.2017.01.045.
3. Chitrakar, S.; Thapa, B.S.; Dahlhaug, O.G.; Neopane, H.P. Numerical Investigation of the Flow Phenomena around a Low Specific Speed Francis Turbine's Guide Vane Cascade. *IOP Conf. Ser. Earth Environ. Sci.* **2016**, *49*, doi:10.1088/1755-1315/49/6/062016.
4. Koirala, R.; Thapa, B.; Neopane, H.P.; Zhu, B.; Chhetry, B. Sediment Erosion in Guide Vanes of Francis Turbine: A Case Study of Kaligandaki Hydropower Plant, Nepal. *Wear* **2016**, *362–363*, 53–60, doi:10.1016/j.wear.2016.05.013.
5. Koirala, R.; Zhu, B.; Neopane, H.P. Effect of Guide Vane Clearance Gap on Francis Turbine Performance. *Energies* **2016**, *9*, 275, doi:10.3390/en9040275.
6. Liu, Y.; Han, Y.; Tan, L.; Wang, Y. Blade Rotation Angle on Energy Performance and Tip Leakage Vortex in a Mixed Flow Pump as Turbine at Pump Mode. *Energy* **2020**, *206*, 118084, doi:10.1016/j.energy.2020.118084.
7. Chitrakar, S.; Dahlhaug, O.G.; Neopane, H.P. Numerical Investigation of the Effect of Leakage Flow through Erosion-Induced Clearance Gaps of Guide Vanes on the Performance of Francis Turbines. *Eng. Appl. Comput. Fluid Mech.* **2018**, *12*, 662–678, doi:10.1080/19942060.2018.1509806.
8. Chitrakar, S.; Neopane, H.P.; Dahlhaug, O.G. Particle Image Velocimetry Investigation of the Leakage Flow through Clearance Gaps in Cambered Hydrofoils. *J. Fluids Eng. Trans. ASME* **2017**, *139*, doi:10.1115/1.4036269.
9. Gautam, S.; Neopane, H.P.; Thapa, B.S.; Chitrakar, S.; Zhu, B. Numerical Investigation of the Effects of Leakage Flow from Guide Vanes of Francis Turbines Using Alternative Clearance Gap Method. *J. Appl. Fluid Mech.* **2020**, *13*, 1407–1419, doi:10.36884/JAFM.13.05.30792.
10. Liu, Y.; Tan, L.; Wang, B. A Review of Tip Clearance in Propeller, Pump and Turbine. *Energies* **2018**, *11*, doi:10.3390/en11092202.
11. Kobro, E. Measurement of pressure pulsations in Francis turbines. Ph.D. Thesis, **2010**, NTNU Trondheim, Norway.
12. Zhang, Y.; Liu, K.; Xian, H.; Du, X. A Review of Methods for Vortex Identification in Hydroturbines. *Renew. Sustain. Energy Rev.* **2018**, *81*, 1269–1285, doi:10.1016/j.rser.2017.05.058.
13. Qian, R. Flow field measurements in a stator of a hydraulic turbine. Ph.D. Thesis, **2008**, Laval University, Quebec, Canada.
14. Chakraborty, P.; Balachandar, S.; Adrian, R.J. On the Relationships between Local Vortex Identification Schemes. *J. Fluid Mech.* **2005**, *535*, 189–214, doi:10.1017/S0022112005004726.
15. Elsas, J.H.; Moriconi, L. Vortex Identification from Local Properties of the Vorticity Field. *Phys. Fluids* **2017**, *29*, doi:10.1063/1.4973243.
16. ANSYS Inc. ANSYS CFD-Post User's Guide. In *Vortex Core Region*; ANSYS Inc: Canonsburg, PA, USA, 2017.
17. Hunt, J.C.R.; Wray, A.A.; Eddies, P.M. Streams, and Convergence Zones in Turbulent Flows. In *Center for Turbulence Research, Proceedings of the Summer Program*; Stanford University, California, USA, **1988**; pp 193–208.

18. Jeong, J.; Hussain, F. On the Identification of a Vortex. *J. Fluid Mech.* **1995**, 69–94, doi:10.1017/S0022112095000462.
19. Chong, M.S.; Perry, A.E.; Cantwell, B.J. A General Classification of Three-Dimensional Flow Fields. *Phys. Fluids A* **1990**, *2*, 765–777, doi:10.1063/1.857730.
20. Zhou, J.; Adrian, R.J.; Balachandar, S.; Kendall, T.M. Mechanisms for Generating Coherent Packets of Hairpin Vortices in Channel Flow. *J. Fluid Mech.* **1999**, *387*, 353–396, doi:10.1017/S002211209900467X.
21. Thapa, R.; Sharma, S.; Singh, K.M.; Gandhi, B.K. Numerical Investigation of Flow Field and Performance of the Francis Turbine of Bhilangana-III Hydropower Plant. *J. Phys. Conf. Ser.* **2020**, *1608*, doi:10.1088/1742-6596/1608/1/012010.
22. Acharya, N.; Trivedi, C.; Wahl, N.M.; Gautam, S.; Chitrakar, S.; Dahlhaug, O.G. Numerical Study of Sediment Erosion in Guide Vanes of a High Head Francis Turbine. *J. Phys. Conf. Ser.* **2019**, *1266*, doi:10.1088/1742-6596/1266/1/012004.
23. Gautam, S.; Neopane, H.P.; Acharya, N.; Chitrakar, S.; Thapa, B.S.; Zhu, B. Sediment Erosion in Low Specific Speed Francis Turbines: A Case Study on Effects and Causes. *Wear* **2020**, *442–443*, doi:10.1016/j.wear.2019.203152.
24. IEC 60041: 1991–11; Field Acceptance Tests to Determine the Hydraulic Performance of Hydraulic Turbines, Storage Pumps and Pump-Turbines, **1991**; International Electrotechnical Commission; Geneva, Switzerland.
25. Trivedi, C.; Dahlhaug, O.G. A Comprehensive Review of Verification and Validation Techniques Applied to Hydraulic Turbines. *Int. J. Fluid Mach. Syst.* **2019**, 12, 34-367.
26. Ansys Inc. CFX Solver Modelling Guide, Release 15.0. *ANSYS CFX Solver Model. Guid.* **2013**, *15317*, 724–746.
27. Menter, F.R. Review of the Shear-Stress Transport Turbulence Model Experience from an Industrial Perspective. *Int. J. Comut. Fluid Dyn.* **2009**, *23*, 305–316. doi:10.1080/10618560902773387.
28. Gautam, S.; Lama, R.; Chitrakar, S.; Thapa, B.S.; Zhu, B.; Neopane, H.P. Numerical Investigation on the Effects of Leakage Flow from Guide Vane-Clearance Gaps in Low Specific Speed Francis Turbines. *J. Phys. Conf. Ser.* **2020**, *1608*, doi:10.1088/1742-6596/1608/1/012016.
29. Trivedi, C.; Cervantes, M.J.; Dahlhaug, O.G. Numerical Techniques Applied to Hydraulic Turbines: A Perspective Review. *Appl. Mech. Rev.* **2016**, *68*, 1–18, doi:10.1115/1.4032681.
30. Arispe, T.M.; de Oliveira, W.; Ramirez, R.G. Francis Turbine Draft Tube Parameterization and Analysis of Performance Characteristics Using CFD Techniques. *Renew. Energy* **2018**, *127*, 114–124, doi:10.1016/j.renene.2018.04.055.
31. Celik, I.B.; Ghia, U.; Roache, P.J.; Freitas, C.J.; Coleman, H.; Raad, P.E. Procedure for Estimation and Reporting of Uncertainty Due to Discretization in CFD Applications. *J. Fluids Eng. Trans. ASME* **2008**, *130*, 0780011–0780014, doi:10.1115/1.2960953.
32. Trivedi, C.; Cervantes, M.J.; Gandhi, B.K.; Dahlhaug, O.G. Experimental and Numerical Studies for a High Head Francis Turbine at Several Operating Points. *J. Fluids Eng. Trans. ASME* **2013**, *135*, 1–17, doi:10.1115/1.4024805.
33. Shingai, K.; Okamoto, N.; Tamura, Y.; Tani, K. Long-Period Pressure Pulsation Estimated in Numerical Simulations for Excessive Flow Rate Condition of Francis Turbine. *J. Fluids Eng. Trans. ASME* **2014**, *136*, 1–9, doi:10.1115/1.4026584.
34. Chitrakar, S.; Neopane, H.P.; Dahlhaug, O.G. Development of a Test Rig for Investigating the Flow Field around Guide Vanes of Francis Turbines. *Flow Meas. Instrum.* **2019**, *70*, 101648, doi:10.1016/j.flowmeasinst.2019.101648.
35. Chitrakar, S.; Thapa, B.S.; Dahlhaug, O.G.; Neopane, H.P. Numerical and Experimental Study of the Leakage Flow in Guide Vanes with Different Hydrofoils. *J. Comput. Des. Eng.* **2017**, *4*, 218–230, doi:10.1016/j.jcde.2017.02.004.
36. Trivedi, C.; Agnalt, E.; Dahlhaug, O.G.; Brandastro, B.A. Signature Analysis of Characteristic Frequencies in a Francis Turbine. *IOP Conf. Ser. Earth Environ. Sci.* **2019**, *240*, doi:10.1088/1755-1315/240/7/072008.
37. Laouari, A.; Ghenaiet, A. Predicting Unsteady Behavior of a Small Francis Turbine at Several Operating Points. *Renew. Energy* **2019**, *133*, 712–724, doi:10.1016/j.renene.2018.08.111.
38. Trivedi, C.; Cervantes, M.J.; Gandhi, B.K. Investigation of a High Head Francis Turbine at Runaway Operating Conditions. *Energies* **2016**, *9*, doi:10.3390/en9030149.

39. Dorji, U.; Ghomashchi, R. Hydro Turbine Failure Mechanisms: An Overview. *Eng. Fail. Anal.* **2014**, *44*, 136–147, doi:10.1016/j.engfailanal.2014.04.013.
40. Arpe, J.; Nicolet, C.; Avellan, F. Experimental Evidence of Hydroacoustic Pressure Waves in a Francis Turbine Elbow Draft Tube for Low Discharge Conditions. *J. Fluids Eng. Trans. ASME* **2009**, *131*, 0811021–0811029, doi:10.1115/1.3155944.
41. Zhou, X.; Shi, C.; Miyagawa, K.; Wu, H.; Yu, J.; Ma, Z. Investigation of Pressure Fluctuation and Pulsating Hydraulic Axial Thrust in Francis Turbines. *Energies* **2020**, *13*, doi:10.3390/en13071734.
42. Anup, K.C.; Thapa, B.; Lee, Y.H. Transient Numerical Analysis of Rotor-Stator Interaction in a Francis Turbine. *Renew. Energy* **2014**, *65*, 227–235, doi:10.1016/j.renene.2013.09.013.
43. Nicolle, J.; Cupillard, S. Prediction of Dynamic Blade Loading of the Francis-99 Turbine. *J. Phys. Conf. Ser.* **2015**, *579*, doi:10.1088/1742-6596/579/1/012001.

Paper 4

Development of simplified model for prediction of sediment induced erosion in Francis turbine's sidewall gaps

N. Acharya, S. Gautam, S Chitrakar and O. G. Dahlhaug
IOP Conference Series: Earth and Environmental Science **1037** 012016
doi:10.1088/1755-1315/1037/1/012016

Development of simplified model for prediction of sediment induced erosion in Francis turbine's sidewall gaps

N Acharya[1*], C Trivedi[1], S Gautam[2] and O G Dahlhaug[1]
[1]Waterpower Laboratory, Department of Energy & Process Engineering, Norwegian University of Science and Technology, NO-7491, Trondheim, Norway
[2]Turbine Testing Lab, Department of Mechanical Engineering, Kathmandu University, Dhulikhel, Nepal

*Corresponding author (nirmal.acharya@ntnu.no)

Abstract. Sediment induced erosion in exposed components of hydraulic turbines has been a major issue in most of the sediment laden hydropower projects. Gradual removal of material can change the components profile which can lead to change in flow characteristics and compromise in the efficiency as well. Among several components in Francis turbine, this study focusses on the runner sidewall gaps to develop a numerical model for erosion prediction. A prototype high head Francis runner with specific speed of 85.4 has been considered as the reference case. A simplified numerical model based on the concept of rotating disc apparatus (RDA) is conceptualized to make analogy with the gap available between runner blades and guide vanes (GVs). Fillet gaps were introduced in the model to emulate the gaps available between runner blade and GV for real case scenario. Four samples with 90° separation of each are mounted on the disc rotating at 750 rpm. Sediment size of 150 µm diameter with particle mass flow rate based on the maximum amount of sediment passing through the reference turbine was used. Numerical calculation was done in ANSYS® with Tabakoff erosion model. Results give an indication of critical zones in the gap region. Erosion pattern, rate density and vorticity were compared with the actual turbine.

Keywords: Erosion, Fillet, Francis turbine, Numerical analysis, Sediment

1. Introduction

Sidewall gaps in Francis turbine refers to the clearance region between stationary and rotary components. For hydro turbines operating with sediment contained water, sediment can enter through these gaps and erode the parent material. Due to continuous effects of abrasion and erosion, these side wall clearance region increases and consequently the leakages. This volumetric loss induces the reduction in the efficiency. The leakage flow and its consequent effect due to sediment was investigated in the studies [1-6]. This leakage flow was developed from the clearance gap region between guide vanes and top-bottom covers. At GVs the clearance region increases due to the continuous effects of erosion wear. This also increases the leakage vortex from the GV. Erosion towards the inlet of the runner is mainly due to these leakage vortices from the GV. Besides the erosion due to the leakage from GV, due to continuous interaction between sediment and turbine material while flow is escaping from rotor-stator clearance region, erosion can be observed at these locations. As sidewall gaps are the area of interest for this research work, detailed view of the flow region is shown in Figure 1.

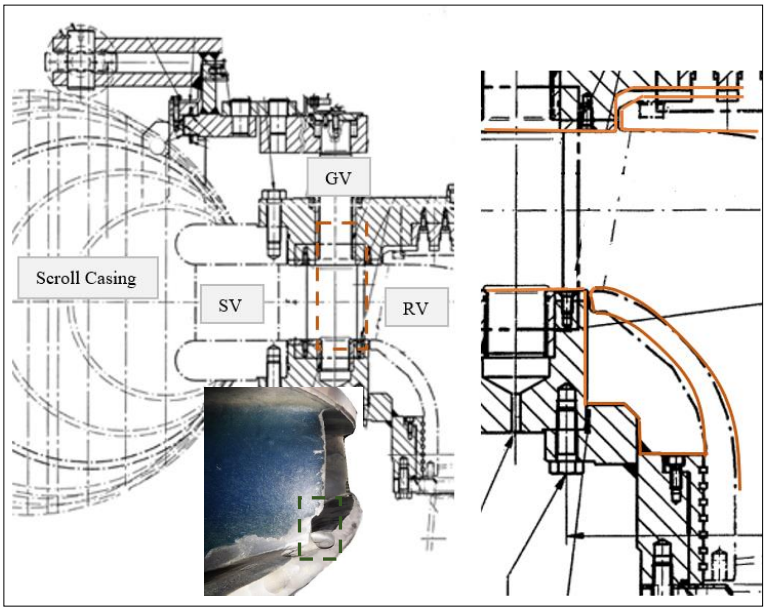

Figure 1. Cross section of reference case with the detailed view of the sidewall gaps and the section of runner from the reference site for illustration of area of interest

Wear and tear of turbine material due to sediment flow is one of major challenges for hydropower plants operating in Himalayan regions of Nepal [2,6-11]. While past studies were limited to study the erosion at GV and runner blade of Francis turbine, erosion towards the hub and shroud region at circumferential locations were not examined at all. Some studies claimed that the erosion at overall circumference of the runner hub-shroud was due to leakage vortex. However, this hypothesis is only true at the certain locations of the runner where the leakage vortex hits directly. Figure 2 shows the oblique location of the rotating runner eroded due to sediment. This study aims to examine the cause of erosion at that location of the runner using numerical technique.

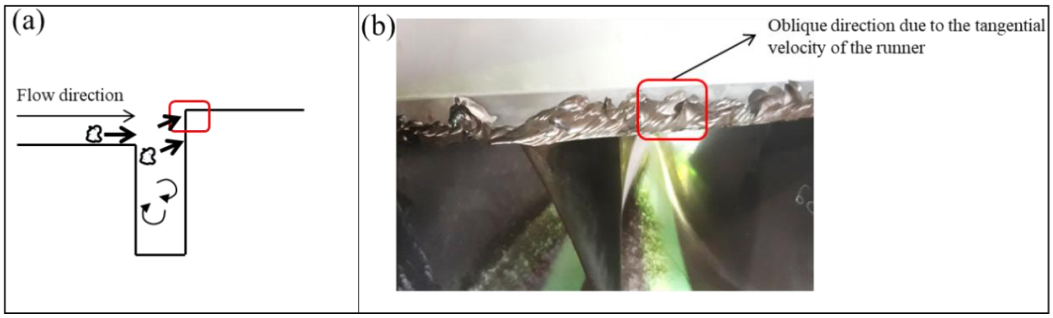

Figure 2. Effect of sediment contained flow on the turbine material (a) Nature of sediment contained flow and (b) Erosion effects towards runner band

2. Development of the reference case

Figure 3 presents the two-dimensional representation of the reference geometry presented in this study. In Figure 2(a) top view of the geometry is given that shows two specimens S1 and S2 placed at the two opposite ends of the circle. Figure 2(b) and 2(c) shows two different geometries similar in all geometrical aspects but only different with the height of the opposite ends of the gap 's'. This arrangement gives the basis for comparing the difference in the flow field with respect to slot gap and the difference in height 'δh'. CAD model of Rotating Disc Apparatus (RDA) is shown in Figure 4 where specimens were mounted for experiments.

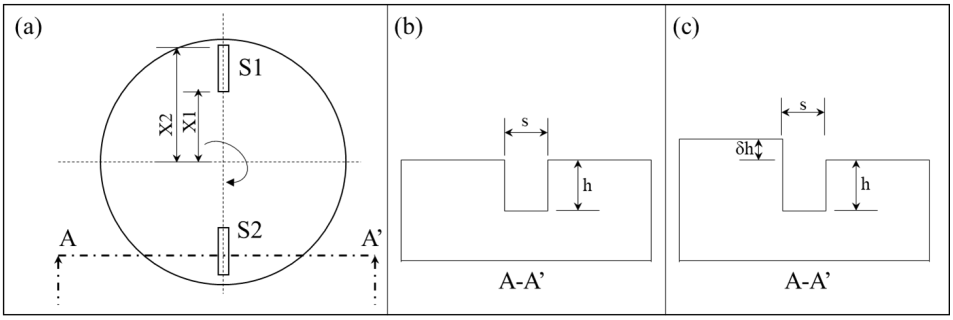

Figure 3. 2-D view of reference geometry (a) Top view (b) Section A-A' for geometry with equal heights and (c) Section A-A' for geometry with unequal heights

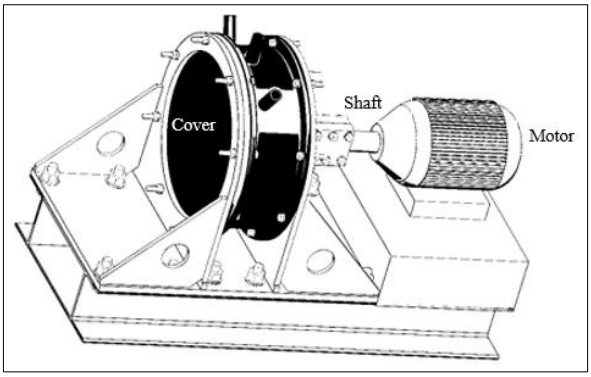

Figure 4. CAD model of RDA used for experiments

1.1 Numerical model and mesh

A simplified numerical model is developed that depicts the gap between the rotor-stator component. There are two different models of the gap in this study. First model has equal height of opposite to the slot gap and second model has unequal heights. The numerical model consists of a cylindrical domain, with the slot gaps in the opposite end of the cylinder exactly at 180 degrees. The 3-D geometry of the simplified model is discretized with structured hexahedral grid using ANSYS ICEM CFD. Near the wall of the gaps, boundary layer is refined to maintain the y+ less than 10. Minimum quality of the grid was less than 0.4. Figure 5 shows the model discretized with hexahedral cells.

For the numerical study, Unsteady Reynolds-Averaged Navier-Stokes (URANS) equations were used to model the flow field and solved using element-based finite volume method. Buoyancy model was activated in the simulation to achieve the gravity effect in the numerical model keeping the

constant gravity term 9.81m/s^2. The simulations were performed using transient flow condition considering 5 revolutions of the domain at rotational speed 750 RPM. For erosion modelling, Tabakoff and Grantt erosion model was used based on the effectiveness of the numerical model from previous literatures.
Sediment properties used in the numerical model are listed in Table 1.

Table 1: Sediment properties used in numerical model

S.N.	Parameters	Value	Unit
1	Density	2650	kg/m^3
2	No. of particles	5000	-
3	Shape factor	0.7	-
4	Size	150	µm

Figure 5. Mesh developed for the numerical study, (a) Fine grid for equal slot height and (b)

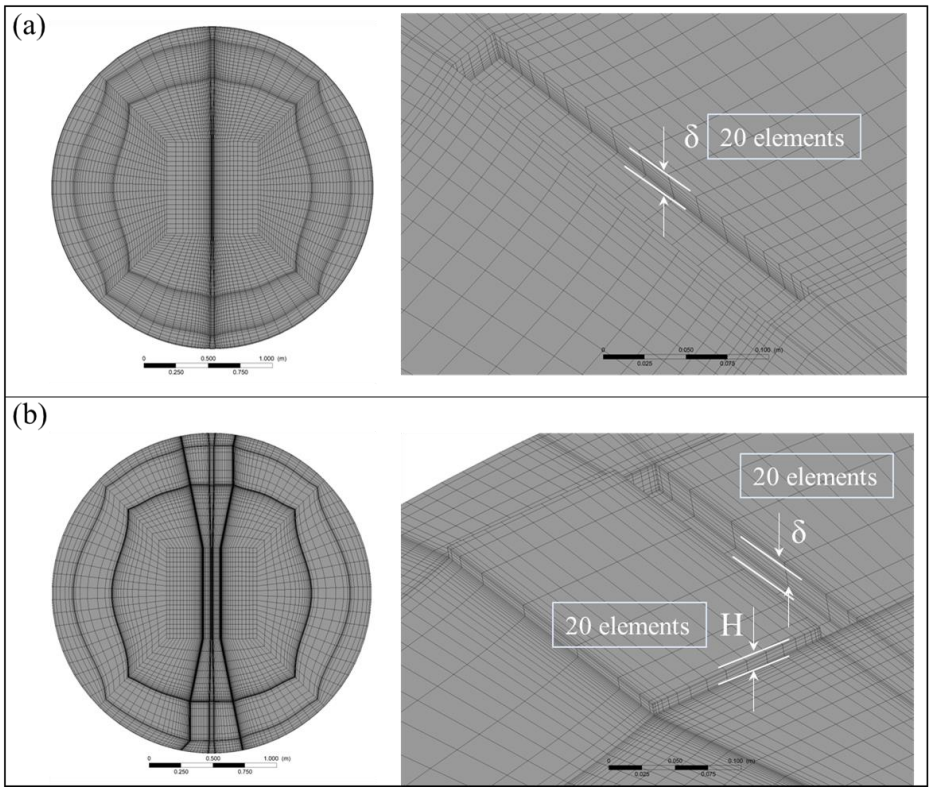

Fine grid for unequal slot height

3. Results and discussion

3.1 Vortex formation inside slot

As shown in Figure 3, that the two opposite ends of slot are at different distance from the centre of rotation, effect of centrifugal force on the vortex formation and propagation can be observed clearly at two different ends. As the centrifugal force is the function of distance to the centre and rotational speed, the evolution of vortex can be observed from shorter radius to the greater one, where the re-circulating flow is pushed away from the centre of rotation.

In a rotating domain, the presence of a gap induces the flow disturbance. In this study a whole domain is rotating at an angular speed of 750 RPM which corresponds to the rpm of reference runner. The presence of slots at two opposite ends of the domain, gives rise to the flow recirculation. Thus, the distinct region of flow recirculation is observed inside the slot that induces the vortex flow. In figure 6, recirculating flow is observed inside the gap and at the stepped end in the direction of rotation.

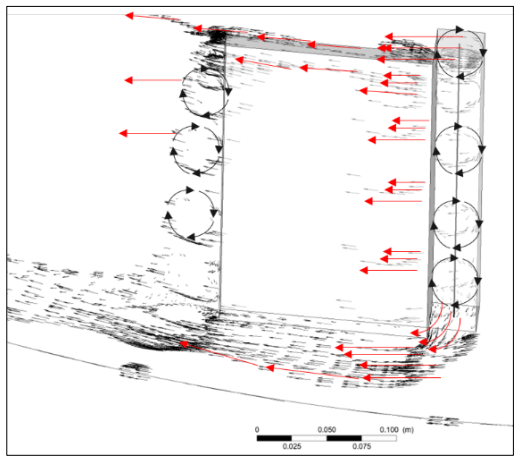

Figure 6. Velocity vector from slot

3.2 Vortex formation inside slot and sediment erosion

Sediment erosion is directly related with the corresponding flow field. Literatures [12-13] suggested that the presence the strong vortices along with sediment particle induces the severe effect of sediment erosion problem. In Figure 7, the presence of strong vortex with highest flow velocity is observed. Since, the velocity of fluid is directly related to the velocity particle and consequently the sediment erosion effect as suggested by Truscott [14], erosion problem is pre-dominant in the region corresponding the highest flow re-circulations. The erosion towards the corner of the gaps where the combined effect of centrifugal force in sediment contained flow and flow re-circulations is highest can be predicted with this nature of vortex.

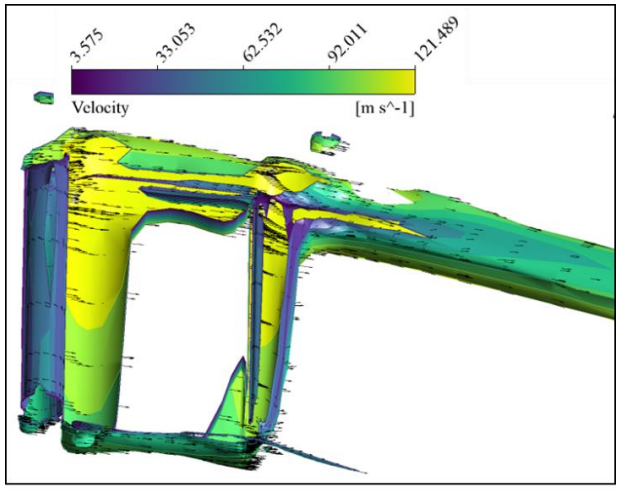

Figure 7. Velocity of fluid in the vortex inside the slot

3.3 Vorticity propagation

Figure 8 shows the intensity of vortex at the two different specimens: (i) with slot only and (ii) with both slot and height difference. For both cases, the vorticity is increasing corresponding the geometrical location i.e., increasing with the distance from the centre of the numerical domain. As discussed in previous section, this increasing vortex tendency is obvious due to higher centrifugal force acting in the working fluid at higher radius. Therefore, the region of sediment erosion can be observed due to the presence of vortices. However, in case of the specimen with slot only the intensity of vorticity was higher compared to slot and height. This is due to shifting of vortex core region at other geometrical location to that of specimen with slot only. In both the cases comparison was made assuming that the vortex core region occurs at same geometrical location. Moreover, added to the central vortex core region inside the slot the vortex flow is also observed at the stepped region. Due to this reason the erosion effects can be seen at two different locations: one inside the gap and the other towards the corner of stepped geometry due to difference in height.

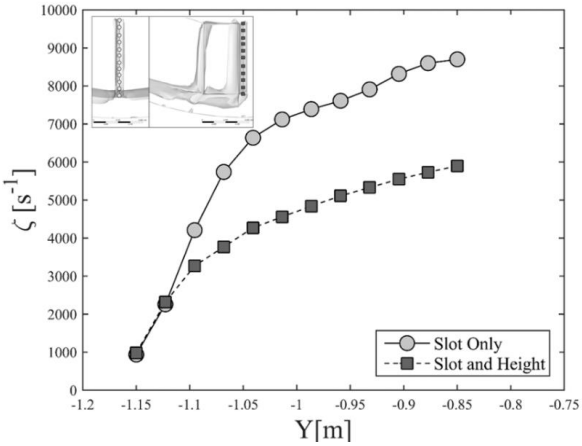

Figure 8. Vorticity distribution inside slot (X-axis shows non-dimensional spacing inside the slot and Y-axis shows the intensity of the vorticity)

3.4 Comparison with experimental results

A simplified test rig was developed as a part of this research to predict the sediment erosion effects due to the presence of slot gap. The rig is Rotational Disc Apparatus (RDA) developed by Rajkarnikar et. al. [15], where four different samples were assembled in a rotor-disc and rotated inside the sediment contained water.

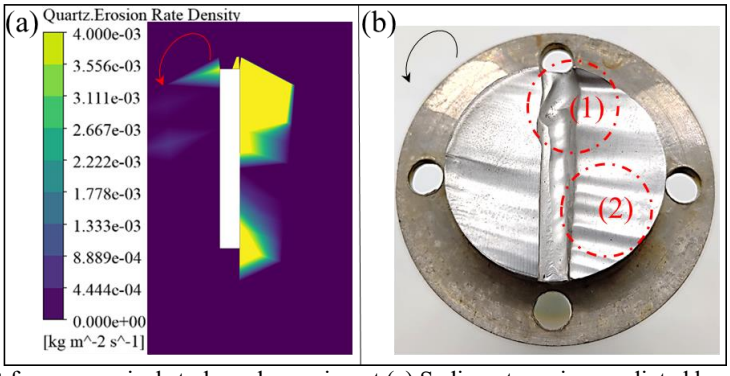

Figure 9. Result from numerical study and experiment (a) Sediment erosion predicted by numerical study and (b) Erosion predicted by the experiment for same case

Experiments were conducted at the same rotational speed as in numerical model and nearly 50,000 ppm of sediment with average shape factor 0.68 and size less than 150 μm was used inside the experimental set up. Figure 9 presents the results from both numerical study and the experiment. It can be inferred from above figure that the erosion is highest towards the opposing end of the gap due to abrasion of sediment particle. The result from experiment presented in Figure 9(b) shows two different regions of erosion. Region 1 is at the farthest end from the centre where all the vortices accumulate, has the distinct region of erosion due to flow re-circulation. In Region 2, the scaled effect of erosion at an angle less than 90 degrees to the slot length is observed. This angular region of erosion is due to the resultant effect of radial and circumferential velocity component acting in the sediment particle.

4. Conclusion

Overall, this study presented a simplified numerical model to predict the flow field inside the gap that can be related to rotor-stationary gap of Francis turbine and the corresponding sediment erosion effects. The presence of gap induces the vortices that has severe effect due to sediment contained flow. The continuous interaction between the sediment particle and the surface of material gives rise to erosive and abrasive wear.

A detailed flow physics based upon the nature of vortex development, propagation and the erosion were studied. It was found that inside the gap of a model rotating at certain angular speed, the vortex develops from lower radius, accumulates to the higher radius and leaves with high intensity. This phenomenon can be observed for both cases having equal heights between the slot gaps and unequal height. However, in the case of the model having unequal heights another region of vortex development was also observed. This can be directly related to the difference in guide vane outlet height and runner inlet height in case of Francis turbine. Finally, the numerically predicted erosion pattern was examined with the experiment. The numerical model was well suitable to predict the erosion effects induced by the gap.

Future Works

Experimental works in RDA are being continued with the variation of slot width and fillet radii as well. With these various measured set of parameters, authors expect to come up with mathematical model for prediction of erosion in the stated area of interest.

Acknowledgments

This work was conducted under research project FME-Hydrocen. This project (No. 90148312) was funded by Norwegian Research Council and Norwegian Hydropower Industries. Authors would like to thank Turbine Testing Lab (TTL), Kathmandu University (KU), Nepal for the availability and usage of the test facilities needed for this research work.

References

[1] Gautam S, Neopane H P, Thapa B S, Chitrakar S and Zhu B 2020 Numerical investigation of the effects of leakage flow from guide vanes of Francis turbines using alternative clearance gap method *J. Appl. Fluid Mech.* **13** 1407–19.

[2] Chitrakar, S.; Neopane, H. P.; Dahlhaug, O. G. Study of the Simultaneous Effects of Secondary Flow and Sediment Erosion in Francis Turbines. *Renew. Energy* **2016**, *97*, 881–891. https://doi.org/10.1016/j.renene.2016.06.007.

[3] Gautam, S.; Neopane, H. P.; Acharya, N.; Chitrakar, S.; Thapa, B. S.; Zhu, B. Sediment Erosion in Low Specific Speed Francis Turbines: A Case Study on Effects and Causes. *Wear* **2020**, *442–443*. https://doi.org/10.1016/j.wear.2019.203152.

[4] Koirala, R.; Thapa, B.; Neopane, H. P.; Zhu, B.; Chhetry, B. Sediment Erosion in Guide Vanes of Francis Turbine: A Case Study of Kaligandaki Hydropower Plant, Nepal. *Wear* **2016**, *362–363* (May 2016), 53–60. https://doi.org/10.1016/j.wear.2016.05.013.

[5] Chitrakar, S.; Dahlhaug O G and Neopane H P 2018 Numerical investigation of the effect of leakage flow through erosion-induced clearance gaps of guide vanes on the performance of francis turbines *Eng. Appl. Comput. Fluid Mech.* **12** 662–78.

[6] Acharya, N.; Trivedi, C.; Wahl, N. M.; Gautam, S.; Chitrakar, S.; Dahlhaug, O. G. Numerical Study of Sediment Erosion in Guide Vanes of a High Head Francis Turbine. *J. Phys. Conf. Ser.* **2019**, *1266* (1). https://doi.org/10.1088/1742-6596/1266/1/012004.
[7] Thapa, B. Sand Erosion of Hydraulic Machinery, 2004.
[8] Panta, S.; Lamsal, M.; Thapa, B.; Thapa, B. S. Prediction of Turbine Needed For Future Hydropower Projects in Nepal. *Hydro Nepal J. Water, Energy Environ.* **2014**, *14*, 23–26. https://doi.org/10.3126/hn.v14i0.11250.
[9] Neopane, H. P.; Dahlhaug, O. G.; Cervantes, M. J. The Effect of Sediment Characteristics for Predicting Erosion on Francis Turbines Blades. *Int. J. Hydropower Dams* **2012**, *19* (1), 79–83.
[10] Neopane, H. P. Sediment Erosion in Hydro Turbines, Norwegian University of Science and Technology, 2010.
[11] Thapa, B. S.; Thapa, B.; Dahlhaug, O. G. Current Research in Hydraulic Turbines for Handling Sediments. *Energy* **2012**, *47* (1), 62–69. https://doi.org/10.1016/j.energy.2012.05.014.
[12] B. S. Thapa, O. G. Dahlhaug, and B. Thapa, "Sediment erosion induced leakage flow from guide vane clearance gap in a low specific speed Francis turbine," Renew. Energy, vol. 107, no. January, pp. 253–261, **2017**, doi: 10.1016/j.renene.2017.01.045.
[13] B. S. Thapa, O. G. Dahlhaug, and B. Thapa, "Effects of sediment erosion in guide vanes of Francis turbine," Wear, vol. 390–391, no. July, pp. 104–112, **2017**, doi: 10.1016/j.wear.2017.07.012.
[14] Truscott, G. F. A Literature Survey on Abrasive Wear in Hydraulic Machinery. *Wear* **1972**, *20* (1), 29–50. https://doi.org/10.1016/0043-1648(72)90285-2.
[15] Rajkarnikar, B.; Neopane, H. P.; Thapa, B. S. Development of Rotating Disc Apparatus for Test of Sediment-Induced Erosion in Francis Runner Blades. *Wear* **2013**, *306* (1–2), 119–125. https://doi.org/10.1016/j.wear.2013.07.011.

Paper 5

Application of hydro-abrasive erosion model from IEC 62364:2019 standard in Francis turbines

N. Acharya, S. Gautam, S Chitrakar, C Trivedi and O. G. Dahlhaug
Paper accepted: IOP Conference Series: Earth and Environmental Science

Paper 6

Experimental investigation on hydro-abrasive erosion due to geometrical positioning of Francis turbine's rotor-stator components

N. Acharya, S. Gautam, S Chitrakar, and O. G. Dahlhaug
Paper Submitted.

Part III

Additional Papers

Paper A

Sediment erosion in low specific speed Francis turbines: A case study on effects and causes

Saroj Gautam, Hari Prasad Neopane, Nirmal Acharya, Sailesh Chitrakar, Biraj Singh Thapa and Baoshan Zhu

Wear 2020; 203152:442-3.

ABSTRACT

Hydraulic turbines experience severe operational and maintenance challenges when operated in sediment-laden water. The combined effect of erosive and abrasive wear in turbine components deteriorates their life and efficiency. The quantity and pattern of sediment erosion depends on the nature of the flow and the amount of hard minerals contained in water. Localized erosion patterns are observed mostly in guide vanes, runner blades and facing plates of Francis turbines due to different natures of fluid flow in those regions. Accelerating flow around the guide vanes and its shaft causes abrasive and erosive wear in its surface, which causes increase in the size of the clearance gap between the facing plates and the guide vanes. Flow leaving the clearance gap forms a vortex filament due to the leakage from high pressure side to the low-pressure side of the guide vane, which eventually strikes the rotating runner blades. This paper presents a case study of a power plant in India with low specific speed Francis turbines, which is severely affected by sediment erosion problems. A numerical analysis of the flow is conducted inside the turbine to study causes of various erosion patterns in the turbine components. The results from CFD are compared with the actual erosion in turbines. Erosion in guide vanes and runner blades are taken into consideration in this paper, due to the complex flow phenomena around these regions. It is found that the leakage flow through clearance gaps of guide vanes is the primary cause of erosion at the inlet of the runner blades. Furthermore, the effects of size and shape of quartz particles are studied which shows that erosion is directly proportional to these parameters.

Relevance to this thesis

This paper investigates the erosion phenomenon and its possible causes in the Francis turbine components for the reference hydropower plant. It helped to understand and estimate the extent of sediment erosion for some hydro-mechanical components of the reference power plant during background study of this PhD work.

The author of the thesis was collaborating with the main author in FranSed project and has contributed to this paper by providing the turbine components drawing, assisting during numerical setups. In addition, author of this thesis was involved during discussion and analysis of the results.

Paper B

Correlating sediment erosion in rotary-stationary gaps of Francis turbines with complex flow patterns

Saroj Gautam, Nirmal Acharya, Arun Pandey, Sailesh Chitrakar, Hari Prasad Neopane, Igor Iliev and Ole Gunnar Dahlhaug

Submitted to : Renewable and Sustainable Energy Reviews

ABSTRACT

A gap between guide vanes and top-bottom covers and rotating-stationary geometries induces the secondary flows in Francis turbines. These flow from the gap between the rotor-stator component enter the upper and lower labyrinth region. When operated with sediment-laden water, Francis turbines, sediment contained flows affect these gaps, thus increasing the size of the gap and increasing the leakage flow. This work examines the secondary flows developing at these locations of Francis turbine and consequent sediment erosion effects. A reference Francis turbine of Bhilangana III Hydropower Plant (HPP) with a specific speed 85.4 severely affected by sediment erosion problem was selected for this study. Different turbine locations with complex secondary flows and consequent sediment erosion effects were examined separately, developing a numerical model. The simultaneous results of secondary flows and sediment erosion at the complex geometries were found to affect the overall performance of the turbine.

Relevance to this thesis

This paper investigates several locations of the Francis turbine where the simultaneous effects of secondary flows and sediment erosion occur. Numerical model is developed to understand complex secondary flows and consequent sediment erosion effects. As this PhD study is intended to find the possible factors and areas for erosion in Francis turbine and way forward to improve erosion handling ability, results from this paper can be an important milestone for designing the turbines operated in sediment laden water.

The author of the thesis has contributed to this paper by taking part during numerical setups and deciding about the operating scenarios to be simulated.